hexagon:2611.01000v1

Towards a conformal field theory
of critical percolation. III.

Quantitative mixed fusion and subleading fields

Alberto Gandolfi[1,2]

[1]Division of Science, New York University Abu Dhabi,
PO Box 129188, Abu Dhabi, United Arab Emirates.

[2]NYUAD Center for Interdisciplinary Data Science & AI (CIDSAI),
NYUAD Research Institute, New York University Abu Dhabi,
PO Box 129188, Abu Dhabi, UAE.

Email: ag189@nyu.edu

22 November 2026

Abstract

How does the field produced by closing a small disk arise when two density marks approach each other in critical site percolation on the triangular lattice? We show that the contribution proportional to the scalar field E° accumulates over the scales at which the two marked clusters can first merge. After subtracting this logarithmic term from the rescaled, centered density pair, we construct a local field L_ℓ at reference length ℓ. The limit holds in variation norm on the full connectivity record of a surrounding circle, which allows us to derive its conformal transformation law before choosing an exterior observation. We then bring E° or L_r to distance r from a further density mark. After angular averaging and subtraction of the leading density, we obtain expansions with error $O(r^{61/40})$ at fixed observation radius. The scalar null identity cancels the possible $r^{55/48}$ term for E°, leaving $r^{3/2}\Psi$. For L_r we identify the coefficient of $r^{3/2}\Psi$ and isolate a possible contribution of order $r^{55/48}$. The passage to arbitrary exterior observations uses joint convergence of the connections among interior marks and labelled boundary arcs in the domains left by an exploration.

Status of this version. This is a preliminary preprint. The detailed verification of the mathematical arguments and their dependencies is ongoing and is not yet complete. The manuscript is being made public to make the arguments available for scrutiny and discussion while this verification continues. Its mathematical claims should therefore be regarded as provisional.

Contents

1 Introduction 1

2 Related work 1

3 Main results 2

4 Local fields and connectivity records 3

5 The finite part of the density pair 5

6 Conformal action and normalization of the logarithmic field 28

7 The leading logarithmic–density fusion 32

8 Nested density collisions and the symmetric triple coefficient 34

9 Two disjoint density pairs 37

10 The logarithmic coefficient from the scalar null equation 39

11 Connections between interior roots and boundary arcs 42

12 Local Ward estimates and conformal images of circles 49

13 The one-arc equation and its first scalar correction 52

14 Radial exploration with four boundary tips 59

15 A radial recurrence in a quadrilateral 63

16 Expansion on an arbitrary observation circle 66

17 Cancellation for the scalar field 68

18 The subleading field and the stationary logarithmic coefficient 70

Conclusion 72

Use of generative AI 72

1 Introduction

How much does closing a small disk change the probability that two distant sites are connected? In critical site percolation on the triangular lattice, the change is of order $r^{5/4}$ for a disk of radius r. After dividing by $r^{5/4}$ and shrinking the disk, we recover the scalar field E° constructed in Paper II [2, Theorems 4.3–4.4]. Here we show how the same field appears when two density marks approach each other, even though their connection experiment involves no obstacle.

To see where E° enters, surround the close pair by a circle and follow the two marked clusters outwards. If they first join in a given annulus, part of the change seen by a distant observer is proportional to E°. These contributions accumulate over the scales between the pair separation and the observation circle. In the four-density correlation they give the logarithm found by Camia and Feng [17, Theorem 1.1]. We subtract the disconnected pair contribution and this logarithmic multiple of E°. The finite part defines a field L_ℓ, where ℓ is the length used in the subtraction. Changing ℓ adds a multiple of E° to L_ℓ. In this sense the two fields form a logarithmic pair. Section 5 constructs the limit while retaining the connections among all clusters that reach the circle.

What does a third density mark see when it approaches the resulting pair? For E°, Paper II found a subleading field Ψ by testing against distant field insertions. Here we allow the observer to distinguish every cluster that reaches the surrounding circle. After subtracting the leading density and averaging over the direction of approach, the first correction for E° is still $r^{3/2}\Psi$. For L_r, with the reference length equal to the separation, we find the coefficient of the same field and isolate a possible earlier term at order $r^{55/48}$. Both expansions have error $O(r^{61/40})$ at fixed observation radius (Theorem 18.1).

The two powers come from different boundary configurations. With one open arc left, the power $3/2$ comes from the evolution of its angular width. With four alternating arcs, two interfaces can approach the source together, and it is the probability of this joint approach, after density rescaling, that accounts for the power $55/48$ (Figure 4). The scalar null identity cancels this contribution for E°. To carry the calculation back to the original observation circle, we need to know which boundary arc each interior mark reaches, even when two arcs are opposite banks of the same slit. Theorem 11.1 proves joint convergence of precisely these observations.

2 Related work

Camia constructed the cluster-sign density and its conformally covariant correlations [3, (1.8)–(1.11), Theorem 1.5]. The full interface scaling limit and convergence of a single exploration are due to Camia and Newman [6, 7]. The arm exponents used here are those of Lawler, Schramm and Werner and of Smirnov and Werner [8, 9]. Garban, Pete and Schramm coupled configurations conditioned on four arms and a specified crossing state [19, Section 3, Proposition 3.1]. Our use of this coupling must control the error even for an incoming state of arbitrarily small probability. Zhan's two-curve Green function and radial transition law enter the analysis of the quadrilateral [11, Theorem 1.1 and Sections 4–5].

Camia and Feng described logarithms in geometric percolation correlations [16], proved the close-pair logarithm for the four-density function [17, Theorem 1.1], and defined a microscopic energy and a logarithmic partner with two- and three-point formulas [18, (1.8)–(1.9), (1.23)–(1.28)]. Paper II identifies the normalized microscopic energy with E° assuming their asymptotic formula for one energy and two densities [2, Theorem 4.9]. Here we fix the unit density two-point normalization and a particular subtraction for the finite part.

The additional information is the comparison of its full local connectivity measures and its response to further fusions. The triangular Ward action is familiar from logarithmic conformal field theory [22, (17)–(22)]. The null-vector method and the scalar block ratio have precedents in [14] and [15, Appendix A.1].

In probabilistic Liouville theory, local Ward identities and four-point fusion asymptotics are obtained from collision estimates [23, Theorems 2.1–2.3][24, arXiv v1, Theorem 1.1]. Here we measure the error before attaching the exterior percolation configuration. This allows us to use a single local estimate for different surrounding clusters.

3 Main results

The finite part of a density pair. We write Φ for the density, E° for the scalar field obtained by closing a disk and ℓ for a reference length. Section 4 fixes their normalizations. In Theorem 5.1 we construct

$$L_\ell(z) = \lim_{r\downarrow 0} \left\{ r^{-25/24}\left[\Phi(z-r/2)\Phi(z+r/2) - r^{-5/24}\mathbf{1}\right] - \kappa \log(\ell/r) E^\circ(z) \right\}.$$

Here $\mathbf{1}$ is the identity insertion and κ is the coefficient of logarithmic mixing fixed in (5.81). At an observation circle of radius d, the error for $\ell = d$ is at most $Cd^{-5/4}(r/d)^\eta[1+\log(d/r)]$ for some $\eta > 0$. The limit is independent of the direction of the pair. In each chiral Ward identity the logarithmic term is $-\kappa E^\circ/2$ (Theorem 6.1). Proposition 6.3 identifies the same finite constant C_{LL} in the two-logarithm and logarithm–two-density correlations.

Further density collisions. Theorem 7.1 identifies the leading density term when $L_r(z)$ approaches a density at distance r. Theorem 8.1 estimates the two errors when a third density approaches a much closer pair. For two disjoint pairs an unusually small separation in one pair can magnify a geometric correction in the other. Keeping this correction in the subtraction recovers C_{LL} at all relative rates (Proposition 9.1). Section 10 determines the separated correlation of L_ℓ, Φ, Ψ from the inhomogeneous scalar null equation.

Mixed fusion on the observation circle. Let M_r and N_r denote the angular averages for E° and L_r against a density at distance r, after rescaling and subtracting the leading density as in (10.1) and (10.2). At fixed observation radius d, Theorem 18.1 gives

$$\begin{aligned} M_r &= r^{3/2}\Psi + O_{d,*}(r^{61/40}), \\ N_r &= r^{55/48}\Omega + \left(\frac{C_{LL}}{C_\circ} - \frac{18\kappa}{5}\right) r^{3/2}\Psi + O_{d,*}(r^{61/40}). \end{aligned}$$

The errors are uniform over all tests of absolute value at most one on the observation circle. The coefficient $C_\circ$ is fixed by the scalar three-point function (4.3). The quadrilateral coefficient Ω has scaling dimension $5/4$ and may vanish. The absence of its counterpart in M_r follows from the scalar null identity (Proposition 17.2).

Interior marks and boundary arcs. In Section 11 we follow the connections from interior marks to labelled open arcs after an exploration. Theorem 11.1 proves convergence of the weight of each partition, with density normalization at each root. The weights transform covariantly even in the presence of closed holes, and convergence is uniform on compact families of separated data. This uniformity lets us condition the mixed-fusion calculation on the explored exterior while preserving the labels of the clusters that still meet the source component.

4 Local fields and connectivity records

An observer on a circle must distinguish clusters that have joined inside the circle from clusters that may still join outside. We describe this observation first at lattice mesh a and normalize the two local fields, the density and the response to closing a disk. We then give the norm that measures the largest change visible on the circle. Finally we recall the exploration rule and the scalar null identity of Paper II, which we will use in Section 10.

4.1 Boundary records and normalization

On the triangular lattice $a\mathbb{T}$ of mesh a, each site is open or closed independently with probabilities $1/2$. A site is represented by its hexagonal cell. We use the inner-cell convention of [1, Section 4.1 and Appendix D]. For a disk $D = B_d(z)$ the frontier consists of its cells adjacent to the exterior. A *record* specifies their colors, the partition of the open frontier cells according to connection inside D, and for each block the parity of the number of marked sites in its cluster. A *row* is a signed measure on these records. Integrating over the inside colors leaves a row on which the exterior can act. We call the places where a connection meets the cut its ports. A frontier word lists the colors in boundary order. The two sides of an explored slit are separate boundary arcs, called its banks. Joining inner and outer blocks adds their parities modulo two. When a block disappears, summing its symmetric cluster sign assigns zero weight if its parity is odd and erases the block if its parity is even. This is the cluster-sign average of [3, (1.8)–(1.11)] and the marked completion of [2, Section 4.2, Lemma 4.1].

Give each open cluster an independent symmetric sign, and a closed site value zero. A density root is a marked site carrying this variable, multiplied by a fixed constant divided by π_a, the probability of an open path from a site to distance one [3, (2.1)]. We choose the constant by the plane two-point function in (4.2) below. An arm crosses an annulus from its inner to its outer boundary. We write $\alpha_k^a(s,t)$ for the probability of k disjoint alternating arms between scales $s < t$ for even k, and α_1^a for an open arm. For mixed sequences we specify the colors as needed. We use the arm events of [19, Section 2.1] and the separation and quasi-multiplicativity estimates of [20, Theorem 10, Proposition 17]. Quasi-multiplicativity compares the arm probability to the product of its probabilities on the two sides of an intermediate cut.

The bulk dimensions of the density and scalar are x and y. We denote the relative subleading fusion exponent of Paper II by p and the holomorphic weights by h_Φ, h_E. Thus

$$x = \frac{5}{48}, \qquad y = \frac{5}{4}, \qquad p = \frac{3}{2}, \qquad h_\Phi = \frac{x}{2}, \qquad h_E = \frac{y}{2}. \tag{4.1}$$

We denote by E° the scalar field of Paper II obtained by closing a disk. We recall its lattice definition after (4.3). We use $\mathbf{1}$ for the identity insertion and angle brackets for continuum correlations, with a subscript for boundary conditions. In the plane, the density normalization and the scalar–density three-point function are

$$\langle \Phi(u)\Phi(v)\rangle = |u-v|^{-2x}, \tag{4.2}$$

$$\langle E^\circ(z)\Phi(u)\Phi(v)\rangle = C_\circ \frac{|u-v|^{y-2x}}{|z-u|^y |z-v|^y}, \qquad C_\circ > 0. \tag{4.3}$$

Equation (4.2) is the chosen version of Camia's normalization. Equation (4.3) and the construction of E° are proved in [2, Theorems 4.3–4.5]. Its lattice regulator of radius r uses the cells entirely contained in $B_r(z)$, denoted by $B_r(z)^a$. It is the source $r^{-y}(1 - H^a_{B_r(z)})$,

where $H^a_{B_r(z)} = 2^{N_a(r,z)}\mathbf{1}_{\{B_r(z)^a \text{ closed}\}}$ and $N_a(r,z)$ counts the sites in $B_r(z)^a$. Thus its pairing is the ordinary expectation minus the expectation with that disk forced closed, divided by r^y. This is the normalization used in [2, Section 4.4, (4.2)–(4.4)].

The holomorphic stress T is the normalized second angular coefficient of a small closed ellipse [1, (4.8), Theorems 9.1 and 17.1]. We write $\bar{T}$ for its conjugate. Separated sources have disjoint closed neighborhoods. We write $O_{\mathcal{D}'}(r^b)$ when each compactly supported smooth test on the configurations of distinct source coordinates gives an error bounded by Cr^b, with the test seminorms and fixed separation included in C.

4.2 The norm at a fixed cut

We measure the largest change that any bounded observation on the cut can detect.

For a signed row ν on a finite record space this is its variation norm,

$$\|\nu\|_{\mathrm{var}} = \sup_{|f|\le 1} |\nu(f)|. \tag{4.4}$$

The test in (4.4) can depend on the mesh. Different annulus fillings and different merger histories may cancel if they give the same final record.

For separated fields, $\|\cdot\|_{d,*}$ denotes the upper variation norm obtained by first taking the mesh upper limit at fixed positive source regulators and then removing those regulators. Every difference uses one common mesh and one common outer cut before either operation. This is the convention of [1, Section 9.2] and [2, Section 4.2].

When a limiting row is constructed below, completion means the norm completion of these admissible same-mesh row families after quotienting by zero upper seminorm. An exterior completion is a Markov kernel or a deterministic push-forward, and therefore has norm at most one in (4.4).

The earlier source estimates give

$$\|\Phi\|_{d,*} \le Cd^{-x}, \qquad \|E^\circ\|_{d,*} \le Cd^{-y}, \qquad \|T\|_{d,*} + \|\bar{T}\|_{d,*} \le Cd^{-2}. \tag{4.5}$$

The scalar regulator is Cauchy with normalized rate $11/15$, and the stress regulator with rate $1/4$ [2, Theorems 4.3–4.4][1, Theorem 9.1 and Section 9.3]. Disjoint local rows can be glued before their regulators are removed. This constructs each finite separated stress word, that is, a product of stress insertions at distinct points.

Writing $\mathrm{av}_\phi = (2\pi)^{-1}\int_0^{2\pi} d\phi$ for the circular average, the leading fusion estimate and weak subleading expansion of Paper II read, for $0 < \gamma < x$,

$$\|r^y E^\circ(z)\Phi(z + re^{i\phi}) - C_\circ \Phi(z)\|_{d,*} \le Cd^{-x}(r/d)^\gamma, \tag{4.6}$$

$$\mathrm{av}_\phi\, r^y E^\circ(z)\Phi(z + re^{i\phi}) = C_\circ\Phi(z) + r^p\Psi(z) + 25C_\circ r^2\partial_z\partial_{\bar{z}}\Phi(z) + O_{\mathcal{D}'}(r^{2+\gamma}). \tag{4.7}$$

The first bound is uniform in ϕ, whereas the second is a source-distribution statement against separated field words [2, Theorems 4.5 and 4.10, Section 12]. The field Ψ has weights $(77/96, 77/96)$, and its finite separated products are constructed in [2, Theorem 4.11 and Sections 13.6–13.7]. With the positive block constant $\mathfrak{k}$ of Paper II, the two-point normalization takes the form [2, (4.20) and Section 14.2]

$$\langle\Psi(z)\Psi(w)\rangle = -\mathfrak{k}^2 C_\circ^2 |z-w|^{-77/24}, \qquad \mathfrak{k} = \frac{5}{12}\left[\frac{\Gamma(1/4)}{\Gamma(3/4)}\right]^2, \qquad z \ne w. \tag{4.8}$$

4.3 Exploration and the scalar null identity

A finite-tip domain is a simply connected domain with a cyclically ordered even number of boundary prime ends, called tips, and alternating open and closed boundary arcs. A wired open arc is one connected open boundary class. A quadrilateral, or quad, has four tips. The interfaces pair the tips without crossing, and we call this pairing their link pattern. We use the separate slit banks, lattice approximations and disk coordinates of [1, Sections 7.1–7.2, 8.1–8.4] and [2, Sections 4.7 and 7.1]. A protected disk is a disk which the exploration leaves unqueried. After a transcript (the list of queries, answers and resulting boundary labels) is fixed, the remaining colors have their product law. The saved labels determine a contraction from the remaining partition to the original record [1, Lemma 8.1 and Theorem 8.4].

The local descendant $L_{-2}E^{\circ}(z)$ is defined by inserting $(2\pi i)^{-1}\oint T(w)\,dw/(w-z)$ on a positively oriented circle enclosing only z. The conjugate contour defines $\bar{L}_{-2}$. Paper II proves

$$(L_{-2}-\tfrac{2}{3}\partial_z^2)E^{\circ}(z)=(\bar{L}_{-2}-\tfrac{2}{3}\partial_{\bar{z}}^2)E^{\circ}(z)=0 \tag{4.9}$$

as source distributions against fixed separated density, scalar and stress words [2, Theorems 4.7 and 9.1]. The coordinatewise scalar identity for four and six boundary tips is [2, Propositions 8.2–8.3].

5 The finite part of the density pair

As we enlarge a disk around the two marks, we ask at which scale their clusters first connect (Figure 1). Before that scale the boundary sees two distinct marked clusters. After it, their common cluster carries even parity. Sections 5.1–5.2 describe how these two kinds of records pass through an annulus. We then use E° and distant density marks to normalize the leading terms. In Sections 5.5–5.7 we sum over the annulus of first connection and compare two initial separations at the same observation circle. The sum produces the logarithm. Its coefficient is identified in Section 5.8.

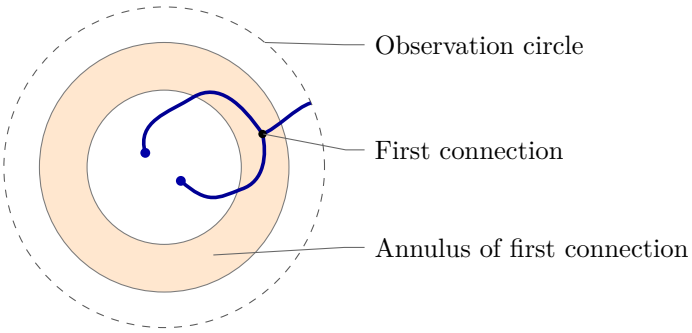

Figure 1: The two inner dots mark the density sites. The blue paths are open. Inside the smaller circle the two marks belong to different clusters. Filling the shaded annulus joins them. If the two clusters remain distinct all the way to the observation circle, their contribution is counted separately.

For a fixed center z, direction θ, radius r, and cut $D=B_d(z)$, put $z_{\pm}=z\pm re^{i\theta}/2$ and let $z_{\pm}^a$ be their nearest lattice sites, with a fixed tie rule. Write $p_a=\mathbb{P}_a(z_-^a\leftrightarrow z_+^a)$ for their full-plane connection probability. A neutral record has even parity on every block. In the augmented record we also retain the possible pair of odd blocks. Let $\mathsf{M}_r^{a,D}$ be the following positive row, divided by p_a. A closed root gives zero weight. If the roots have joined, their record is neutral. If both reach the cut separately, their two blocks are odd. A configuration

in which one of those blocks disappears contributes zero. Write ι for embedding neutral rows in the augmented space, μ_d^a for the unforced neutral row, and $\nu_{B_r}^{a,D}$ for the row obtained with all cells of the smaller disk forced closed. Define

$$\mathsf{Q}_r^{a,D} = r^{-y}(\mathsf{M}_r^{a,D} - \iota\mu_d^a), \tag{5.1}$$

$$R_r^{a,D} = r^{-y}(\mu_d^a - \nu_{B_r}^{a,D}), \tag{5.2}$$

$$\mathsf{D}_{r,b}^{a,D} = \mathsf{Q}_{br}^{a,D} - \mathsf{Q}_r^{a,D} - \kappa\log(1/b)\,\iota R_r^{a,D}, \qquad 1/2 \le b \le 1. \tag{5.3}$$

Let Π_2 project an augmented row onto its two-odd-block summand. All differences in this section are at the same mesh and cut. The normalization by p_a has the continuum density-pair normalization after the mesh limit [3, Theorem 1.5]. Here κ denotes the coefficient of the logarithmic subtraction in the theorem below.

For the circular source, [2, Theorem 4.3] gives

$$\sup_{0<s\le\epsilon} \limsup_{a\downarrow 0} \|R_s^{a,D} - R_\epsilon^{a,D}\|_{\mathrm{var}} \le Cd^{-y}(\epsilon/d)^{11/15}. \tag{5.4}$$

We will use its three-point normalization (4.3) to identify the coefficient of the logarithm.

Theorem 5.1 (The finite part of the density pair)**.** *Take $\kappa = C_{\log}/C_\circ > 0$, where $C_{\log}$ is the four-density logarithmic coefficient of [17, Theorem 1.1, (1.9)] and $C_\circ$ is the scalar three-point coefficient in (4.3). Section 5.8 identifies the coefficient produced by the annular sum with this ratio in (5.81). Let δ_C, δ_E be the positive exponents for propagation of two marked blocks and of a neutral difference in Theorem 5.6 below. With $\eta = \frac{1}{4}\min\{\delta_C, \delta_E, 11/15\} > 0$, we have*

$$\sup_{1/2\le b\le 1} \limsup_{a\downarrow 0} \|\mathsf{D}_{r,b}^{a,D}\|_{\mathrm{var}} \le Cd^{-y}(r/d)^{\eta}[1+\log(d/r)]. \tag{5.5}$$

The surviving two-odd-block endpoint separately satisfies

$$\sup_{1/2\le b\le 1} \limsup_{a\downarrow 0} \|(br)^{-y}\Pi_2\mathsf{M}_{br}^{a,D} - r^{-y}\Pi_2\mathsf{M}_r^{a,D}\|_{\mathrm{var}} \le Cd^{-y}(r/d)^{\delta_C}. \tag{5.6}$$

For every fixed $\ell > 0$, the mesh-first collision therefore defines

$$L_\ell(z) = \lim_{r\downarrow 0}\left\{r^{-25/24}[\Phi(z - re^{i\theta}/2)\Phi(z + re^{i\theta}/2) - r^{-5/24}\mathbf{1}] - \kappa\log(\ell/r)E^\circ(z)\right\}. \tag{5.7}$$

It is independent of θ and exists jointly for every fixed finite separated word of densities, scalars, stresses, and such logarithmic fields. With Q_r denoting the first term in braces,

$$\|Q_r - \kappa\log(d/r)E^\circ - L_d\|_{d,*} \le Cd^{-y}(r/d)^{\eta}[1+\log(d/r)], \tag{5.8}$$

$$\|L_\ell\|_{d,*} \le Cd^{-y}(1 + |\log(\ell/d)|). \tag{5.9}$$

The bounds are uniform over bounded tests of the entire outgoing record at each mesh.

For the proof, define $Z_r^{a,D} = \mathsf{Q}_r^{a,D} - \kappa\log(\ell/r)\iota R_r^{a,D}$. Subtracting the expressions at the two radii, we obtain

$$Z_{br} - Z_r = \mathsf{D}_{r,b} - \kappa\log(\ell/(br))\iota(R_{br} - R_r). \tag{5.10}$$

By (5.4), the second term has a summable bound $Cd^{-y}(r/d)^{11/15}[1+\log(d/r)]$ for fixed ℓ/d. It remains to control the centered first-merger row.

5.1 Marked clusters in an annulus

We call a state with two odd blocks *charged*. A collar is the annulus between two nested cuts. Its through-components are its open clusters adjacent to the inner cut that also meet the outer frontier. A state is realizable if it can be obtained by an inner coloring with the designated marks. We write $\|\cdot\|_1 = \|\cdot\|_{\mathrm{var}}$ on these finite state spaces. Operator norms are induced by variation, and $h \otimes \nu$ sends a row v to $v(h)\nu$. For the linear algebra only, allow also formal joined neutral partitions when joining two blocks would not be planar. No extra randomness or probability weight is assigned to that formal join. Let V_s^0 and V_s^2 denote signed neutral rows and signed rows on realizable charged states, respectively, and let $V_s^{0,*} = \{v \in V_s^0 : v\mathbf{1} = 0\}$ be the zero-total-mass neutral rows in this auxiliary space. For deterministic nested cuts $s < t$, independent filling acts on the two kinds of records by the block kernel

$$\mathcal{K}_{s,t}^a = \begin{pmatrix} P_{s,t}^a & 0 \\ B_{s,t}^a & Q_{s,t}^a \end{pmatrix}. \tag{5.11}$$

The neutral kernel P also acts on a formal joined partition. For each filling we take the equivalence relation generated by the incoming blocks and the open collar connections, then restrict it to the outgoing frontier. This operation is defined for every incoming partition, and averaging it over the collar colors makes P stochastic. The kernel Q records separate survival of both odd blocks, and B records their merger. Hence $B\mathbf{1} + Q\mathbf{1} \le 1$.

Let J_s send a charged state to the neutral record with its two designated blocks joined minus the neutral record with their marks erased but their blocks separate. Then

$$\|J_s\| \le 2, \qquad J_s P_{s,t} = Q_{s,t} J_t. \tag{5.12}$$

For each fixed collar filling, a merger in the collar makes both neutral outputs equal. Disappearance of one odd block does the same. If both survive distinctly, their difference is precisely the join-minus-separate output at t. This proves the identity before averaging. The map J_s can have a kernel when further boundary blocks are present. The ensuing bounds are valid on the auxiliary neutral space and hence on the rows from lattice colorings.

Let $w_s(c)$ be the probability that the two odd blocks eventually merge in a fresh exterior. Then

$$\mu_s P_{s,t} = \mu_t, \qquad w_s = B_{s,t}\mathbf{1} + Q_{s,t} w_t, \qquad 0 \le w_s \le 1. \tag{5.13}$$

Define the centered conversion

$$\widehat{B}_{s,t} = B_{s,t} - (B_{s,t}\mathbf{1}) \otimes \mu_t. \tag{5.14}$$

Its output has mass zero, and, rowwise,

$$\|\widehat{B}_{s,t}(c,\cdot)\|_{\mathrm{var}} \le 2B_{s,t}\mathbf{1}(c), \qquad \|\widehat{B}_{s,t}\| \le 2. \tag{5.15}$$

Block multiplication and (5.13) give

$$\widehat{B}_{s,u} = \widehat{B}_{s,t} P_{t,u} + Q_{s,t} \widehat{B}_{t,u}. \tag{5.16}$$

5.1.1 Clusters crossing a collar

For a single collar, denote its cuts by D_i, D_j, with radii $R_i < R_j$. For one fixed collar configuration ω, delete the incoming region and examine the open components of the collar alone. Let $k(\omega)$ be the number of its components that meet both the incoming and outgoing frontiers. Boundary sites and buffers can be allocated so these components depend only on the sampled collar variables. The argument applies also to the formal neutral partitions just defined.

Lemma 5.2 (At most two through-components)**.** *Fix the colors in the collar.*

(i) If $k \le 1$, the outgoing neutral state is independent of every incoming neutral state, and no charged state survives.

(ii) If $k = 2$, write H_1, H_2 for the two through-components. Every outgoing neutral state is either the collar's separate outer partition n_{sep} or the partition n_{join} obtained by joining the two outer blocks of H_1, H_2. Every surviving charged output is the same state c_ω, with those two blocks odd and all other blocks even.

(iii) Let J denote join-minus-separate. If $\xi J_i = 0$, then $\xi Q_\omega = 0$ whenever $k \le 2$.

Proof. An incoming identification can change outgoing connectivity only by joining distinct collar components that both reach the outgoing frontier and both touch the incoming frontier. There are no such pairs if $k \le 1$. Two odd components cannot then reach the outgoing frontier separately.

When $k = 2$, the collar fixes every outgoing component that misses the incoming frontier, so an incoming connection can change the output only by joining H_1 to H_2. For a charged state to survive, its two odd blocks must reach these through-components separately. Any further identification through an even block would join them and destroy survival. Thus every surviving state has the same charged output c_ω.

Thus $\xi Q_\omega = t c_\omega$ for some scalar t when $k = 2$. Applying the intertwining identity to this row, we find

$$(\xi Q_\omega) J_j = (\xi J_i) P_\omega = 0.$$

Since $c_\omega J_j = n_{\mathrm{join}} - n_{\mathrm{sep}} \neq 0$, one has $t = 0$. The case $k \le 1$ follows from the first assertion. □

5.1.2 Transmission of boundary connections

Put

$$\beta_2^a(i,j) = \mathbb{P}_a[k(\omega) \ge 2], \qquad \beta_3^a(i,j) = \mathbb{P}_a[k(\omega) \ge 3].$$

For concentric deterministic disk collars, two distinct open components crossing the annulus force four alternating arms, and three force six. One may use fixed inner and outer buffers to avoid conventions on the cut layers. Hence, for universal fixed $c_0 > 1$ and R_j/R_i sufficiently large,

$$\beta_2^a(i,j) \le C\alpha_4^a(c_0 R_i, R_j/c_0), \qquad \beta_3^a(i,j) \le C\alpha_6^a(c_0 R_i, R_j/c_0). \tag{5.17}$$

The planar implication uses closed radial separators between consecutive distinct open crossing clusters. It is the cluster interpretation of alternating even-arm events recorded in [9, Theorem 4 and the paragraph following it]. We count the components in the collar before any boundary identifications.

Proposition 5.3 (Unnormalized propagation)**.** *On the full finite state spaces,*

$$\|Q_{i,j}\|_{1\to 1} \le \beta_2^a(i,j), \tag{5.18}$$

$$\|\nu P_{i,j}\|_1 \le \beta_2^a(i,j)\|\nu\|_1, \qquad \nu \in V_i^{0,*}, \tag{5.19}$$

$$\sup_x \|P_{i,j}(x,\cdot) - \mu_j\|_1 \le 2\beta_2^a(i,j). \tag{5.20}$$

Proof. Couple all incoming states with the same unconditioned collar. Charged survival is impossible on $k \le 1$, proving (5.18). On that same event every neutral input produces the same output, so a zero-mass signed combination vanishes. On $k \ge 2$, stochasticity is a

variation contraction. Integrating proves (5.19). Couple input x and an independent input of law μ_i with the same collar. Their outputs agree on $k \le 1$, and the second output has law μ_j. This proves (5.20). □

Write $y = 5/4$. The continuum four-arm bound from [17, Corollary 2.4], with scale invariance and monotonic interpolation, implies

$$\limsup_{a\downarrow 0} \beta_2^a(i,j) \le C(R_i/R_j)^y. \tag{5.21}$$

Short collars can be absorbed into the constant. Numerical limsups of finite-mesh operator norms therefore satisfy the same bound.

5.1.3 Six arms and the kernel of the joining map

Theorem 5.4 (The intertwiner kernel propagates at the six-arm scale)**.** *For every finite-mesh signed charged row ξ satisfying $\xi J_i = 0$,*

$$\|\xi Q_{i,j}\|_1 \le \beta_3^a(i,j)\|\xi\|_1. \tag{5.22}$$

Proof. Lemma 5.2(iii) makes the integrand zero whenever $k \le 2$. On the remaining configurations Q_ω is substochastic and hence a variation contraction. Integrate the resulting bound. □

The polychromatic six-arm exponent is $(6^2-1)/12 = 35/12$ [9, Theorem 4, including its continuum discussion]. We use only its consequence with an arbitrarily small loss. For every $\varepsilon > 0$,

$$\limsup_{a\downarrow 0} \beta_3^a(i,j) \le C_\varepsilon(R_i/R_j)^{35/12-\varepsilon}.$$

Combining this with (5.22) gives

$$\limsup_{a\downarrow 0} \sup_{\substack{\xi J_i = 0 \\ \|\xi\|_1 \le 1}} (R_j/R_i)^{5/4}\|\xi Q_{i,j}\|_1 \le C_\varepsilon(R_i/R_j)^{5/3-\varepsilon}. \tag{5.23}$$

For $R_j/R_i = 2^b$, the right side is summable over b whenever $0 < \varepsilon < 5/3$.

5.1.4 A representation by two marked clusters

The same geometry controls the range of $\widehat{B}$. A long collar can carry a component outside $\operatorname{im} J$ only on the six-arm event.

Theorem 5.5 (Two crossing clusters and the six-arm remainder)**.** *There are linear maps*

$$L_{i,j} : V_i^{0,*} \longrightarrow V_j^2, \qquad E_{i,j} : V_i^{0,*} \longrightarrow V_j^{0,*}$$

such that

$$\nu P_{i,j} = (\nu L_{i,j})J_j + \nu E_{i,j}, \quad \|L_{i,j}\| \le \tfrac{1}{2}\beta_2^a(i,j), \quad \|E_{i,j}\| \le \beta_3^a(i,j). \tag{5.24}$$

In particular, after any later collar,

$$\widehat{B}_{i,i+1}P_{i+1,j} = V_{i,j}J_j + \mathcal{E}_{i,j}, \tag{5.25}$$

$$V_{i,j} := \widehat{B}_{i,i+1}L_{i+1,j}, \qquad \|V_{i,j}\| \le \beta_2^a(i+1,j),$$

$$\mathcal{E}_{i,j} := \widehat{B}_{i,i+1}E_{i+1,j}, \qquad \|\mathcal{E}_{i,j}\| \le 2\beta_3^a(i+1,j). \tag{5.26}$$

Both maps use the unnormalized collar law.

Proof. Fix a collar configuration with $k = 2$ and use the states in Lemma 5.2. For each incoming neutral state x, let $a_\omega(x) \in \{0, 1\}$ indicate whether its output is n_{join} instead of n_{sep}. Since $\nu\mathbf{1} = 0$,

$$\nu P_\omega = \nu(a_\omega)(n_{\mathrm{join}} - n_{\mathrm{sep}}) = \big(\nu(a_\omega)c_\omega\big)J_j.$$

Moreover $|\nu(a_\omega)| \le \|\nu\|_1/2$. Define

$$\nu L_{i,j} = \mathbb{E}_a[\mathbf{1}_{\{k=2\}}\nu(a_\omega)c_\omega], \qquad \nu E_{i,j} = \mathbb{E}_a[\mathbf{1}_{\{k\ge 3\}}\nu P_\omega].$$

On $k \le 1$ the output is zero. This proves the identity and the two bounds. The range of E has zero mass because each neutral P_ω is stochastic. Compose with $\widehat{B}$, whose range has zero mass and whose norm is at most two by (5.15), to obtain the remaining statements. □

5.2 The leading terms of the two annular kernels

Set $\alpha_a(r) = \alpha_4^a(a, r)$ and $\lambda^a(s, t) = \alpha_a(t)/\alpha_a(s)$. At an intermediate cut the two factors telescope. Quasi-multiplicativity and the arm-ratio limit give

$$\lambda^a(s, t) \asymp \alpha_4^a(s, t), \qquad \lim_{a\downarrow 0} \lambda^a(s, t) = (s/t)^y \tag{5.27}$$

for fixed positive scales [19, Proposition 4.9 and (4.28)]. We sometimes write $\lambda^a_{s,t}$ for the same quantity.

Theorem 5.6 (Leading terms of the charged and neutral annular kernels)**.** *There are uniformly bounded columns h^a_s, ℓ^a_s and rows ν^a_s, e^a_s such that $\nu^a_s \ge 0$, $e^a_s = \nu^a_s J_s$, $e^a_s\mathbf{1} = 0$, and, for positive δ_C, δ_E,*

$$\|Q^a_{s,t}/\lambda^a(s, t) - h^a_s \otimes \nu^a_t\|_{1\to 1} \le C(s/t)^{\delta_C}, \tag{5.28}$$

$$\|P^a_{s,t}|_{V^{0,*}_s}/\lambda^a(s, t) - \ell^a_s \otimes e^a_t\|_{1\to 1} \le C(s/t)^{\delta_E}. \tag{5.29}$$

The first estimate is on realizable charged inputs and their signed span. Both estimates retain the entire outgoing partition, including even blocks. The exact normalizations and propagation rules are

$$\nu_s h_s = 1, \qquad e_s\ell_s = 1, \qquad J_s\ell_s = h_s, \tag{5.30}$$

$$\nu_s Q_{s,t} = \lambda(s, t)\nu_t, \qquad Q_{s,t}h_t = \lambda(s, t)h_s, \tag{5.31}$$

$$e_s P_{s,t} = \lambda(s, t)e_t, \qquad P_{s,t}\ell_t = \lambda(s, t)\ell_s \quad \text{on } V^{0,*}_s. \tag{5.32}$$

We first take $D_r = [-r, r]^2$ centered at the source. We return to circular cuts at the end of this subsection. Allocate every site to one region and use a buffered cut layer. We use the Russo–Seymour–Welsh crossing bounds (RSW), positive association of increasing events under the product law (FKG), arm separation and extension, and the constructive four-face coupling of [19, Proposition 3.1]. That coupling retains the internal crossing bit and decides success before filling the final interior. The needed relative extra-arm estimate is

$$\alpha^a_{5+}(u, v) \le C(u/v)^{d_5}\alpha^a_4(u, v), \qquad d_5 > 0; \tag{5.33}$$

here 5+ means five or more disjoint arms of the corresponding mixed color type. A positive relative six-arm exponent ζ is also available. These consequences of separation and the arm exponents are used with a small loss, as shown in [9, Theorem 4] and [20, Theorem 10].

5.2.1 Comparison at the inner boundary

A four-face domain is bounded by four alternating monochromatic lattice paths, as in [19, Section 3, pp. 29–30]. The two open paths are its open faces. A row supported on a rare configuration needs an error proportional to the probability of that configuration. In a four-face domain containing D_L, let $W \geq 0$ depend only on $D_{L/4}$ and write $p = \mathbb{E}_a W$. For the open-face crossing U, compare the two outside events U^+ and U^- obtained by forcing the core entirely open and entirely closed. If C is an open circuit in the buffered annulus $D_{3L/4} \setminus D_{L/2}$, then

$$U^+ \cap C \subset U^-.$$

An open connection using the forced core can be rerouted along C. Since the two events on the left are increasing functions of the outside variables,

$$\mathbb{P}(U^-) \geq \mathbb{P}(U^+ \cap C) \geq c_{\mathrm{scr}} \mathbb{P}(U^+).$$

For every deterministic filling of the core, its conditional crossing probability lies between these two extremes. Integration against W proves

$$c_{\mathrm{scr}} p \leq \mathbb{E}(W \mid U = \tau) \leq c_{\mathrm{scr}}^{-1} p, \qquad \tau \in \{0, 1\}; \tag{5.34}$$

for $\tau = 0$ use the dual closed crossing and a closed circuit. The argument applies to arbitrary nonnegative W. The screening annulus lies strictly inside the unfilled domain.

We apply [19, Proposition 3.1] with inner radius L and outer radius T. The event $\mathcal{A}_\Theta(L, T)$ requires four alternating arms from the indicated faces of Θ to the inner square. It is determined outside the open square D_L. The additional bit U_Θ says whether the two open faces connect inside Θ. Two comparisons with the reference square in that proposition couple two laws with the same bit. In the sector $U_\Theta = 0$, both comparisons reverse the colors relative to the reference, so the two resulting face colors agree.

To bound the error for a rare input, we first couple the outer configurations up to their induced faces at L, using the coupling of the induced-face histories in the proof of [19, Proposition 3.1]. On the event of agreement we fill their common remaining domain identically, conditional on the common crossing bit. For an unmatched history we may additionally reveal everything outside D_L before sampling its interior. For each exterior that can occur, the arm event is then decided. The only remaining condition on the independent colors in D_L is its specified value of U_Θ. The circuit proof of (5.34) applies for each fixed exterior because the two endpoints lie outside the screening circuit, and every path through the core can be rerouted on the circuit. For a closed crossing we interchange the two colors. This bounds the conditional mean of W by Cp even when the unmatched boundary has more than four faces. Equivalently one may couple the outer configurations first by their induced-face data and resample conditional on those data. In that coupling the choice of success reveals no core color.

If $|f|, |f'| \leq 1$ and the two tests agree on a common interior with the same face labels, their matched contributions cancel. The two unmatched contributions are bounded by Cp times the unmatched probability. Consequently

$$\left|\mathbb{E}_\Theta[Wf] - \mathbb{E}_{\Theta'}[W'f']\right| \leq Cp(L/T)^\eta \tag{5.35}$$

for some $\eta > 0$. Here $\mathbb{E}_\Theta$ and $\mathbb{E}_{\Theta'}$ denote expectations for the two laws conditioned on the four arms and their common crossing value, and W' is the same function of the second core.

For a realizable charged state c at radius r, set $L = 16r$. Let W_c indicate its underlying unmarked state in a fresh product filling of D_r, and let $p_c = \mathbb{P}(W_c) > 0$. Choose one fixed

frontier representative in each designated block. With outer faces Θ, put

$$E_\Theta = \mathcal{A}_\Theta(L,T) \cap \{U_\Theta = 0\}, \qquad z_\Theta = \mathbb{P}_a(E_\Theta).$$

Let $k_a(c,\Theta)$ be the probability, with input c and independent exterior colors, of reaching different open faces distinctly. On distinct attachment, planar duality supplies a closed crossing between the two closed faces. It separates the two open paths from the designated representatives, so it intersects every connected set containing both representatives, in particular D_L. Its two end segments and the two open paths give the required alternating arms. Thus

$$k_a(c,\Theta) = \frac{z_\Theta}{p_c}\mathbb{E}[W_c f_c \mid E_\Theta]. \tag{5.36}$$

Here f_c is the indicator of distinct attachment of the two designated representatives. Its value is determined by the common interior and induced faces. The two designated roots are exchangeable for this test, which counts both face assignments. Applying (5.35) with mean p_c, *then* dividing by p_c, gives a uniform Cauchy estimate for $k_a(c,\Theta)/z_\Theta$. Comparing separated reference faces at radii tending to infinity defines a bounded $H_r^a(c)$ and yields

$$|k_a(c,\Theta) - H_r^a(c) z_\Theta| \le C z_\Theta (r/T)^\eta, \qquad 0 \le H_r^a(c) \le C. \tag{5.37}$$

To see the Cauchy assertion, compare the two conditional expectations in (5.36) for reference circuits at T and $T' \ge T$. Equation (5.35) bounds their difference, after division by p_c, by $C(r/T)^\eta$. The same comparison with a reference circuit at $T' \to \infty$ gives (5.37) for every four-face boundary at T.

5.2.2 Exploration of the outer partition

Choose $r \ll u \ll v \ll R$, with fixed buffers. We reveal the interface pieces in a fixed order.

Reveal the product configuration between D_v and D_R, including the cut layer. From every interface edge crossing the inner boundary of this revealed region, trace the interface piece in the annulus between u and v, stopping at its first visit to the inner cut or to the outer cut. If it encounters previously queried hexagons, follow the determined interface without resampling until the piece is completed or reaches new unqueried sites. The trace stops at the inner boundary, leaving the protected square unqueried. We order the finitely many starting edges and trace each piece once.

Success requires a revealed four-face circuit Θ_H enclosing the protected square, with its interior $D_{\Theta_H} \subset D_v$ unqueried. Equivalently, the circuit separates the inner square from the outer cut with exactly two open boundary arcs, the remaining two arcs closed. Use the boundary of the unqueried central component, with the usual simple-face extraction and the lattice buffer. Once this is certified, fill every other unqueried component outside D_{Θ_H}, retaining the whole outgoing partition.

The four-face construction of [19, Section 3, pp. 29–30 and proof of Proposition 3.6] gives this separator on $\mathcal{A}_4(u,v) \setminus \mathcal{A}_{5+}(u,v)$. On this event there are four crossing interface pieces, and consecutive pieces have neighboring hexagons in common: a strip separating their adjacent hexagons would carry a fifth disjoint arm. Their revealed neighbouring hexagons surround the protected inner square and its central complementary component has four alternating faces. Additional returning interface pieces cannot enter that central component because its monochromatic face arcs cannot be crossed by a percolation interface, and its four colour-changing entrances belong to the four crossing pieces. An additional piece entering through the protected inner boundary would be an additional crossing piece. Thus tracing the other outer-started pieces does not reveal the unexplored interior on this event. Fixed one-layer discrepancies are covered by the protected-square buffer.

The conditional filling law. Every next query and every stopping decision depends on the observed answers. For each history H, every filling of the remaining unqueried region gives the same history. Under a Bernoulli product law, the conditional law of that remaining region is therefore the original product law with the observed boundary colours. The absence of an extra arm guarantees success of the search. The observed history alone specifies the conditional filling law.

Eligible histories. The two open faces must each be attached through the now filled complement to the outer frontier, and the corresponding two outer blocks must be distinct. Keep a history in the charged measure only when both conditions hold. If the faces are joined outside, no charged input can survive through them. If one face fails to reach the outer frontier, there is likewise no charged output, even though $k_a(c, \Theta_H)$ may be positive.

For an eligible history, write Z_H for the full outer partition obtained through its two separate open faces, with both corresponding blocks odd and every other block even. This is independent of the unfilled interior *on the event that the two incoming odd blocks attach distinctly*. Every open access to that interior uses one of the two open faces. The faces themselves are connected boundary arcs. Hence distinct attachment cannot change any remaining outgoing even block or the partition of the filled complement.

Proposition 5.7 (Decomposition at a separating four-face domain)**.** *Let Λ be the restriction of the history law to certified, eligible histories, so its total mass is the probability that both conditions hold. Then*

$$Q^a_{r,R}(c, \cdot) = \int k_a(c, \Theta_H)\delta_{Z_H}(\cdot)\, d\Lambda(H) + \mathcal{D}^a_{r,R}(c, \cdot), \tag{5.38}$$

where $\mathcal{D}$ is positive and

$$\sup_c \|\mathcal{D}^a_{r,R}(c, \cdot)\|_1 \le C\alpha^a_4(r, R)(u/v)^{d_5}. \tag{5.39}$$

The constants are independent of the number of outgoing even blocks and of the realization probability of the incoming state.

Proof. Disintegrate the product collar law over the queried histories. Since the exploration stops before querying the interior, its conditional law is the product law there. On an eligible history each successful attachment produces Z_H, so the conditional charged output is the attachment probability times δ_{Z_H}. On an ineligible certified history there is no charged output. All remaining charged histories form the positive remainder, proving (5.38).

If charged survival occurs on a geometrically failed history, there are two distinct open crossing components and hence four alternating arms across the inner and outer buffered bands. If the middle band had four arms and no extra arm, the preceding certificate construction would succeed. Its exterior would be eligible because survival occurs. Therefore failure forces the extra-arm event there. Because the buffered bands are disjoint, we can bound their joint probability by

$$C\alpha^a_4(r, u)\alpha^a_{5+}(u, v)\alpha^a_4(v, R).$$

Use (5.33) and quasi-multiplicativity to get (5.39). □

Set $N^a_{r,R} = \int z_{\Theta_H}\delta_{Z_H}\, d\Lambda(H)$. Its mass is at most $C\alpha^a_4(r, R)$. To verify this, take one realizable input with separated macroscopic open arcs. By arm extension the reference state satisfies $H^a_r(c_*) \ge c > 0$. For r/u small, (5.37) makes its good attachment probability at

least $(c/2)z_{\Theta_H}$ on every history. The four-arm bound for the total charged survival of c_* then bounds N. The finite range of shorter ratios is absorbed in the constant.

Apply (5.37) in (5.38). For logarithmically equally spaced r, u, v, R, reducing the exponent slightly to accommodate fixed buffers gives

$$Q^a_{r,R} = H^a_r \otimes N^a_{r,R} + \mathcal{R}^a_{r,R}, \qquad \|\mathcal{R}^a_{r,R}\|_{1\to 1} \le C\alpha^a_4(r,R)(r/R)^\delta, \tag{5.40}$$

for some $\delta > 0$.

5.2.3 Normalization by a four-arm source

Fix a microscopic seed σ_a at radius $r_* = O(a)$, with two separated open branches and two closed separators and propagate it to the input cut by setting

$$m^a_r = \sigma_a Q^a_{r_*,r}. \tag{5.41}$$

The measure m^a_r carries the mass of seed configurations surviving to radius r. Extending the four separated arms to the outer scale, we obtain

$$c\alpha_a(r) \le \|m^a_r\|_1 \le C\alpha_a(r). \tag{5.42}$$

Set $H^a_{*,r} = m^a_r(H^a_r)$.

Apply the row-uniform factorization (5.40) to m^a_r. Positivity and (5.42) immediately give

$$\left\|\sigma_a Q^a_{r_*,R} - H^a_{*,r} N^a_{r,R}\right\|_1 \le C\alpha_a(r)\alpha^a_4(r,R)(r/R)^\delta. \tag{5.43}$$

The bounds $H^a_{*,r} \asymp \alpha_a(r)$ can also be checked without a new limit interchange. The upper bound follows from boundedness of H^a_r and (5.42). For the lower bound, take R/r sufficiently large in (5.43). The left source has total mass at least $c\alpha_a(R)$, whereas the error is at most a small fixed multiple of $\alpha_a(R)$ by quasi-multiplicativity. Since $\|N^a_{r,R}\|_1 \le C\alpha^a_4(r,R)$, it follows that

$$H^a_{*,r} \ge c' \frac{\alpha_a(R)}{\alpha^a_4(r,R)} \ge c''\alpha_a(r).$$

Define

$$\nu^a_r = \frac{m^a_r}{\alpha_a(r)}, \qquad h^a_r = \frac{\alpha_a(r) H^a_r}{H^a_{*,r}}. \tag{5.44}$$

The masses $\|\nu^a_r\|_1$ are bounded above and below, h^a_r is uniformly bounded and nonnegative, and $\nu^a_r(h^a_r) = 1$.

From (5.43),

$$N^a_{r,R} = \frac{\alpha_a(R)}{H^a_{*,r}} \nu^a_R + O_{\mathrm{var}}\left(\alpha^a_4(r,R)(r/R)^\delta\right).$$

Insert this in (5.40) and divide by $\lambda^a_{r,R} \asymp \alpha^a_4(r,R)$. This proves

$$\left\| \frac{Q^a_{r,R}}{\lambda^a_{r,R}} - h^a_r \otimes \nu^a_R \right\|_{1\to 1} \le C(r/R)^\delta. \tag{5.45}$$

Take $\delta_C = \delta > 0$.

Exact compatibility. By (5.41) we have $\nu_r^a Q_{r,R}^a = \lambda_{r,R}^a \nu_R^a$. For the column identity use the source-ratio expression, where Θ_S is a regular separated reference face circuit at radius S,

$$h_r^a(c) = \alpha_a(r) \lim_{S\to\infty} \frac{k_a(c,\Theta_S)}{k_a(\sigma_a,\Theta_S)}.$$

At fixed a, r, R, the state set at R is finite, and distinct attachment to the remote reference forces charged survival to R. Hence $k_a(c,\Theta_S) = Q_{r,R}^a k_a(\cdot,\Theta_S)(c)$ and the finite sum passes through the limit. Thus

$$Q_{r,R}^a h_R^a = \lambda_{r,R}^a h_r^a. \tag{5.46}$$

Together with $\nu_R^a(h_R^a) = 1$, the two exact identities prove composition of the rank-one family.

5.2.4 The neutral transition kernel

Suppress the mesh superscript. Set $e_r = \nu_r J_r$. The seed can be chosen so that its artificial join is realized by changing the seed coloring and has no third open block to cross. Consequently this reference contrast propagates to realizable neutral rows, although the auxiliary algebra allowed more general formal joins. The intertwiner gives

$$e_r P_{r,R} = \lambda_{r,R} e_R, \qquad \|e_R\|_1 \le C.$$

A fixed left–right crossing test $0 \le \varphi_R \le 1$ satisfies $e_R(\varphi_R) \ge c > 0$. To see this, extend the seed's two open components to the left and right arcs, and its closed separator across the other two arcs, so that adding the artificial join changes the crossing from zero to one. Separation and fixed-buffer RSW give event mass $c\alpha_a(R)$ before the normalization in ν_R.

Theorem 5.5 gives, on zero-mass neutral rows,

$$P_{r,s} = L_{r,s} J_s + E_{r,s}, \qquad \|L_{r,s}\| \le C\lambda_{r,s}, \quad \|E_{r,s}\| \le C\lambda_{r,s}(r/s)^\zeta. \tag{5.47}$$

By Lemma 5.2, with at most one open through-component the output of a zero-mass row is zero. With exactly two through-components its output is a scalar times join-minus-separate, so it has a lift to realizable charged states. Three or more through-components give the remainder, controlled by six arms. We can therefore apply (5.45) to the lifted rows. The remainder still has total mass zero. We realize the lift by closing the protected core and placing one odd mark on each of the two sampled through-components. Thus the charged estimate applies even if a neutral input was formally enlarged.

Let $\ell_{r;s} = \lambda_{r,s}^{-1} L_{r,s} h_s$. Propagating (5.47) to R gives

$$\left\| \lambda_{r,R}^{-1} P_{r,R}|_{V_r^{0,*}} - \ell_{r;s} \otimes e_R \right\| \le C\big[(s/R)^\delta + (r/s)^\zeta\big]. \tag{5.48}$$

Here the E term is propagated using the *zero-mass four-arm bound* $\|P_{s,R}|_{V_s^{0,*}}\| \le C\lambda_{s,R}$, not merely stochastic contraction by one. This factor is necessary for the normalized estimate.

Compare (5.48) at intermediate radii s, t, test by the same φ_R, and then send $R \to \infty$ at fixed mesh. The detecting bound yields

$$\|\ell_{r;s} - \ell_{r;t}\| \le C\big[(r/s)^\zeta + (r/t)^\zeta\big].$$

Thus $\ell_r = \lim_{s\to\infty} \ell_{r;s}$ exists in norm. Balancing the two powers by

$$\log(s/r) = \frac{\delta}{\delta+\zeta} \log(R/r)$$

proves

$$\left\| \frac{P^a_{r,R}|_{V_r^{0,*}}}{\lambda^a_{r,R}} - \ell^a_r \otimes e^a_R \right\| \le C(r/R)^{\delta_E}, \qquad \delta_E = \frac{\delta\zeta}{\delta+\zeta} > 0. \tag{5.49}$$

We now prove the compatibility identities. Apply (5.49) to e_r and use its exact propagation and the detecting test to obtain $\ell_r(e_r) = 1$. Compare $P_{r,T} = P_{r,R}P_{R,T}$ at a common remote target T to get $P_{r,R}\ell_R = \lambda_{r,R}\ell_r$. Finally apply the two mixing estimates to $J_r P_{r,R} = Q_{r,R}J_R$ and test at the same remote boundary to get $J_r\ell_r = h_r$. All differences reduce to a scalar multiple of the uniformly detected e_R. The remainders tend to zero. This proves the normalization and compatibility in Theorem 5.6.

Using circular cuts. The mixing estimates can be transferred from square cuts to disk cuts by inserting square buffers. For example, for $R > 8r$ factor

$$Q^a_{B_r,B_R} = Q^a_{B_r,D_{2r}} Q^a_{D_{2r},D_{R/2}} Q^a_{D_{R/2},B_R}.$$

Apply Theorem 5.6 to the middle factor. Define the incoming disk column by propagating h^a_{2r} through the first buffer and dividing by $\lambda^a_{r,2r}$. Define the outgoing disk row by propagating $\nu^a_{R/2}$ through the last buffer and dividing by $\lambda^a_{R/2,R}$. The fixed-ratio factors have uniformly bounded normalized norms. The errors consequently retain a positive power of r/R.

These definitions agree with the microscopic-seed and remote-reference definitions made directly at disk cuts. In particular, normalization $\nu^a_r h^a_r = 1$ follows by propagating the seed through the first buffer, and exact compatibility follows from the Markov property and the remote-reference limit. The neutral argument is the same on the zero-mass subspace, using its four-arm norm bound. Hence disk cuts may be used below, without changing the insertion. They are useful for rotations of the source.

5.3 Normalization by the scalar field

Translate the center to zero. Use a fixed two-density probe outside B_d by placing its roots at $-2d, 2d$ and multiplying its normalized completion by d^{2x}. Denote the resulting neutral test by ϕ^a_d. The two root arms cross disjoint disks, so their independent probabilities bound $\|\phi^a_d\|_\infty$ by a constant at small mesh. We also need this probe to detect the difference between a join and a separation. For the seed defining ν^a_d, separated-arm extension implies

$$0 < c \le t^a_d := e^a_d(\phi^a_d) \le C. \tag{5.50}$$

For the lower bound, attach one external root to each of the two seed components, keeping them distinct until the artificial join. By RSW and separated-arm extension this event has mass at least a fixed multiple of the seed four-arm probability times the two root-arm probabilities. Dividing by the seed and density normalizations leaves the positive lower bound in (5.50). The upper bound for the completion is that of [1, Section 9.2].

Evaluating the three-point function (4.3) at these roots fixes the continuum normalization

$$A_d := \langle E^\circ(0), \phi_d \rangle = 2^{-5/12} C_\circ d^{-y} > 0. \tag{5.51}$$

At each mesh define the bounded reference rows

$$\mathcal{E}^a_d = A_d \frac{e^a_d}{t^a_d}, \qquad \mathcal{C}^a_d = A_d \frac{\nu^a_d}{t^a_d}. \tag{5.52}$$

They satisfy $\mathcal{C}^a_d J_d = \mathcal{E}^a_d$ and have norms at most Cd^{-y}. They are finite-mesh reference rows. No cross-mesh measure limit is assigned to them.

Lemma 5.8 (Scalar alignment in the complete neutral norm)**.** *For $s < cd$ and $\delta_0 = \min\{\delta_E, 11/15\}$,*

$$\limsup_{a\downarrow 0} \|R_s^{a,D} - \mathcal{E}_d^a\|_{\mathrm{var}} \le C d^{-y} (s/d)^{\delta_0}. \tag{5.53}$$

For each fixed $d < D$,

$$\lambda^a(d,D)\frac{t_D^a}{t_d^a} \longrightarrow \frac{A_D}{A_d} = (d/D)^y. \tag{5.54}$$

Proof. At a cut cs around the source, $R_s = s^{-y}\zeta_s P_{cs,d}$, where $\zeta_s = \mu_{cs} - \nu_{B_s}^{cs}$ has mass zero and norm at most two. Apply (5.29). Subtracting the same row's value on ϕ_d^a times e_d^a/t_d^a gives

$$\limsup_a \left\| R_s - R_s(\phi_d^a)\frac{e_d^a}{t_d^a} \right\|_{\mathrm{var}} \le C d^{-y}(s/d)^{\delta_E}.$$

The fixed-s mesh limit of $R_s(\phi_d^a)$ exists. Its difference from A_d is at most $Cd^{-y}(s/d)^{11/15}$ by (5.4) and the bounded probe. This proves (5.53).

Filling the annulus between the cuts gives the identity $R_s^{a,B_d} P_{d,D}^a = R_s^{a,B_D}$. Insert (5.53) on the two sides and test by ϕ_D^a. Use (5.32) and (5.50). For each fixed s, d, D take the mesh upper limit, and then send $s \downarrow 0$. The errors vanish and give (5.54).

□

5.4 Scale invariance of source amplitudes

We determine how much a density pair contributes to the leading direction of each annular kernel. Exact scale independence matters because the number of annuli grows logarithmically.

5.4.1 Connections at fixed radii

We shall test the same coloring at several radii. At an inner cut we may ask whether two marked clusters are still distinct and whether each reaches the cut. At an outer cut we may ask whether they have joined, and a distant pair of density marks may test the resulting connection. A new, independent coloring is used only when the experiment calls for a reset.

Fix finitely many point marks and deterministic cuts. A connection may be tested in the plane, in the interior of a cut, or in the collar between cuts. Its ends can be marks, positive-radius targets, or specified boundary arcs. An arc used as a target records contact; wiring an arc also identifies its open contacts. We use disks, squares and regular deformations of these configurations. In a fixed family the incidence and wiring of the arcs are fixed, the smooth pieces vary in C^2 charts, and the finitely many corners have angles bounded away from 0 and 2π on compact subfamilies. Distinct cuts used as the boundaries of a collar, distinct targets in a connection test, and roots and cuts are separated. We call a finite list of these data and connection decisions a *template*. Boolean combinations of the decisions include nonconnections and first mergers between successive cuts. A point mark carries the normalization π_a^{-1} of Section 4 whenever the event requires an open arm from that mark across a fixed disk of its own.

Lemma 5.9 (Connections of marked points at fixed radii)**.** *For each event in such a template that requires an arm from each of its m density roots, the probability divided by π_a^m has a mesh limit. This includes finite products for independent resets, with the point normalizations counted in the copies where the marks occur. The limits are continuous in the separated data, and convergence is uniform on compact subfamilies. Rotations preserve the limiting weights. Dilating the entire configuration by $\lambda > 0$ multiplies a weight with m density roots by λ^{-mx}.*

Proof. Connections at positive scales. First replace each point by a disk of fixed positive radius and wire its cells open. We read the connections in each test domain from the portion of the original sample lying in that domain. To include the wiring, make a graph of the labelled targets: a sampled cluster supplies an edge when it touches two targets, counting an incident cell at a wired set. Splitting a path at its visits to the wired sets shows that a chain of edges describes precisely a connection after wiring [1, Section 11.1]. Only wired targets may be intermediate vertices of the chain. In particular, to test whether two clusters reach a frontier separately, we test each for contact with the frontier and test their mutual connection in the original wiring. Making the whole frontier a single wired block in this last test would join the very clusters we want to distinguish.

We explain why these tests converge in one sample, including when their domains overlap. Use the common coupling of the quad-crossing configurations and interface loops of [4, Section 4.2, Remark 4.17 and Theorem 7.1]. In a bounded simply connected piecewise smooth domain, Theorem 7.1 of that work matches the clusters of diameter above a fixed positive threshold in probability, in Hausdorff distance. Its clusters are the components obtained *after restriction* to the domain, so a path that travels outside the cut cannot supply an edge inside it. For separated targets we can take the threshold smaller than their separation. For an open target, meeting a slightly smaller target is a lower test and meeting a slightly larger one is an upper test. The matching decides these buffered tests in the limit: one may choose the buffer widths at continuity values of the distances from the limiting clusters to the targets. There are almost surely only finitely many clusters above the threshold. For a boundary arc we take the buffered targets to be thin neighborhoods on the domain side; the side estimate below compares near contact to contact with the arc itself. We use the same coupling for each of the finitely many domains. Arm and circuit indicators in fixed smooth annuli, including arms landing on specified arcs, also converge in probability in this coupling [19, Lemma 2.9 and Remarks 2.11–2.12].

Here is the boundary estimate which allows the buffers to be removed. Set aside disks of radius u about the finitely many corners and arc endpoints, and take a buffer of width $h \ll u$ on each remaining smooth piece. A change of a macroscopic contact near one of the excluded points requires a sampled arm from that disk to a fixed distance. A sequence of disjoint annuli with fixed radius ratio separates the two scales, so the RSW circuit bound makes this probability tend to zero with u. Away from these disks, cover a displaced side by $O(h^{-1})$ tiles and move it by one tile at a time. If extending a wired target gains a connection, the newly attached open component previously avoided the target. Its path toward the other target therefore has a closed separator on either side. If removing a tile from the allowed domain breaks a connection, the two surviving open branches reach the tile from distinct components. A closed arm must run between them, since an open crossing between the branches would restore their connection. These are three sampled arms on the domain side of the cut. The same comparisons apply when a cluster is tested for contact with an unwired target: stop the path at its first contact. A whole frontier used only as a target may be covered by finitely many arcs in this manner. The side comparison for quadrilateral crossings is detailed in [21, Appendix A, Lemmas A.1–A.2], and the corresponding target comparison in [1, Section 11.1].

At fixed u the three arms run from scale $O(h)$ to a positive distance depending only on the separated geometry and u. The half-plane three-arm bound, applied in boundary charts as in [1, Sections 4 and 11.1], bounds the sum over tiles by $C_{u,\xi}h^{1-\xi}$ for any sufficiently small $\xi > 0$ [9, Theorem 3]. A closed separator for a lost connection lies between the open branches, while the separators for a gained contact lie alongside a branch that avoided the wired bank. Thus the assigned boundary color cannot supply any of these three arms. Taking first the mesh limit, then $h \downarrow 0$ and finally $u \downarrow 0$ proves stability under the small displacements used

above. It also permits inward and outward approximations of a moving regular domain by fixed ones. In the plane we first work inside a large box: a connection between bounded targets that needs to leave the box entails an arm from a fixed enclosing circle to that box. Its probability tends to zero as the box grows.

Connections confined to a collar. A collar has a hole. To apply the simply connected cluster-matching theorem, we open the collar in two different places and record where a path can pass from one opened domain to the other. Choose two disjoint, positively separated thin closed strips joining the inner to the outer boundary of the collar. Deleting either strip opens the collar into a simply connected domain. Between the two strips choose a finite union of smooth transverse arcs separating them in the collar (for example, the two sides of a slightly wider strip around the first one). These arcs lie in the overlap of the two opened domains and have positive distance from both deleted strips. Cover them by $O(h^{-1})$ little disks of radius h. Choose a fixed threshold $b > 0$ smaller than one quarter of both this distance and the separation of the two targets under test, at a continuity value of cluster diameters in the two opened domains.

In each opened domain keep the clusters of diameter above b and record which targets and covering disks each cluster meets. Link clusters from different domains when both meet the same covering disk. At fixed h the preceding cluster matching and boundary comparison apply to this finite incidence graph. For a target on an original boundary, its portion in a chart is an arc or a finite union of arcs; choose the strip ends transversely and use the endpoint comparison at the new corners. Disk radii may be varied in $(h, 2h)$ to use continuity values while maintaining the cover. Every sampled path between the targets is represented in this graph. A path avoiding one strip stays in one opened domain. Otherwise, list its visits to the strips, grouping successive visits to the same strip. Between the last visit in one group and the first in the next, the path crosses a separating arc. Switch domains there. Each resulting piece visits a strip and reaches a separating arc, so it belongs to a cluster of diameter above b, including the first and last pieces.

Conversely, a false connection in this graph would require two distinct clusters in the original collar to meet the same covering disk and both extend a distance at least $b/3$ from it. Away from the ends of the separating arcs this requires four alternating arms: the two open branches are separated on both sides by closed branches as long as their components remain distinct. With endpoint disks of radius u removed, the outer arm scale can be chosen to be a fixed positive number smaller than $b/3$ and the distance to the collar boundary. The bulk four-arm exponent $5/4$ bounds the sum over the covering disks by $C_{u,b,\xi} h^{1/4-\xi}$ for $0 < \xi < 1/4$ [9, Theorem 4]. Within the endpoint disks even a single such cluster requires an arm from scale $O(u)$ to scale $b/3$. Thus the probability of a false link between distinct original components tends to zero, first in h and then in u. This recovers connections in the collar using only restricted clusters in simply connected domains. In all these approximations, the probability of an error in the whole finite list is at most the sum of the individual error probabilities. Its joint law, and hence the probability of any Boolean combination, converges.

Restoring the point marks. Choose disjoint disks $B(q_i, d_i)$ about the m roots, inside every test domain involving that root and away from the cuts and the other targets. Let A_i require an open arm from the lattice root to the boundary of its disk and put $A = \bigcap_i A_i$. For the event E in the statement, $E \subset A$. Independence in the root disks and the one-arm ratio of [3, (2.1)] give

$$\frac{\mathbb{P}_a(E)}{\pi_a^m} = \left(\prod_{i=1}^{m} \frac{\mathbb{P}_a(A_i)}{\pi_a} \right) \mathbb{P}_a(E \mid A), \qquad \prod_{i=1}^{m} \frac{\mathbb{P}_a(A_i)}{\pi_a} \longrightarrow \prod_{i=1}^{m} d_i^{-x}.$$

It remains to compare the conditional probability with one involving only positive radii.

Let E_t be the same list of decisions with $B(q_i, t)$ wired in place of each root, where $8t < \min_i d_i$. Under A_i the root cluster crosses from the small disk to $\partial B(q_i, d_i/2)$. If every open branch crossing between these two circles belongs to the root component in $B(q_i, d_i)$, wiring cannot change any decision: a path that uses the wired disk to join two macroscopic branches can instead join them through the root component. A path ending at the disk can likewise be continued to the root. These replacements stay in each domain in which the mark is tested, since the entire root disk lies in all of them. The root disks are disjoint, so the replacements can be made at all the marks in the same sample.

A failure at q_i requires the crossing branch of the root cluster and a branch in a different component of $B(q_i, d_i)$. Between radii $2t$ and $d_i/4$, planar duality gives a closed crossing on each side between these two open arms: an open connection on either side would put the two branches in the same component inside the root disk. This is the four-arm separation in [3, (2.54)–(2.59)]. The event A_i also requires an open arm from the root to $t/2$, in cells disjoint from these four arms. All other root disks are independent and their conditioning factors cancel. Writing $\triangle$ for symmetric difference, we obtain

$$\limsup_{a\downarrow 0} \mathbb{P}_a(E \triangle E_t \mid A) \;\le\; C \sum_{i=1}^{m} (d_i/t)^x (t/d_i)^y \;=\; C \sum_{i=1}^{m} (t/d_i)^{55/48}.$$

Here $(d_i/t)^x$ comes from dividing the inner one-arm probability by $\mathbb{P}_a(A_i)$, using [3, (2.1)]. The four-arm factor follows from quasi-multiplicativity and the fixed-scale ratio (5.27). This estimate controls positive and negative decisions together, since both are read from the same partitions.

For $0 < \varepsilon < t/2$, let H_ε require a sampled arm from radius ε to radius d_i about every q_i. Camia's coupling, applied independently in the disjoint root disks, compares the laws conditioned on A and on H_ε [3, Lemma 2.1, Remark 2.2 and (2.14)–(2.20)]. Except on an event whose mesh upper probability tends to zero with ε at fixed t, the two samples agree outside common open circuits inside the disks of radius t. All the cells that can then differ are filled when evaluating E_t. Thus we may replace $\mathbb{P}_a(E_t \mid A)$ by

$$\frac{\mathbb{P}_a(E_t \cap H_\varepsilon)}{\mathbb{P}_a(H_\varepsilon)}$$

with that same error. The arm indicators in this ratio are read in the original colors before wiring. At fixed ε, t, the joint positive-scale limit above applies to the numerator, and the denominator has a positive limit by RSW and independence. Given any error tolerance, first choose t to make the wiring error small and then choose ε to make the coupling error small. The resulting ratio has a limit and approximates $\mathbb{P}_a(E \mid A)$ to that tolerance in mesh upper limit. This proves convergence of the normalized probability.

Merger observations and changes of scale. For two labels to survive separately to a cut, each must reach it and their mutual connection in its interior must fail. Their first merger between that cut and the next is the intersection of separate survival at the first cut with their connection inside the next one. This description tests the same coloring twice, so a subsequent observation can be included in the joint list without assigning it an independent coloring. For an artificial join, we identify the two named vertices in the connection graph before reading the observation. For an independent reset we instead multiply the merger probability by the unmarked observation probability. These rules explain how the fixed-radius limits enter the distant probes in Lemma 5.10, the numerator and denominator in (5.69)–(5.70), and the merger rows tested in (5.73). Division by a pair probability uses its positive normalized limit at fixed separation [3, Theorem 1.1]. Positivity of the denominator of the two-buffer ratio is established in Lemma 5.11 below.

The same comparisons hold along a sequence of templates converging to separated data. We can choose common root radii along the sequence. At each fixed buffer width, test a positive connection first in a slightly smaller limiting domain with smaller targets, then in a larger one with larger targets. The moving connection indicator lies between the two. By the preceding arm bounds their disagreement probability tends to zero as the offsets shrink. We make this comparison for each positive decision before taking complements or intersections. Thus the lattice weights along the sequence converge to the weight of its limiting template. To see continuity of the continuum weight, approximate the jth template by a mesh smaller than $1/j$ with weight error at most $1/j$, using the fixed-template convergence. This sequence has the same limit. On a compact family any sequence has a converging subsequence, so the same argument also proves uniformity. Finally, the positive-scale laws are rotation and dilation invariant [4, Theorem 9.5]. A template with no point roots has only the positive-scale probabilities. When roots are present, dilation changes their fixed radii to λd_i, so the product of one-arm factors acquires precisely λ^{-mx}. □

By a packet we mean a signed local row, here specified by a finite linear combination of these connection experiments. Suppose that a packet at $c_\zeta r$ is given by dilating one such fixed configuration and has uniformly bounded variation as $a/r \to 0$. We allow two cases, a neutral row of total mass zero and a row carrying two odd blocks. Its pairing after propagation to a far probe, multiplied by r^{-y}, then has dilation degree $-y$ because the probe has its factor D^{2x}, and the pair's source normalization is the ratio to p_a. Only the packets in Sections 5.5 and 5.7 will be used in the final theorem.

Lemma 5.10 (Normalization by distant density marks)**.** *For a neutral packet ζ_r^a as above, the scalar*

$$a_{\zeta,r}^a(d) = r^{-y}\lambda^a(c_\zeta r, d)\zeta_r^a(\ell_{c_\zeta r}^a)\frac{t_d^a}{A_d} \tag{5.55}$$

has a mesh limit b_ζ independent of the scale r and the output cut d. For a charged packet c_r^a, the corresponding scalar is

$$a_{c,r}^a(d) = r^{-y}\lambda^a(c_c r, d)c_r^a(h_{c_c r}^a)\frac{t_d^a}{A_d}, \tag{5.56}$$

and has a similarly scale-independent limit b_c. This assertion is uniform on each fixed regular compact template family. A rotation of a disk-based template leaves its coefficient unchanged.

The reference direction in the far-probe argument is supplied in the full norm by Lemma 5.8.

Proof. Consider the neutral case first. Complete the propagated row at a far radius D by ϕ_D^a, and denote its fixed-r, D mesh limit by

$$F_{\zeta,r}(D) = \lim_{a\downarrow 0} r^{-y}\zeta_r^a P_{c_\zeta r,D}^a \phi_D^a.$$

This limit is a finite combination of the regular history probabilities just described. Mixing and the bounded probe give

$$\limsup_a \left| a_{\zeta,r}^a(D) - \frac{F_{\zeta,r}(D)}{A_D} \right| \le C_\zeta (r/D)^{\delta_E}. \tag{5.57}$$

The coefficient's exact cut ratio is $\lambda^a(d, D)t_D^a/t_d^a$. After division by the corresponding A ratio, (5.54) shows that $a_{\zeta,r}^a(D) - a_{\zeta,r}^a(d) \to 0$ for fixed r, d, D. All these coefficients are bounded, by mixing normalization and the packet norm. Apply (5.29) before the probe. Use the exact native compatibility and Lemma 5.8. Fixed template sizes are absorbed in C_ζ.

For two large far radii, (5.57) and this cut comparison show that $F_{\zeta,r}(D)/A_D$ is Cauchy as $D \to \infty$. They also show that the original scalar (5.55) has that limit as $a \downarrow 0$. Call it $b_\zeta(r)$. The ratio is scale invariant because the numerator and denominator have the same dilation degree, namely $-y$. Indeed,

$$F_{\zeta,\lambda r}(\lambda D) = \lambda^{-y} F_{\zeta,r}(D), \qquad A_{\lambda D} = \lambda^{-y} A_D.$$

Taking $D \to \infty$ proves $b_\zeta(\lambda r) = b_\zeta(r)$, so the same coefficient applies at every r.

For a charged packet, use

$$F_{c,r}(D) = \lim_a r^{-y} c_r^a Q^a_{c_c r, D} J_D \phi_D^a.$$

The product $\nu_D^a J_D \phi_D^a = t_D^a$ is the same detector. The error in (5.57) is now $C_c(r/D)^{\delta_C}$. The join-minus-separate test is a difference of two finite marked connectivity rules, so its fixed-scale limit belongs to the same test class. For the density source it equals the normalized probability that the two central roots belong to different global clusters and attach to the two distant density roots separately. The argument just given applies unchanged.

The coefficient does not depend on the chosen regular detecting probe. Indeed, (5.53) places both calibrated probes in the direction e_d, so the ratio compares them to the same scalar coefficient. Rotating the template rotates such a probe, while the scalar reference is rotationally covariant. This proves the rotation assertion. The fixed-scale root limits and all errors are uniform on a fixed compact template family, proving the final uniformity assertion.

□

5.5 Two clusters surviving to the observation circle

Choose once and for all $c > 1$ sufficiently large, and put $r_0 = cr$. At that initial cut, let n_r^a, c_r^a be the neutral and charged parts of the pair row, including division by p_a but not r^{-y}. Thus $n_r^a \geq 0$, $c_r^a \geq 0$, and

$$\|n_r^a\| + \|c_r^a\| \leq C, \qquad n_r^a \mathbf{1} + c_r^a w_{r_0}^a = 1. \tag{5.58}$$

The bound follows by extracting the two disjoint local root-arm probabilities before division by p_a. RSW joining bounds p_a below by a fixed multiple of their product. The equality partitions global root connection into an inner merger and eventual merger from the surviving marked state.

Let b_Φ be the coefficient in Lemma 5.10 for the row c_r^a. Charged mixing gives

$$\limsup_{a \downarrow 0} \|r^{-y} c_r^a Q^a_{r_0,d} - b_\Phi \mathcal{C}_d^a\|_{\mathrm{var}} \leq C d^{-y} (r/d)^{\delta_C}. \tag{5.59}$$

Indeed its projected part is $a^a_{c,r}(d)\mathcal{C}_d^a$, whose scalar coefficient tends to b_Φ for every fixed r, d. Subtract the same reference row at r and br to obtain (5.6).

The compensating neutral term enters through the bounded map

$$\mathcal{T}_d(v) = (-[v w_d]\mu_d,\ v), \qquad \|\mathcal{T}_d(v)\| \leq 2\|v\|. \tag{5.60}$$

Its first coordinate is neutral and its second is charged. Thus (5.59) also proves convergence of the charged tail *together with* its compensating neutral term to the common reference $b_\Phi \mathcal{T}_d(\mathcal{C}_d^a)$, with the same norm estimate. The bound on $\mathcal{T}_d$ follows from $0 \leq w_d \leq 1$.

5.6 The logarithm from the first merger

The exact centered pair decomposition is

$$\mathsf{Q}_r^d = \iota r^{-y}\big[(n_r - (n_r\mathbf{1})\mu_{r_0})P_{r_0,d} + c_r\widehat{B}_{r_0,d}\big] + \mathcal{T}_d(r^{-y}c_rQ_{r_0,d}). \tag{5.61}$$

Substitute (5.14) and $1 = n_r\mathbf{1} + c_rB_{r_0,d}\mathbf{1} + c_rQ_{r_0,d}w_d$ from (5.58) to verify it. Both the marked tail and its compensation occur in this identity.

For every $s < t$ define

$$\gamma^a(s,t) = \frac{\nu_s^a\widehat{B}_{s,t}^a\ell_t^a}{\lambda^a(s,t)}. \tag{5.62}$$

Its exact cocycle and local bound are

$$\gamma^a(s,u) = \gamma^a(s,t) + \gamma^a(t,u), \qquad |\gamma^a(s,t)| \le C \quad (1 < t/s \le 2). \tag{5.63}$$

They follow from (5.16), (5.31)–(5.32), and the bounded conversion. The output after $\widehat{B}$ has mass zero, so the neutral harmonic-column identity applies.

The fixed-scale continuum coefficient exists and satisfies

$$\lim_{a\downarrow 0}\gamma^a(s,t) = \chi\log(t/s). \tag{5.64}$$

For the next ratio only, write $\gamma_a(r,R) = \gamma^a(r,R)$, $\lambda_{r,R}^a = \lambda^a(r,R)$, and use square cuts. The disk-buffer transfer proved above applies unchanged.

Take $s < r < R < t$, with substantial buffers $s \ll r$ and $R \ll t$. At the inner cut D_s, choose a deterministic source σ_s^a whose frontier has two macroscopically separated open arcs, each internally connected, separated by closed arcs. These two blocks are odd. It is a frontier state realized by two open caps and a closed separating interior. At D_t, let $\varphi_t^a \in \{0,1\}$ test connection between two separated, fixed-fraction left and right boundary arcs.

Choose the templates with the separated extension used in Theorem 5.6. Then, uniformly for sufficiently fine meshes,

$$\sigma_s^a h_s^a \ge c_0, \qquad e_t^a(\varphi_t^a) \ge c_0. \tag{5.65}$$

The first bound follows by extending the two source arcs, with their closed separators, through a fixed collar and then to separated reference faces. The second is the macroscopic detecting test constructed in the proof of Theorem 5.6. This uses only regular templates, not a lower bound for every incoming state.

Define

$$N_a(s,r,R,t) = \sigma_s^aQ_{s,r}^a\widehat{B}_{r,R}^aP_{R,t}^a\varphi_t^a, \tag{5.66}$$

$$D_a(s,t) = \sigma_s^aQ_{s,t}^aJ_t^a\varphi_t^a. \tag{5.67}$$

Joining the two odd blocks preserves any existing crossing, so the denominator is nonnegative. It is positive because separated arm extension realizes configurations in which the join creates a crossing.

Lemma 5.11 (Two-buffer probability ratio)**.** *For R/r in a fixed compact subinterval of $(1,\infty)$ and sufficiently long buffers,*

$$\left|\frac{N_a(s,r,R,t)}{D_a(s,t)} - \gamma_a(r,R)\right| \le C\left[(s/r)^{\delta_C} + (R/t)^{\delta_E}\right]. \tag{5.68}$$

The comparison is uniform in the mesh because the common denominator $D_a(s,t)$ is comparable to $\lambda_{s,t}^a$.

Proof. Write $T^C = Q/\lambda$, $T^E = P|_{V^{0,*}}/\lambda$, and $V = \widehat{B}_{r,R}/\lambda_{r,R}$. All common scalar factors cancel in N/D. Put $a_s = \sigma_s h_s$ and $b_t = e_t \varphi_t$. By Theorem 5.6,

$$\sigma_s T^C_{s,r} = a_s \nu_r + O_{\mathrm{var}}((s/r)^{\delta_C}), \qquad T^E_{R,t}\varphi_t = b_t \ell_R + O_{\mathrm{dual}}((R/t)^{\delta_E}).$$

The second estimate may be used after V because its output has mass zero. Uniform boundedness of V and the rows and columns gives

$$\frac{N_a}{\lambda^a_{s,t}} = a_s b_t \gamma_a(r,R) + O((s/r)^{\delta_C} + (R/t)^{\delta_E}).$$

Charged mixing and $e_t = \nu_t J_t$ similarly give

$$\frac{D_a}{\lambda^a_{s,t}} = a_s b_t + O((s/t)^{\delta_C}).$$

Use (5.65), take the buffers long enough to keep the denominator above $c_0^2/2$, and use the local bound in (5.63). The denominator error is absorbed in the displayed bound. □

Connection events in the ratio. Sample the collar from s to t with the source template inserted. Let S_u mean that its two marked components remain distinct and both reach the frontier at u. Let $F_{r,R}$ mean S_r and merger of the two components by radius R. If an odd component is lost, it cannot merge later, so these descriptions agree with $Q_{s,r}B_{r,R}$. Let φ_t be evaluated on the final neutral connectivity. Since $\mu_R P_{R,t} = \mu_t$,

$$N_a = \mathbb{P}^a_{\sigma_s}(F_{r,R}, \varphi_t = 1) - \mathbb{P}^a_{\sigma_s}(F_{r,R})\mathbb{P}^a_{\text{unmarked } \mathrm{D_t}}(\varphi_t = 1). \tag{5.69}$$

Similarly, let $\varphi_t^{\mathrm{join}}$ be the crossing test after artificially joining the two source arcs. On S_t this is equivalent to joining their two surviving odd blocks at the outer frontier. Therefore

$$D_a = \mathbb{P}^a_{\sigma_s}(S_t, \varphi_t^{\mathrm{join}} = 1, \varphi_t = 0). \tag{5.70}$$

All marks in these formulas are macroscopic boundary arcs. Their signed subtraction retains the true merger mass and unmarked background.

Both probabilities involve only regular marked histories at fixed positive radii, so Lemma 5.9 applies to each. RSW bounds the denominator away from zero at each such geometry. For $s_m = 2^{-m}r$ and $t_m = 2^m R$, let G_m be the mesh limit of their ratio. By (5.68), with $\epsilon_m = C(2^{-m\delta_C} + 2^{-m\delta_E})$,

$$|G_m - G_k| \le \epsilon_m + \epsilon_k, \qquad \limsup_{a \downarrow 0} |\gamma^a(r,R) - \lim_m G_m| \le 2\epsilon_m.$$

Letting $m \to \infty$ proves the limit of $\gamma^a(r,R)$ and its independence of the regular probes. Dilation covariance of the regular probabilities makes the limit a function of R/r alone. Exact additivity in (5.63) and the local bound make it a locally bounded additive function of $\log(R/r)$, proving (5.64). At a fixed collision radius the sum has finitely many collars, so we can take this limit term by term before sending the collision radius to zero.

Write

$$T_C(s,t) = Q_{s,t}/\lambda(s,t), \quad T_E(s,t) = P_{s,t}|_{V_s^{0,*}}/\lambda(s,t),$$
$$\Pi_C(s,t) = h_s \otimes \nu_t, \quad \Pi_E(s,t) = \ell_s \otimes e_t, \quad D_C = T_C - \Pi_C, \quad D_E = T_E - \Pi_E.$$

For a finite chain $r_0 < r_1 < \cdots < r_n = d$, set $V_j = \widehat{B}_{r_j,r_{j+1}}/\lambda(r_j, r_{j+1})$. On ratio-at-most-two collars these operators are uniformly bounded. The normalized first-merger sum has the exact expansion

$$\begin{aligned}\sum_{j=0}^{n-1} T_C(r_0, r_j) V_j T_E(r_{j+1}, d) = \gamma^a(r_0, d)(h_{r_0} \otimes e_d) \\ + \sum_j D_C(r_0, r_j) V_j \Pi_E(r_{j+1}, d) \\ + \sum_j \Pi_C(r_0, r_j) V_j D_E(r_{j+1}, d) \\ + \sum_j D_C(r_0, r_j) V_j D_E(r_{j+1}, d). \end{aligned} \tag{5.71}$$

At a zero-length interval $T_C = T_E = I$. Its residual is $I - \Pi$.

5.7 Comparison of pair separations

To compare two nearby separations we use the same annuli near the observer. The first few annuli around each pair can then be accounted for by scalar coefficients.

The endpoint comparison is made in the original full-record norm. Outgoing endpoint rows need not acquire separate continuum limits. We compare them at the same mesh for every collision radius being compared.

5.7.1 Contributions near the marked pair

The initial neutral packet

$$\zeta_{0,r} = n_r - (n_r \mathbf{1})\mu_{cr}$$

is a regular zero-mass dilation template of bounded norm. Lemma 5.10 and neutral mixing give a constant b_{in} such that

$$\limsup_a \|r^{-y}\zeta_{0,r} P_{cr,d} - b_{\mathrm{in}} \mathcal{E}^a_d\| \le C d^{-y}(r/d)^{\delta_E}. \tag{5.72}$$

For the source-anchored cuts $r_j = c2^j r$ define the merger rows

$$\zeta_{j,r} = c_r Q_{cr,r_j} \widehat{B}_{r_j,r_{j+1}}, \qquad j \ge 0. \tag{5.73}$$

Each has mass zero. Its positive term is the first-merger event by the next cut with its outgoing neutral record. Its negative term is the probability of that event times a fresh neutral law. The p_a factor is kept in c_r. At fixed j and $r > 0$, Lemma 5.9 applies to the pairing with a regular geometric observation. In the first term we read the merger and the observation in the same sample. In the second we multiply the merger probability by the probability of the observation after an independent reset.

Let b_j be their projected amplitude from Lemma 5.10, using the multiplier r^{-y}. Set

$$u_j = b_j - b_\Phi \chi \log 2. \tag{5.74}$$

In the second line of (5.71), the incoming residual is

$$r^{-y}\lambda(r_{j+1}, d)\zeta_{j,r}(\ell_{r_{j+1}})e_d - a^a_{c,r}(d)\gamma^a(r_j, r_{j+1})\mathcal{E}^a_d.$$

Its scalar coefficient converges to u_j for every fixed j, r. Charged mixing on the left, bounded V_j, and bounded projection on the right give

$$|u_j| \le C2^{-\delta_C j}. \tag{5.75}$$

To see that the constant is independent of j, the factor $r^{-y}\lambda(cr, d)$ is bounded by Cd^{-y} after the mesh limit, while the left residual costs $2^{-\delta_C j}$. Test with ϕ^a_d and divide by $A_d \asymp d^{-y}$. The normalized initial source has bounded norm by (5.58).

5.7.2 Contributions near the observation circle

Use terminal-anchored cuts

$$s_k = d2^{-(k+1)}, \qquad t_k = d2^{-k}, \qquad k \ge 0.$$

At a mesh small compared with s_k, define the neutral row

$$\mathcal{W}^a_{k,d} = \frac{A_d}{t^a_d}\,\nu^a_{s_k}\,\frac{\widehat{B}^a_{s_k,t_k}}{\lambda^a(s_k, t_k)}D^a_E(t_k, d). \tag{5.76}$$

Here t^a_d is the detector in (5.50), not the terminal radius t_k. It follows directly that

$$\|\mathcal{W}^a_{k,d}\|_{\mathrm{var}} \le Cd^{-y}2^{-\delta_E k}. \tag{5.77}$$

For a source at r, the corresponding term in the third line of (5.71) is precisely $a^a_{c,r}(d)\mathcal{W}^a_{k,d}$.

In particular, for each fixed finite K,

$$\lim_{a\downarrow 0}\left\|[a^a_{c,r}(d) - b_\Phi]\sum_{k<K}\mathcal{W}^a_{k,d}\right\|_{\mathrm{var}} = 0.$$

5.7.3 Annuli of noninteger logarithmic width

Put

$$N = \lfloor \log_2(d/(cr))\rfloor, \qquad m = \lfloor N/2\rfloor, \qquad k = N - m.$$

Use m full source-anchored collars and k full terminal-anchored collars, with one middle collar of ratio in $[1, 2)$ connecting them. If its ratio is one it is omitted. The first K source windows and last K terminal windows are unchanged when $K < \min(m, k)$. The middle conversion has bounded normalized norm. Its nonprojected terms cost $C(2^{-\delta_C m} + 2^{-\delta_E k})$. Its projected term is kept through the exact total $\gamma^a(cr, d)$.

Set $\delta = \min(\delta_C, \delta_E)$. On this chain the double-residual last line of (5.71), including the one middle collar, has variation norm at most

$$Cd^{-y}(N + 1)2^{-\delta(N-2)}.$$

The omitted incoming and outgoing tails after K windows have norm at most $Cd^{-y}2^{-\delta K}$. These follow by multiplying the two residual estimates in the bulk and summing the two one-sided geometric tails.

5.7.4 A reference measure at the outer cut

Set $\kappa_* = b_\Phi \chi$. For each finite K define, on the augmented record at d,

$$\mathcal{L}^a_{\ell,d,K} = \left[b_{\mathrm{in}} + \sum_{j<K} u_j + \kappa_* \log \frac{d}{c\ell} \right] \iota \mathcal{E}^a_d + b_\Phi \sum_{k<K} \iota \mathcal{W}^a_{k,d} + b_\Phi \mathcal{T}_d(\mathcal{C}^a_d). \tag{5.78}$$

This row has uniformly bounded norm $Cd^{-y}(1 + |\log(\ell/d)|)$. For fixed finite $K' > K$, its difference from $\mathcal{L}^a_{\ell,d,K'}$ has mesh upper norm at most $Cd^{-y}2^{-\delta K}$. All its terms are at the same mesh. The integer K is held fixed when taking that mesh limit. The common reference expression contains the incoming constant, outgoing correction, surviving marked tail, and its neutral compensation.

Use (5.61) and (5.71), first at fixed r, K, and take $a \downarrow 0$. By Lemma 5.10 the projected source coefficient tends to b_Φ, so summing the collar contributions by (5.64) leaves $\kappa_* \log(d/(cr))\, \iota \mathcal{E}^a_d$ in the same-mesh comparison sense. The incoming coefficients become the u_j in (5.78). The outgoing terms and the tail use the same rows as that reference. Only scalar coefficient differences vanish in this mesh limit.

Replace the counterterm R^d_r by $\mathcal{E}^a_d$ using Lemma 5.8. The difference of the two leading logarithms is $\kappa_* \log[d/(c\ell)]$. Combining the errors for $K < \min(m, k)$ and sufficiently small r/d, we obtain

$$\begin{aligned} &\limsup_{a\downarrow 0} \left\| \mathsf{Q}^{a,D}_r - \kappa_* \log(\ell/r) \iota R^{a,D}_r - \mathcal{L}^a_{\ell,d,K} \right\|_{\mathrm{var}} \\ &\quad \le Cd^{-y} \left[2^{-\delta K} + (N+1)2^{-\delta N/2} + (1 + |\log(\ell/r)|)(r/d)^{\delta_0} \right]. \end{aligned} \tag{5.79}$$

Initial neutral and charged mixing errors are absorbed in this bound. The middle collar's two residuals have the displayed $2^{-\delta N/2}$ bound, with harmless changes for integer parts.

Since the endpoint coefficients and terminal grid of (5.78) are independent of r, we can compare the radii r and br, $1/2 \le b \le 1$, to that same row with $K = \lfloor N/3 \rfloor - 1$. Adding the two error bounds, we obtain

$$\sup_{1/2\le b\le 1} \limsup_a \|Z_{br} - Z_r\|_{\mathrm{var}} \le C_{\ell/d} d^{-y} (r/d)^\eta [1 + \log(d/r)], \quad \eta = \tfrac{1}{4} \min(\delta_C, \delta_E, 11/15). \tag{5.80}$$

For boundedly short chains enlarge the constant. The loss from $\delta/3$ to the displayed η absorbs all fixed cut factors and integer parts. Equation (5.10), with (5.4), proves (5.5) with κ_*. Since that defect does not contain ℓ, one may choose $\ell = d$ for its bound.

5.8 Identification of the mixing constant

To compute the coefficient $\kappa_* = b_\Phi \chi$ in the plane normalization, we pair (5.79) with two separated densities. Because the reference row is bounded, its pairing with the two densities contributes only $O(1)$. Thus

$$\langle Q_r(z,\theta)\Phi(u)\Phi(v)\rangle = \kappa_* \log(\ell/r) \langle E^\circ(z)\Phi(u)\Phi(v)\rangle + O(1).$$

[17, Theorem 1.1, (1.9)] identifies the coefficient on the left as $C_{\log}|u-v|^{25/24}/(|z-u|^{5/4}|z-v|^{5/4})$. Comparing logarithmic coefficients using (4.3), we conclude that

$$\kappa_* C_\circ = C_{\log}, \qquad \kappa_* = \kappa = C_{\log}/C_\circ > 0. \tag{5.81}$$

The geometric sum of (5.80), with a final ratio in $[1/2, 1]$, proves a same-mesh Cauchy estimate for all positive radii. Its tail is bounded by

$$Cd^{-y}(r/d)^{\eta}[1 + \log(d/r)]. \tag{5.82}$$

Replacing R_r by E° costs the summable error in (5.4). This proves (5.7) with the same bound against every fixed finite separated stress, scalar and density word. To compare directions, rotate a disk source template and its detecting probe together. Detector independence against the scalar reference then identifies its projected coefficient with that of the unrotated template. Consequently b_{in}, b_Φ, and each b_j, u_j are independent of θ, while the terminal reference in (5.78) is independent of direction by construction. Two directions are thus compared to the same row at the same mesh, proving direction independence in the original norm.

The same estimate constructs any fixed finite number of mutually separated L_ℓ insertions jointly with stresses, scalars, and densities. At fixed positive pair separations, expansion of the finitely many counterterms reduces to previously available finite-hole density correlations. Each Z_r has uniformly bounded augmented-row norm, so finite multilinear telescoping controls their joint removal at arbitrary relative rates. All odd marks are joined before the final cluster-sign parity test. Here the finite cluster-sign rule is [3, (1.9)], and the multilinear completion is [1, Section 9.3].

5.8.1 Similarities and two-point correlations

Changing the reference length changes the logarithmic subtraction by a scalar multiple of E°. Subtracting the two definitions, we find

$$L_{\ell'} = L_\ell - \kappa \log(\ell'/\ell)E^\circ. \tag{5.83}$$

Exact similarity covariance at fixed regulators and the joint limits give, in correlation notation,

$$L_\ell(\lambda z) = \lambda^{-y}\big[L_\ell(z) + \kappa \log\lambda\, E^\circ(z)\big], \qquad \lambda > 0, \tag{5.84}$$

with the usual factors for other insertions. Rotation and translation act scalarly at the L slot. Section 6 extends these similarity identities to finite conformal transport and the logarithmic Ward action.

Taking the centered density-pair limit in (4.3), using $\langle E^\circ E^\circ\rangle = 0$ from [2, Theorem 4.4 and Section 5], gives

$$\langle E^\circ(z)E^\circ(w)\rangle = 0, \qquad \langle L_\ell(z)E^\circ(w)\rangle = C_\circ|z-w|^{-5/2}. \tag{5.85}$$

The joint two-L limit, translations, rotations, and (5.84) imply

$$\langle L_\ell(z)L_\ell(w)\rangle = \frac{C_{LL} + 2\kappa C_\circ \log(|z-w|/\ell)}{|z-w|^{5/2}}. \tag{5.86}$$

The pair subtraction fixes C_{LL}. Dilating both points by λ adds $2\kappa C_\circ \log\lambda$ to the bracket, because both cross pairings in (5.85) contribute. This agrees with (5.83).

6 Conformal action and normalization of the logarithmic field

A change of coordinates changes the distance between the two roots. Because the subtraction depends logarithmically on this distance, its change is proportional to E°. To compute it, set $s = re^{i\theta}$ and

$$Q_s(z) = r^{-25/24}[\Phi(z - s/2)\Phi(z + s/2) - r^{-5/24}\mathbf{1}], \qquad Z_s = Q_s - \kappa \log(\ell/r)E^\circ. \tag{6.1}$$

By Theorem 5.1, Z_s converges jointly to L_ℓ with the uniform bound (5.8). We use a smooth average in separation and angle to compute the Ward action of this limit.

6.1 The logarithmic Ward action

The stress insertion differentiates a separated correlation. At a logarithmic slot, it also replaces that slot by the scalar field.

Theorem 6.1. *In the plane, for every finite separated word $X = \prod_i \mathcal{O}_i(z_i)$ with $\mathcal{O}_i \in \{\Phi, E^\circ, L_\ell, T, \bar{T}\}$,*

$$\begin{aligned}\langle T(w)X\rangle = \sum_i \left[\frac{\partial_{z_i}}{w-z_i} + \frac{h_i}{(w-z_i)^2}\right]\langle X\rangle \\ - \frac{\kappa}{2}\sum_{i:\mathcal{O}_i=L_\ell} \frac{\left\langle E^\circ(z_i)\prod_{j\neq i}\mathcal{O}_j(z_j)\right\rangle}{(w-z_i)^2},\end{aligned} \tag{6.2}$$

where $h_\Phi = 5/96$, $h_{E^\circ} = h_L = 5/8$, $h_T = 2$, and $h_{\bar{T}} = 0$. The conjugate identity holds with the corresponding antiholomorphic derivatives and weights. Each L_ℓ contributes $-\kappa E^\circ/2$ in either chiral identity. There is no central fourth-order term at a T slot in this construction.

6.2 An exact finite-separation identity

First let X contain only fields whose Ward action is known, and set $G_X = \langle X\rangle$. Write $v(\zeta) = (w-\zeta)^{-1}$, $v_\pm = v(z \pm s/2)$, and $v'_\pm = v'(z \pm s/2)$. The operator $\mathcal{D}_w^X$ is the known sum of coordinate and weight terms on X (and, in the induction below, its logarithmic replacements). A prime here differentiates with respect to ζ, so $v'(\zeta) = (w-\zeta)^{-2}$.

Writing the two root derivatives in center/separation coordinates and differentiating the explicit normalization gives

$$\begin{aligned}\langle T(w)Q_s(z)X\rangle = \Bigg[\mathcal{D}_w^X + \frac{v_- + v_+}{2}\partial_z + (v_+ - v_-)\partial_s \\ + \frac{25}{48}\frac{v_+ - v_-}{s} + \frac{5}{96}(v'_- + v'_+)\Bigg]\langle Q_s(z)X\rangle \\ + \frac{5}{96}|s|^{-5/4}\frac{s^2}{[(w-z)^2 - s^2/4]^2}\,G_X.\end{aligned} \tag{6.3}$$

We take all derivatives at positive separation in the distributional sense. This follows by substituting (6.1) in the density Ward identity, including the identity-channel remainder.

The original density pair is $r^{-5/24}G_X + r^{25/24}\langle Q_s X\rangle$. The identity-channel contribution left after subtracting $r^{-5/24}\langle T(w)X\rangle$ is

$$\frac{5}{96}r^{-5/4}\left[v'_- + v'_+ - 2\frac{v_+ - v_-}{s}\right]G_X.$$

Since

$$\frac{v_+ - v_-}{s} = \frac{1}{(w-z)^2 - s^2/4}, \qquad v'_- + v'_+ - 2\frac{v_+ - v_-}{s} = \frac{s^2}{[(w-z)^2 - s^2/4]^2}, \tag{6.4}$$

this is the last line of (6.3). It is $O(r^{3/4})$ on separated compact configurations, because $2 - 5/4 = 3/4$.

6.3 The weak limit of the separation derivative

The limiting weight in the square bracket is

$$\frac{25}{48} + 2\frac{5}{96} = \frac{5}{8}. \tag{6.5}$$

Moreover,

$$s\partial_s \log(\ell/|s|) = -\frac{1}{2}, \qquad s\partial_s = \frac{1}{2}\left(r\partial_r - i\partial_\theta\right). \tag{6.6}$$

These identities suggest the coefficient $-\kappa/2$, but differentiating a convergent cutoff family pointwise would not be justified.

Choose $\chi \in C_c^\infty(\mathbb{R})$ of integral one and average the finite identity over $s = \epsilon \exp(\lambda + i\theta)$ with weight $\chi(\lambda)d\lambda\, d\theta/(2\pi)$. Test z and the other scalar coordinates smoothly on a separated compact set. The joint limit makes this average converge to the same limit as $\epsilon \downarrow 0$.

For the bounded convergent family Z_s, integration by parts gives

$$\int \chi(\lambda)\frac{d\lambda\, d\theta}{2\pi} s\partial_s \langle Z_s X\rangle = -\frac{1}{2}\int \chi'(\lambda)\frac{d\lambda\, d\theta}{2\pi}\langle Z_s X\rangle \longrightarrow 0. \tag{6.7}$$

The angular derivative integrates to zero. The final limit uses direction independence and $\int \chi' = 0$. The estimate (5.8) bounds the remainder after this integration by parts. It does not bound an unsmoothed radial derivative.

In (6.3), $v_+ - v_- = sv'(z) + O(s^3)$ and $(v_- + v_+)/2 = v(z) + O(s^2)$. After integration by parts, their errors have size $O(r^2[1 + |\log r|])$ on the required fixed tests. The multiplication errors have the same bound. Inserting $Q_s = Z_s + \kappa \log(\ell/r)E^\circ$ and subtracting the established scalar Ward identity cancels the terms proportional to $\log(\ell/r)$. The only nonvanishing extra term is

$$-\frac{\kappa}{2}\frac{v_+ - v_-}{s}\langle E^\circ(z)X\rangle \longrightarrow -\frac{\kappa/2}{(w-z)^2}\langle E^\circ(z)X\rangle. \tag{6.8}$$

Together with (6.7), the vanishing identity remainder and (6.5), this proves (6.2) for one new logarithmic slot.

For several logarithmic slots, we first fix the positive pair regulators at all but one slot and apply the identity there. Repeating the argument produces a replacement term at each logarithmic slot. Since the joint Cauchy estimate identifies the iterated limits with the joint limit, we may differentiate against smooth tests after all the pair regulators have been removed. For additional T and $\bar{T}$ slots, keep their mutually disjoint contours fixed while applying the finite mixed Ward hierarchy of [2, Theorem 4.4] at the positive pair regulators. The same integration by parts acts only on the pair variables, so each existing stress contour and either chiral derivative is a fixed bounded completion. Remove the logarithmic regulators by the joint Cauchy estimate and the stress regulators by the predecessor hierarchy. Finite multilinear telescoping identifies all orders with the common raw limit. This proves both chiral Ward identities for every fixed mixed word, including the replacement term at each logarithmic slot.

In particular, the sequential singular expansion is

$$T(w)L_\ell(z) = \frac{(5/8)L_\ell(z) - (\kappa/2)E^\circ(z)}{(w-z)^2} + \frac{\partial_z L_\ell(z)}{w-z} + \text{a term regular in } w \text{ at } z, \tag{6.9}$$

in this common separated testing class. The antiholomorphic identity follows by reflection with the corresponding derivatives. Thus the two dilation weights on (E°, L_ℓ) are triangular, with off-diagonal coefficient $-\kappa/2$ in each chiral part.

6.4 Finite conformal covariance and low-point consequences

Proposition 6.2. *Let $f : U \to U'$ belong to the finite-hole class of [1, Section 10, Theorem 10.1(ii)]. Such a map is conformal between the stated spherical domains and extends holomorphically with nonzero derivative across their analytic boundary components. In separated correlations,*

$$\begin{aligned} E^{\circ}_{f(U)}(f(z)) &= |f'(z)|^{-5/4} E^{\circ}_{U}(z), \\ L_{\ell;f(U)}(f(z)) &= |f'(z)|^{-5/4} \left[L_{\ell;U}(z) + \kappa \log |f'(z)| E^{\circ}_{U}(z) \right]. \end{aligned} \tag{6.10}$$

For several logarithmic slots we expand the product of these brackets. Each remaining scalar primary carries its usual factor.

Proof. Under a fixed analytic map, the midpoint and separation of the transformed pair are

$$\frac{f(z-s/2)+f(z+s/2)}{2} = f(z) + \frac{f''(z)}{8} s^2 + O(s^4), \tag{6.11}$$

$$f(z+s/2) - f(z-s/2) = f'(z)s + \frac{f'''(z)}{24} s^3 + O(s^5). \tag{6.12}$$

The product of the two density covariance factors is $|f'(z)|^{-5/24}[1 + O(r^2)]$. Combining this with the collision normalization gives weight $|f'(z)|^{-5/4}$ for Q_s, plus an identity remainder $O(r^{3/4})$ and a multiplication remainder $O(r^2[1 + |\log r|])$. These estimates are uniform on the separated compact test supports. The identity remainder vanishes because $2 - 5/4 > 0$.

The transformed separation has length $r' = |f'(z)|r[1 + O(r^2)]$, so

$$\log(\ell/r') = \log(\ell/r) - \log |f'(z)| + O(r^2). \tag{6.13}$$

Use the scalar covariance in the counterterm. The last logarithm in (6.13) yields the positive mixing term in (6.10). The sign agrees with (6.8), whose Ward convention differentiates the inverse pullback.

For the midpoint shift and the variable separation, use the same temporary smooth averaging in logarithmic radius and angle as in the Ward proof above. The map of these variables and the midpoint is a smooth diffeomorphism on the fixed compact averaging region, with the Taylor bounds above. Transfer it to the test and use the uniform distributional convergence of Z_s. Its $O(r^2)$ midpoint error acts on a uniformly smooth test rather than on a pointwise derivative of the cutoff correlation. The original raw limit exists independently and has the same average. This proves the assertion with one logarithmic insertion. Finite joint convergence and finite expansion give the assertion for any fixed number of slots. The map class is the finite-hole class of [1, Theorem 10.1 and Section 17.4], for which the input density covariance is available. □

6.5 The finite constants in the two- and three-point functions

Proposition 6.3 (Canonical low-point normalization)**.** *For the pair prescription (5.7), the finite constant in $\langle L_\ell \Phi\Phi \rangle$ is the same C_{LL} as in (5.86). Explicitly,*

$$\langle L_\ell(z)\Phi(u)\Phi(v)\rangle = \frac{|u-v|^{25/24}}{|z-u|^{5/4}|z-v|^{5/4}} \left[C_{LL} + \kappa C_\circ \log \frac{|z-u||z-v|}{\ell|u-v|} \right]. \tag{6.14}$$

Proof. Let

$$F(z;u,v) = \frac{|u-v|^{25/24}}{|z-u|^{5/4}|z-v|^{5/4}}.$$

Möbius covariance in Proposition 6.2 gives

$$\langle L_\ell(z)\Phi(u)\Phi(v)\rangle = F(z;u,v)\left[B + \kappa C_\circ \log\frac{|z-u||z-v|}{\ell|u-v|}\right]. \tag{6.15}$$

Indeed the length inside the logarithm gains the factor $|f'(z)|$ under a Möbius map. Subtracting that logarithm from the correlation divided by F leaves a Möbius-invariant distribution on distinct triples and hence a constant. The displayed function is its smooth representative. This is the logarithmic three-point form of [22, (21)] and [18, (1.24)]. Proposition 6.2 supplies its normalization for the present prescription.

Set $u = w - s/2$, $v = w + s/2$ in (6.15), form the centered pair at w, and subtract its scalar counterterm. Since $\langle L_\ell\rangle = 0$ and (5.85) holds, the sequential limit is

$$|z-w|^{-5/2}\left[B + 2\kappa C_\circ \log(|z-w|/\ell)\right].$$

Comparison with (5.86) yields

$$B = C_{LL}. \tag{6.16}$$

The product $O(|s|^2)\log(1/|s|)$ tends to zero in this fixed-distance limit, justifying the substitution in the logarithm's coefficient. Camia and Feng obtain the corresponding equality for their logarithmic prescription [18, (1.27)–(1.28)].

□

This equality of finite constants uses the canonical pair prescription. For a separately shifted field $L^{(u)} = L + uE^\circ$, the finite $L^{(u)}\Phi\Phi$ coefficient is $C_{LL} + uC_\circ$, whereas the $L^{(u)}L^{(u)}$ constant is $C_{LL} + 2uC_\circ$ because $\langle E^\circ L\rangle = C_\circ|z-w|^{-5/2}$ and $\langle E^\circ E^\circ\rangle = 0$. Subsequent mixed-fusion coefficients use the former coefficient.

7 The leading logarithmic–density fusion

We now bring L_ℓ close to a density mark and ask how well a single density insertion describes what is seen outside a larger disk. Paper II's annular estimate controls the error for every connection visible there. We write η for the exponent in (5.8) and fix $0 < \gamma < x$. At a cut of radius s, equations (4.5) and (5.9) give

$$\|\Phi\|_{s,*} \le Cs^{-x}, \quad \|E^\circ\|_{s,*} \le Cs^{-y}, \quad \|L_\ell\|_{s,*} \le Cs^{-y}(1 + |\log(\ell/s)|). \tag{7.1}$$

7.1 Propagation of an odd number of marks

An annulus can screen the details of a cluster carrying an odd number of marks. At mesh a, let $K^a_{s,d}$ be the annular kernel from a cut of radius s to one of radius d. It acts on the marked partitions of Section 4 by the parity rule. Let F^a_d be the positive outgoing row of one canonically normalized density root at the center, and set

$$m^a_d = F^a_d(\mathbf{1}), \qquad \sigma^a_d = F^a_d/m^a_d. \tag{7.2}$$

Here $m^a_d \asymp d^{-x}$ after the fixed-scale mesh limit, by [2, (6.5)]. The row F^a_d includes the root normalization. $K^a_{s,d}$ retains its original subprobability mass.

For any signed row ξ supported on realizable inputs of odd total parity, Paper II's signed screening estimate gives

$$\|\xi K^a_{s,d} - (\xi K^a_{s,d}\mathbf{1})\sigma^a_d\|_{\mathrm{var}} \le C\alpha^a_1(s,d)\alpha^a_1(2s,d/4)\|\xi\|_{\mathrm{var}}, \tag{7.3}$$

$$\|\xi K^a_{s,d}\|_{\mathrm{var}} \le C\alpha^a_1(s,d)\|\xi\|_{\mathrm{var}}. \tag{7.4}$$

These are [2, (6.6)–(6.7)]. α_1^a denotes the ordinary open one-arm probability, with fixed geometric buffers absorbed in C. Their hypotheses permit three odd blocks, and any number of even blocks. An open circuit joins the surviving odd marks into a single block. The bound includes the probability of survival of each input. By the one-arm ratio and quasi-multiplicativity in [2, (6.8)], the first arm factor is at most $C(s/d)^x$ after the fixed-scale mesh limit. The second is at most $C_\gamma(s/d)^\gamma$. Write $\limsup_{\mathrm{reg}}$ for the upper limit with the mesh removed first as in Section 4. If $\limsup_{\mathrm{reg}} \|\xi_s^a\|_{\mathrm{var}} \le Cs^{-x}$, then

$$\limsup_{\mathrm{reg}} \|\xi_s^a K_{s,d}^a - b_s^a F_d^a\|_{\mathrm{var}} \le C_\gamma d^{-x}(s/d)^\gamma, \qquad b_s^a = \frac{\xi_s^a K_{s,d}^a \mathbf{1}}{m_d^a}. \tag{7.5}$$

This is [2, (6.9)]. The coefficients b_s^a are bounded in the same order of limits, by (7.4).

7.2 Fusion at a running reference length

Choosing the reference length equal to the distance to the density removes the scale logarithm and isolates the leading amplitude.

Theorem 7.1 (Leading logarithmic–density fusion)**.** *For $|u| = 1$ and $0 < \rho < cd$, with $c > 0$ a sufficiently small fixed geometric constant,*

$$\big\|\rho^y L_\rho(z)\Phi(z+\rho u) - C_{LL}\Phi(z)\big\|_{d,*} \le C_\gamma d^{-x}(\rho/d)^\gamma. \tag{7.6}$$

At any fixed reference length $\ell > 0$ this gives

$$\begin{aligned}\big\|\rho^y L_\ell(z)\Phi(z+\rho u) - [C_{LL} + \kappa C_\circ \log(\rho/\ell)]\Phi(z)\big\|_{d,*} \\ \le C_\gamma d^{-x}(\rho/d)^\gamma[1 + |\log(\rho/\ell)|].\end{aligned} \tag{7.7}$$

The constants are uniform in the pair direction. These are complete-record estimates, including mesh-dependent bounded tests. For a fixed finite separated spectator word, its completion bound is included in C_γ.

Proof. Translate z to zero. Use disjoint local disks of radius $\rho/8$ around 0 and ρu, and enclose them by the cut $s = 3\rho$. Keep the logarithmic pair regulator smaller than $\rho/100$ while removing the mesh. Remove this regulator at the fixed positive distance ρ. Let ξ_ρ^a denote the resulting admissible row family for the packet

$$\rho^y L_\rho(0)\Phi(\rho u). \tag{7.8}$$

At the logarithmic source cut, the reference length ρ differs from the cut radius $\rho/8$ by a fixed factor. Equation (7.1) therefore bounds its row by $C\rho^{-y}$. The separate density row has mass at most $C\rho^{-x}$. Filling the remaining region and joining the two partitions is a substochastic operation. It follows that

$$\limsup_{\mathrm{reg}} \|\xi_\rho^a\|_{\mathrm{var}} \le C\rho^y\rho^{-y}\rho^{-x} = C\rho^{-x}. \tag{7.9}$$

Before we add the density, each term of the finite logarithmic regulator has zero or two local odd blocks. The density adds one odd mark, so a surviving record has one or three odd blocks. A merger may reduce three to one, but it preserves total parity and we still record the even blocks. These are the hypotheses for the projection (7.5), which we now apply to (7.9):

$$\limsup_{\mathrm{reg}} \|\xi_\rho^a K_{3\rho,d}^a - b_\rho^a F_d^a\|_{\mathrm{var}} \le C_\gamma d^{-x}(\rho/d)^\gamma. \tag{7.10}$$

The remaining task is to identify b_ρ^a to the required accuracy at this same cut.

Put a remote density at $v = 2d$, outside $B_d(0)$. Multiply its exterior completion by d^x and denote the resulting test by φ_d^a. Its own necessary root arm makes it uniformly bounded on every outgoing odd record. Evaluating the normalized density two-point function at the two centers, we find

$$\limsup_{a\downarrow 0} \|\varphi_d^a\|_\infty \le C, \qquad F_d^a(\varphi_d^a) \longrightarrow 2^{-2x} d^{-x} > 0. \tag{7.11}$$

These are the detector and its positive calibration in [2, (6.12)]. The detector joins the entire outgoing partition to the remote-root experiment before imposing the final even-parity rule.

Testing the difference in (7.10) with φ_d^a bounds $|b_\rho^a - C_{LL}|F_d^a(\varphi_d^a)$ by the projection error times $\|\varphi_d^a\|_\infty$ plus the absolute error in the correlation used as the test. Since $\|F_d^a\|/F_d^a(\varphi_d^a)$ is bounded by (7.2) and (7.11), the triangle inequality gives the same bound, up to a constant, for the row with coefficient C_{LL}.

Taking the reference length $\ell = \rho$ in the logarithmic three-point function (6.14) and dividing by the density two-point function, we obtain

$$\frac{\rho^y \langle L_\rho(0)\Phi(\rho u)\Phi(v)\rangle}{\langle \Phi(0)\Phi(v)\rangle} = \left|1 - \frac{\rho u}{v}\right|^{25/24} \left[C_{LL} - \kappa C_\circ \log\left|1 - \frac{\rho u}{v}\right|\right]. \tag{7.12}$$

The minus sign follows because the logarithm in (6.14) becomes $\log(|v|/|v - \rho u|)$. At $v = 2d$, the right side of (7.12) differs from C_{LL} by $O(\rho/d)$, uniformly in u, since both functions of $\rho u/v$ have bounded first derivatives on its closed disk of radius $1/4$. Consequently

$$\limsup_{\mathrm{reg}} \left|(\xi_\rho^a K_{3\rho,d}^a - C_{LL}F_d^a)(\varphi_d^a)\right| \le C d^{-x}\rho/d. \tag{7.13}$$

Apply this comparison to (7.10) and (7.13). Since $\gamma < x < 1$, the term ρ/d is bounded by $(\rho/d)^\gamma$. This proves (7.6). Uniformity over every bounded completion was supplied by the norm projection before the detector was chosen. The detector determines only the coefficient.

Finally, the reference-length identity (5.83) reads

$$L_\ell = L_\rho + \kappa \log(\rho/\ell) E^\circ. \tag{7.14}$$

Combine (7.6) with the scalar–density fusion [2, Theorem 4.5], in its original norm,

$$\|\rho^y E^\circ(z)\Phi(z + \rho u) - C_\circ \Phi(z)\|_{d,*} \le C_\gamma d^{-x}(\rho/d)^\gamma. \tag{7.15}$$

The triangle inequality and (7.14) give (7.7). □

8 Nested density collisions and the symmetric triple coefficient

The separation inside a density pair and the distance to a third density give two small scales. We keep the scalar counterterm as an insertion because this separates the error made inside the close pair from the error made when the pair approaches the third density.

Let $z_\pm = z \pm re^{i\theta}/2$, and put the third root at $z + \rho u$, where $|u| = 1$ and $0 < r < \rho/100$, $\rho < cd$. With the centered pair notation of Section 5,

$$Q_r(z,\theta) = r^{-25/24}\left[\Phi(z_-)\Phi(z_+) - r^{-5/24}\mathbf{1}\right]. \tag{8.1}$$

The mesh limit and the other local field-regulator limits are taken at fixed positive r, ρ, d before a collision limit.

Theorem 8.1 (Uniform renormalized nested limit)**.** *Under the logarithmic construction and the preceding conventions,*

$$\begin{aligned}&\|\rho^y\left[Q_r(z,\theta)-\kappa\log(\rho/r)E^\circ(z)\right]\Phi(z+\rho u)-C_{LL}\Phi(z)\|_{d,*}\\&\quad\le C_\gamma d^{-x}\left[(r/\rho)^\eta\{1+\log(\rho/r)\}+(\rho/d)^\gamma\right].\end{aligned}\tag{8.2}$$

In particular, the normalized error d^x times the left side tends to zero whenever $r/\rho\to 0$ and $\rho/d\to 0$, at arbitrary relative rates. For a fixed exterior cut this is convergence to $C_{LL}\Phi(z)$ in its complete-record norm.

Proof. Apply (5.8) at the local cut $\rho/8$, with reference length ρ. Fixed changes in the cut radius affect only the constant. Thus

$$\|Q_r(z,\theta)-\kappa\log(\rho/r)E^\circ(z)-L_\rho(z)\|_{\rho/8,*}\le C\rho^{-y}(r/\rho)^\eta[1+\log(\rho/r)].\tag{8.3}$$

Glue this error to the nearby density in a separate disk of radius $\rho/8$, and multiply by ρ^y. Equation (7.1) and contraction of the gluing kernel bound the resulting row on $B_{3\rho}(z)$ by

$$C\rho^{-x}(r/\rho)^\eta[1+\log(\rho/r)].\tag{8.4}$$

This row is supported on inputs of odd total parity, just as in the proof of (7.9). Propagate it to d using (7.4). Its necessary one-arm factor is at most $C(\rho/d)^x$ in the stated order of limits. The propagated bound is consequently

$$Cd^{-x}(r/\rho)^\eta[1+\log(\rho/r)].\tag{8.5}$$

Using only contraction by one at this step would leave the unwanted factor ρ^{-x}. The one-arm mass is needed.

The remaining term is $\rho^y L_\rho(z)\Phi(z+\rho u)$. Theorem 7.1 bounds its difference from $C_{LL}\Phi(z)$ by $C_\gamma d^{-x}(\rho/d)^\gamma$. Adding this bound to (8.5) proves (8.2). Each scale ratio has its own vanishing factor because $t^\eta[1+\log(1/t)]\to 0$ as $t\downarrow 0$. □

To recover the expansion of the original pair, we add the scalar term back into (8.2) and apply (7.15):

$$\begin{aligned}\rho^y Q_r(z,\theta)\Phi(z+\rho u)&=[C_{LL}+\kappa C_\circ\log(\rho/r)]\Phi(z)+\mathcal{R}_{r,\rho},\\\|\mathcal{R}_{r,\rho}\|_{d,*}&\le C_\gamma d^{-x}\left[(r/\rho)^\eta\{1+\log(\rho/r)\}+(\rho/d)^\gamma\{1+\log(\rho/r)\}\right].\end{aligned}\tag{8.6}$$

Here the second error is small only under the additional scale condition indicated by its formula. The theorem's unrestricted statement concerns the expression in (8.2), where the scalar counterterm remains an insertion until after the inner limit has been controlled. Replacing that insertion by its leading density coefficient introduces the product of the outer error with the inner logarithm in (8.6).

8.1 Boundary behavior of the fixed-shape triple coefficient

Paper II constructs a common leading coefficient for a triple of density roots. For distinct fixed points ζ_1,ζ_2,ζ_3, it is

$$\mathcal{C}(\zeta_1,\zeta_2,\zeta_3)=\lim_{R\to\infty}R^{2x}\langle\Phi(\zeta_1)\Phi(\zeta_2)\Phi(\zeta_3)\Phi(R)\rangle.\tag{8.7}$$

The existence and symmetry of this limit, and the bound

$$\left\| \rho^{2x} \prod_{j=1}^{3} \Phi(z+\rho\zeta_j) - \mathcal{C}(\zeta_1,\zeta_2,\zeta_3)\Phi(z) \right\|_{d,*} \le C_{\boldsymbol{\zeta},\gamma} d^{-x} (\rho/d)^{\gamma}, \tag{8.8}$$

are [2, Appendix A, Proposition A.1 and (A.1)]. The constants there are uniform on bounded template families whose three points remain a fixed positive distance apart. The function $\mathcal{C}$ is one four-density correlation with a field at infinity. This construction does not evaluate it at general shapes.

The logarithmic pair estimate determines its behavior near the boundary where two template points merge.

Proposition 8.2 (A logarithmic boundary expansion of the triple)**.** *For $|u| = 1$ and $\epsilon \downarrow 0$,*

$$\begin{aligned} &\epsilon^{2x}\mathcal{C}(-\epsilon e^{i\theta}/2, \epsilon e^{i\theta}/2, u) \\ &\quad = 1 + \epsilon^{y}\left[C_{LL} + \kappa C_{\circ}\log(1/\epsilon) + O(\epsilon^{\eta}[1+\log(1/\epsilon)])\right]. \end{aligned} \tag{8.9}$$

The error is uniform in u and θ. Since the coefficient is symmetric in its three arguments, permutation yields its expansion at the other two close-pair boundaries.

Proof. The pair identity (8.1), with $r = \epsilon$, is

$$\epsilon^{2x}\Phi(-\epsilon e^{i\theta}/2)\Phi(\epsilon e^{i\theta}/2) = \mathbf{1} + \epsilon^{y} Q_{\epsilon}(0,\theta). \tag{8.10}$$

Use (8.3) at a fixed local cut and reference length one to replace Q_ϵ by $L_1 + \kappa\log(1/\epsilon)E^{\circ}$. The local error has norm at most $C\epsilon^{\eta}[1+\log(1/\epsilon)]$. After joining the density at u, its odd packet has the same bound at a fixed enclosing cut.

To see that this error remains bounded uniformly in the far-probe limit, take a cut of radius comparable to R separating the packet from the root at R. Equation (7.4) bounds the propagated error by $CR^{-x}\epsilon^{\eta}[1+\log(1/\epsilon)]$. The remote root's completion has bound CR^{-x} before multiplication by R^{2x}. Thus the normalized four-point error is at most $C\epsilon^{\eta}[1+\log(1/\epsilon)]$ uniformly for large R. This justifies taking the limit in (8.7) after the pair replacement.

The identity term in (8.10) has limit one, since $R^{2x}|R-u|^{-2x} \to 1$. The scalar three-point formula [2, (4.11)] gives

$$\lim_{R\to\infty} R^{2x}\langle E^{\circ}(0)\Phi(u)\Phi(R)\rangle = C_{\circ}. \tag{8.11}$$

Similarly, (6.14) with $\ell = 1$ gives

$$\lim_{R\to\infty} R^{2x}\langle L_1(0)\Phi(u)\Phi(R)\rangle = C_{LL}. \tag{8.12}$$

Indeed, its logarithm is $\log(R/|R-u|)$ and tends to zero, while the nonlogarithmic prefactor tends to one after normalization. Substitute these limits and the uniform error into (8.10). This proves (8.9). Symmetry follows from that of (8.7). □

The proposition relates different close-pair boundaries through one symmetric three-density coefficient. The comparable-scale interior of the triple shape space is still represented by $\mathcal{C}$ itself. A truncated expansion at one boundary cannot be extended into a different collision regime without further estimates. In particular, (8.9) does not determine all subleading odd fields or compare arbitrary overlapping renormalized fusion procedures.

9 Two disjoint density pairs

The same common-row estimates also give a quantitative check with two disjoint pairs. Besides displaying the logarithmic coefficient, this calculation identifies the exact geometric factors that must be kept when one pair collapses much faster than the other.

Take two centers z, w, let $D = |z - w|$, and choose pair separations $re^{i\theta}$ and $se^{i\psi}$ with $r, s < D/100$. Define the normalized four-density correlation

$$G^{(4)}_{r,s} = (rs)^{2x}\langle \Phi(z - re^{i\theta}/2)\Phi(z + re^{i\theta}/2) \cdot \Phi(w - se^{i\psi}/2)\Phi(w + se^{i\psi}/2)\rangle. \tag{9.1}$$

It is divided by the product of the two internal pair correlations. Put $t_r = \log(D/r)$ and $t_s = \log(D/s)$. These logarithms will be written explicitly whenever a bound couples the two scales.

Proposition 9.1 (Two-pair expansion)**.** *With the exponent η reduced if necessary so that $0 < \eta < 2$,*

$$G^{(4)}_{r,s} = 1 + (rs/D^2)^y \left[C_{LL} + \kappa C_\circ \log \frac{D^2}{rs} + \mathcal{E}_{r,s} \right], \tag{9.2}$$

where

$$|\mathcal{E}_{r,s}| \le C\big[(r/D)^\eta(1 + t_r) + (s/D)^\eta(1 + t_s) + t_r(s/D)^2 + t_s(r/D)^2\big]. \tag{9.3}$$

The directions θ, ψ are unrestricted. When r/s remains in a fixed compact subset of $(0, \infty)$ and $\epsilon = \max(r, s)/D \to 0$, the error is $O(\epsilon^\eta[1 + \log(1/\epsilon)])$.

At arbitrary relative rates, the more precise form is

$$G^{(4)}_{r,s} = 1 + (rs/D^2)^y \left[C_{LL} + \kappa C_\circ t_r \left| 1 - \frac{s^2 e^{2i\psi}}{4(z - w)^2} \right|^{-y} + \kappa C_\circ t_s \left| 1 - \frac{r^2 e^{2i\theta}}{4(z - w)^2} \right|^{-y} + \widetilde{\mathcal{E}}_{r,s} \right], \tag{9.4}$$

with

$$|\widetilde{\mathcal{E}}_{r,s}| \le C\big[(r/D)^\eta(1 + t_r) + (s/D)^\eta(1 + t_s)\big]. \tag{9.5}$$

Each term on the right tends to zero with its own radius. Thus the remainder in (9.4) vanishes as soon as r/D and s/D both tend to zero.

Proof. Use reference length $\ell = D$ at both centers. For this proof write

$$Z_r(z) = Q_r(z, \theta) - \kappa t_r E^\circ(z), \qquad Z_s(w) = Q_s(w, \psi) - \kappa t_s E^\circ(w). \tag{9.6}$$

These are the finite pair subtractions with the limiting scalar. At fixed pair separations we first take the mesh limit, then remove the scalar regulators. Rewriting (8.1) at z, we obtain

$$r^{2x}\Phi(z - re^{i\theta}/2)\Phi(z + re^{i\theta}/2) = \mathbf{1} + r^y[Z_r(z) + \kappa t_r E^\circ(z)], \tag{9.7}$$

and the corresponding identity at w. Both Q and its scalar counterterm have zero vacuum mean. Also $\langle E^\circ(z)E^\circ(w)\rangle = 0$, as proved for the scalar prescription in [2, Theorem 4.4 and Section 5]. Multiplying the two identities therefore yields

$$G^{(4)}_{r,s} - 1 = (rs)^y\big[\langle Z_r(z)Z_s(w)\rangle + \kappa t_r\langle E^\circ(z)Z_s(w)\rangle + \kappa t_s\langle Z_r(z)E^\circ(w)\rangle\big]. \tag{9.8}$$

This expansion is performed after the fixed-separation continuum limits, before either pair radius is sent to zero.

Choose disjoint cuts of radius $D/8$ around z and w. Theorem 5.1, including (5.8) and (5.9), gives

$$\begin{aligned} \|Z_r(z) - L_D(z)\|_{D/8,*} &\le CD^{-y}(r/D)^{\eta}(1+t_r), \\ \|Z_s(w) - L_D(w)\|_{D/8,*} &\le CD^{-y}(s/D)^{\eta}(1+t_s), \\ \|Z_r(z)\|_{D/8,*} + \|Z_s(w)\|_{D/8,*} + \|L_D(z)\|_{D/8,*} + \|L_D(w)\|_{D/8,*} &\le CD^{-y}. \end{aligned} \tag{9.9}$$

For the last bound, use the first two and the boundedness of $t^{\eta}[1+\log(1/t)]$ on $(0, 1/100)$. At each finite mesh the two source experiments are independent before the common exterior is glued. The completion pairing has norm at most one. The tensor-product telescoping identity

$$Z_r \otimes Z_s - L_D \otimes L_D = (Z_r - L_D) \otimes Z_s + L_D \otimes (Z_s - L_D) \tag{9.10}$$

and (9.9) consequently imply

$$\left|\langle Z_r(z)Z_s(w)\rangle - \langle L_D(z)L_D(w)\rangle\right| \le CD^{-2y}\left[(r/D)^{\eta}(1+t_r) + (s/D)^{\eta}(1+t_s)\right]. \tag{9.11}$$

We have compared both subtractions at common mesh and cuts, so the inequality passes to their joint limit. The two terms in (9.11) come from changing one factor at a time, which is why each logarithm involves only the radius in its own error term.

The mixed pairings in (9.8) can be evaluated more sharply. The scalar three-point formula [2, (4.11)], the definition of Q_s, and $\langle E^{\circ}E^{\circ}\rangle = \langle E^{\circ}\rangle = 0$ give

$$\begin{aligned} \langle E^{\circ}(z)Z_s(w)\rangle &= C_{\circ}\left|(z-w)^2 - s^2e^{2i\psi}/4\right|^{-y}, \\ \langle Z_r(z)E^{\circ}(w)\rangle &= C_{\circ}\left|(z-w)^2 - r^2e^{2i\theta}/4\right|^{-y}. \end{aligned} \tag{9.12}$$

For example, the numerator s^{y-2x} in that three-point formula cancels the factor $s^{-(y-2x)}$ in Q_s. The two distances to $w \pm se^{i\psi}/2$ multiply to the modulus in (9.12). The logarithmic counterterm contributes zero because it is paired with E°.

Finally, (5.86) at reference length D gives

$$\langle L_D(z)L_D(w)\rangle = C_{LL}D^{-2y}. \tag{9.13}$$

Substituting (9.11)–(9.13) into (9.8), and factoring out $(rs/D^2)^y$, proves (9.4)–(9.5).

To obtain the simpler form, the function $|1-q|^{-y}$ has bounded first derivatives for $|q| \le 1/4$. Hence, uniformly in direction,

$$\left|1 - \frac{s^2e^{2i\psi}}{4(z-w)^2}\right|^{-y} = 1 + O((s/D)^2), \qquad \left|1 - \frac{r^2e^{2i\theta}}{4(z-w)^2}\right|^{-y} = 1 + O((r/D)^2). \tag{9.14}$$

These errors are multiplied by t_r and t_s, respectively. Together with $t_r + t_s = \log(D^2/(rs))$, this proves (9.2)–(9.3). When the radii are comparable, both logarithms are $O(1+\log(1/\epsilon))$ and $\eta < 2$ absorbs the quadratic terms into the stated remainder. □

9.1 Unequal pair separations

The cross terms in (9.3) are substantive. For example, set $s/D = \epsilon$ and $r/D = \exp(-\epsilon^{-3})$. Then both ratios tend to zero but $t_r(s/D)^2 = \epsilon^{-1}$. Thus that particular bound does not give an additive $o(1)$ remainder inside the simplified bracket of (9.2).

Keeping the two geometric factors in (9.4), we can take the two radii to zero independently. By (9.5),

$$\begin{aligned}&(D^2/(rs))^y(G^{(4)}_{r,s} - 1) \\ &\quad - \kappa C_\circ \left[t_r \left| 1 - \frac{s^2 e^{2i\psi}}{4(z-w)^2} \right|^{-y} + t_s \left| 1 - \frac{r^2 e^{2i\theta}}{4(z-w)^2} \right|^{-y} \right] \longrightarrow C_{LL}\end{aligned} \tag{9.15}$$

whenever $r/D, s/D \to 0$. The factors kept in this subtraction are the exact scalar–pair correlations from (9.12). They preserve the small geometric correction that an arbitrarily large logarithm of the other pair can amplify.

10 The logarithmic coefficient from the scalar null equation

The scalar field satisfies a null equation even when the distant experiment includes a logarithmic insertion. This allows us to compute one more three-point function. We use the angular averages

$$M_r(z) = \mathrm{av}_\phi\, r^y E^\circ(z)\Phi(z + re^{i\phi}) - C_\circ \Phi(z), \tag{10.1}$$

$$N_r(z) = \mathrm{av}_\phi\, r^y L_r(z)\Phi(z + re^{i\phi}) - C_{LL}\Phi(z). \tag{10.2}$$

At reference length r, both have dilation degree x by (5.84). We shall determine the constant a_L for which $B_r = N_r - a_L M_r$ has zero order-$r^{3/2}$ coefficient against a separated Ψ.

10.1 The inhomogeneous equation and its normalization

At infinity we use the coordinate $\zeta = 1/w$ with reference length one in that chart. By (6.10), $L(\infty)$ in the plane coordinate is the limit of $|w|^{2y}[L_1(w) - 2\kappa \log|w|\, E^\circ(w)]$ in separated correlations. Thus (6.14) gives

$$\langle L(\infty)\Phi(1)\Phi(0)\rangle = C_{LL}.$$

Define

$$F_0(z,\bar z) = \langle E^\circ(\infty)\Phi(1)E^\circ(z)\Phi(0)\rangle, \qquad G(z,\bar z) = \langle L(\infty)\Phi(1)E^\circ(z)\Phi(0)\rangle. \tag{10.3}$$

The first function and its nonzero second block are computed in [2, Theorem 4.8 and Section 11]. To justify the scalar null equation for the second function, keep the pair regulator defining L positive. It is a finite linear combination of density words from Paper II and the scalar subtraction, so the scalar null identity applies. Move the source derivatives to a compact test and then use (5.8), with a fixed separated stress contour for the L_{-2} term. Its limit is the null identity at the $E^\circ(z)$ insertion in G.

For a real auxiliary parameter δ near zero, introduce the differential operator

$$\mathcal{D}_\delta = \partial_z^2 + \frac{3(1-2z)}{2z(1-z)}\partial_z - \frac{5}{64z^2(1-z)^2} + \frac{3\delta}{2z(1-z)}. \tag{10.4}$$

The parameter has the formal meaning $h_\infty = 5/8 + \delta$. For an ordinary insertion of that weight at infinity, the global Ward identities give

$$\partial_0 F_\delta + \partial_1 F_\delta + \partial_z F_\delta = 0, \qquad \partial_1 F_\delta + z\partial_z F_\delta = (\delta - 2h_\Phi)F_\delta.$$

Substituting these derivatives into the level-two null equation yields $\mathcal{D}_\delta F_\delta = 0$. We use δ only as a parameter in this differential equation.

For G, the infinity Ward action instead contains $-\kappa E^\circ/2$ by (6.9). The corresponding dilation identity is

$$\partial_1 G + z\partial_z G = -2h_\Phi G - \frac{\kappa}{2}F_0.$$

The extra term from the logarithmic insertion becomes the forcing in the equations for G:

$$\mathcal{D}_0 G = \frac{3\kappa}{4z(1-z)}F_0, \qquad \overline{\mathcal{D}}_0 G = \frac{3\kappa}{4\bar{z}(1-\bar{z})}F_0. \tag{10.5}$$

10.2 A single-valued auxiliary solution

Writing $f = [z(1-z)]^{-5/8}u$ in (10.4) gives

$$z(1-z)u'' + \left(\frac{1}{4} - \frac{z}{2}\right)u' + \left(\frac{15}{16} + \frac{3\delta}{2}\right)u = 0.$$

Hence the hypergeometric parameters are

$$c = \frac{1}{4}, \qquad a = -\frac{1}{4} - \sqrt{1 + \frac{3\delta}{2}}, \qquad b = -\frac{1}{2} - a. \tag{10.6}$$

At $\delta = 0$ these are $(-5/4, 3/4, 1/4)$, as in the calculation of [2, Theorem 4.8, Section 11 and Proposition 14.1]. The normalized local blocks are

$$f_{0,\delta}(z) = [z(1-z)]^{-5/8}\,{}_2F_1(a, b; c; z), \tag{10.7}$$

$$f_{1,\delta}(z) = [z(1-z)]^{-5/8} z^{1-c}\,{}_2F_1(a-c+1, b-c+1; 2-c; z). \tag{10.8}$$

Their local powers, $-5/8$ and $1/8$, are independent of δ. These are the standard hypergeometric solutions [13, 15.10.2].

Set $g_j(z) = f_j(1-z)$. Since $a + b = -1/2$, the equation is invariant under $z \mapsto 1 - z$. Gauss's connection formula [13, 15.10.21] gives

$$\begin{pmatrix} f_0 \\ f_1 \end{pmatrix} = \begin{pmatrix} A & B \\ C & D \end{pmatrix} \begin{pmatrix} g_0 \\ g_1 \end{pmatrix},$$

where

$$A = \frac{\Gamma(c)\Gamma(c-a-b)}{\Gamma(c-a)\Gamma(c-b)}, \qquad B = \frac{\Gamma(c)\Gamma(a+b-c)}{\Gamma(a)\Gamma(b)},$$

$$C = \frac{\Gamma(2-c)\Gamma(c-a-b)}{\Gamma(1-a)\Gamma(1-b)}, \qquad D = \frac{\Gamma(2-c)\Gamma(a+b-c)}{\Gamma(a-c+1)\Gamma(b-c+1)}.$$

For real δ sufficiently close to zero, all four coefficients are real and nonzero. Because the two exponents at zero differ by $3/4$, the off-diagonal products acquire a nontrivial phase around zero and cannot occur in a single-valued solution. We must also eliminate the off-diagonal

terms in the basis g_0, g_1 at one. Using the connection matrix above, this fixes the ratio of the two diagonal coefficients as

$$b_{\mathrm{rel}}(\delta) = -\frac{AB}{CD} = -\frac{\Gamma(c)^2\Gamma(1-a)\Gamma(1-b)\Gamma(a-c+1)\Gamma(b-c+1)}{\Gamma(2-c)^2\Gamma(a)\Gamma(b)\Gamma(c-a)\Gamma(c-b)}. \tag{10.9}$$

At $\delta = 0$ this ratio is the signed coefficient $b_{\mathrm{rel}}(0) = -\mathfrak{k}^2$ of Paper II, with $\mathfrak{k}$ as in (4.8). Fixing the ratio leaves a one-dimensional space of single-valued homogeneous solutions. For weak solutions, the same conclusion follows by reducing each ordinary differential equation to its fundamental matrix, as in [2, Theorem 4.8, Section 11 and Proposition 14.1]. Smoothness is a consequence of these equations away from $0, 1, \infty$.

With a leading coefficient independent of δ, define

$$F_\delta = C_\circ^2(|f_{0,\delta}|^2 + b_{\mathrm{rel}}(\delta)|f_{1,\delta}|^2). \tag{10.10}$$

It is real analytic in δ on compact sets away from the punctures. The resonance of exponents at infinity when $\delta = 0$ causes no singularity here because the blocks at zero and the connection coefficients at one used above are regular there. Single-valuedness around zero and one also implies single-valuedness around infinity. At zero the normalization is $F_\delta = C_\circ^2|z|^{-5/4}(1+o(1))$, uniformly near $\delta = 0$.

10.3 Fixing the homogeneous ambiguity

Differentiate $\mathcal{D}_\delta F_\delta = 0$ at zero. From (10.4),

$$\mathcal{D}_0\, \partial_\delta F_\delta|_0 = -\frac{3}{2z(1-z)} F_0,$$

and the conjugate equation holds as well. Consequently $-\kappa\partial_\delta F_\delta|_0/2$ is a particular solution of the inhomogeneous equations (10.5). Subtracting this particular solution from G leaves a single-valued solution of both homogeneous equations, hence a multiple of F_0. The leading fusion and the spherical normalization give

$$\lim_{z\to 0} |z|^{5/4} G(z,\bar z) = C_\circ C_{LL}.$$

The leading coefficient of F_δ in (10.10) is independent of δ, so its derivative contributes nothing to this limit. We obtain

$$G = \frac{C_{LL}}{C_\circ} F_0 - \frac{\kappa}{2}\, \partial_\delta F_\delta|_0\,. \tag{10.11}$$

The leading coefficient of each local block in (10.7)–(10.8) equals one and does not depend on δ. Angular averaging therefore shows that the relative coefficient of the second scalar block in (10.11) is

$$\frac{C_{LL}}{C_\circ} - \frac{\kappa}{2}\, \frac{d}{d\delta} \log|b_{\mathrm{rel}}(\delta)|\Big|_{\delta=0}. \tag{10.12}$$

The first block contributes only at relative order r^2 after angular averaging, so the term of relative order $r^{3/2}$ comes entirely from the second block.

To evaluate the derivative, put $\psi = \Gamma'/\Gamma$. From (10.9), with $b = -1/2 - a$ and $c = 1/4$,

$$\frac{d}{da} \log|b_{\mathrm{rel}}|\Big|_{a=-5/4} = -\psi(9/4) + \psi(1/4) - \psi(-5/4) + \psi(3/4) = -\frac{48}{5}.$$

For the last equality, the recurrence $\psi(v+1) = \psi(v) + 1/v$ [13, 5.5.2] gives $\psi(9/4) = \psi(1/4) + 24/5$ and $\psi(-5/4) = \psi(3/4) + 24/5$. Since $a'(0) = -3/4$ by (10.6), the chain rule yields

$$\frac{d}{d\delta} \log|b_{\mathrm{rel}}(\delta)|\Big|_{\delta=0} = \frac{36}{5}, \qquad a_L = \frac{C_{LL}}{C_\circ} - \frac{18\kappa}{5}. \tag{10.13}$$

10.4 The three-point function with Ψ

The weak extraction at the $E^\circ(z)\Phi(0)$ pair in (10.11) gives

$$\langle L(\infty)\Phi(1)\Psi(0)\rangle = -a_L \mathfrak{k}^2 C_\circ^2. \tag{10.14}$$

To justify the extraction with a separated L, first keep its pair regulator fixed. Paper II's local Euler representation for Ψ applies to each of its separated terms [2, Sections 12–13]. After smooth testing in the center of the fusing pair, the truncated representation and its tail act on any exterior row. The bound for the tail is the exterior variation bound times an integrable power of the radial variable [2, Lemma 13.1, (13.7), and Sections 13.6–13.7]. Equation (5.9) bounds the compensated exterior rows uniformly. We can therefore truncate the radial integral, remove the logarithmic regulator at fixed truncation using (5.8), and then remove the truncation. One may center the extraction at the scalar point while translating the density by $-z$. Moving the center back by $O(|z|)$ translates the smooth test. In the leading primary term the linear displacement has zero circular mean, and the resulting $O(|z|^2)$ term is of higher order than $|z|^{3/2}$. The first angular terms of the scalar–density fusion have order $|z|$ by [2, Section 12], so their change under this translation also costs $O(|z|^2)$. The three-point covariance of E°, Φ, Ψ and the logarithmic Ward action determine all coordinate dependence from (10.14). Explicitly,

$$\begin{aligned}&\langle L_\ell(z)\Phi(u)\Psi(v)\rangle \\ &\quad = -\mathfrak{k}^2 C_\circ^2 \frac{|z-u|^{1/4}}{|z-v|^{11/4}|u-v|^{11/24}} \left[a_L + \kappa \log \frac{|z-u||z-v|}{\ell|u-v|}\right].\end{aligned} \tag{10.15}$$

The corresponding $E^\circ\Phi\Psi$ formula is the same prefactor without the square bracket, by [2, Theorem 4.8, Section 11 and Proposition 14.1]. Since Φ and Ψ have different dimensions, their two-point function is zero. Put $u = z + re^{i\phi}$ and $\ell = r$ in (10.15). After subtracting a_L times the scalar formula, the remaining logarithm is $\log(|z-v|/|z+re^{i\phi}-v|)$. Its first-order term has zero angular average, including the smooth expansion of the prefactor. On compact separated sets this proves

$$\langle B_r(z)\Psi(v)\rangle = O(r^{p+2}) = o(r^p). \tag{10.16}$$

Section 18 uses this correlation to identify the coefficient at order r^p.

11 Connections between interior roots and boundary arcs

Once an exploration has cut a slit, asking whether a marked cluster reaches the slit loses some information, since the cluster may reach one bank, the other, or both. We keep a separate label for each open boundary arc and ask for the whole partition of those labels and the interior marks. The two sides can share a Euclidean location all along the slit, so distance in the original domain does not distinguish them. In a disk coordinate the two banks occupy distinct boundary intervals. We will move these intervals slightly into the disk and estimate the probability that this changes a connection.

We use marked Carathéodory convergence as in [1, Sections 7.1–7.2]. If $g : \mathbb{D} \to U$ is the conformal map onto a simply connected domain with $g(0) = z$ and $g'(0) > 0$, the conformal radius of U at z is $\mathrm{crad}_U(z) = g'(0)$. Along a marked-convergent sequence the normalized maps converge locally uniformly in $\mathbb{D}$, and the inverse images of the labelled boundary prime ends converge in cyclic order. We use the compact families of [2, Section 7.1], with a common protected interior disk, an upper bound on the diameter of the domains, and a positive

lower bound on the separation of the marked angles. The interior roots and closed holes are separated from one another and from the edge of the protected disk. The holes have fixed positive sizes and uniform analytic boundary charts. We also allow the single open arc to shrink to a point or expand to the whole boundary, as described after Lemma 11.3.

Theorem 11.1 (Joint convergence of interior roots and boundary arcs)**.** *Consider critical site percolation on the triangular lattice along a marked-convergent sequence in such a family. Fix alternating boundary colors, give each open arc its own label as in [1, Lemma 7.3], and force the holes closed. For every partition in which each interior root connects to another root or to a labelled arc, the probability of that partition has a limit after density normalization at each root as in Section 4. The vector of limiting weights is continuous in the separated data, and convergence is uniform on compact families.*

Let K and K' be the unions of the closed holes in U and U'. Suppose $f : U\backslash K \to U'\backslash K'$ is a conformal bijection taking each hole boundary to its corresponding boundary and preserving the labels of the outer arcs. In disk coordinates for U and U', assume that f extends conformally across the outer unit circle. Then the weight in $U \setminus K$ equals the weight of the transported partition in $U' \setminus K'$ multiplied by $\prod_i |f'(q_i)|^x$, where q_i are the roots. The assertion includes the one-arc domain and its fully open and fully closed endpoints. Summing the admissible partitions with the parity rule of Section 4 gives the cluster-sign expectations.

11.1 Arm estimates at a boundary prime end

A small change in a boundary arc matters only if paths reach it from some distance away. We estimate those paths in a coordinate that distinguishes the two banks. Normalize the unperforated lattice domain to the disk and take a Möbius coordinate w sending the disk to the upper half-plane and the boundary point in question to 0. An arm across the half-annulus $r < |w| < R$, $\operatorname{Im} w > 0$, joins its two semicircles through sampled cells. Fixed exterior faces do not count toward an arm.

Lemma 11.2. *Choose R so the half-annulus misses the protected sets, and let $0 < r < R$. For $0 < \zeta < 1/3$, the mesh upper limits of the one-arm and alternating three-arm probabilities are bounded, respectively, by*

$$C_\zeta (r/R)^{1/3-\zeta}, \qquad C_\zeta (r/R)^{2-\zeta}.$$

Proof. We first cut the half-annulus at radii $2r$ and $R/2$ and denote the resulting inner and outer sides by I and O. We may take $R > 32r$, since a larger constant covers the remaining ratios. To make the cuts on the lattice, we follow the frontiers of the filled caps as in [2, Lemma 7.1, proof of (7.4)]. In disk coordinates the largest cell diameter tends to zero, so a path from radius r to radius R crosses both frontiers. The radial margins let us trim it to a sampled path from I to O. The frontier construction in the cited lemma also controls the marked corners. Short crosscuts about each corner separate it from the other three, so the corresponding marked angles converge in the disk of the cut domain. We can therefore apply ordinary quadrilateral crossing convergence to bound a single arm by the crossing probability in the round half-annulus, whose exponent is $1/3$ [9, Section 3, Theorem 3].

For three arms we need their order as well. Keep all sampled colors and give the quadrilateral an open exterior along I and a closed exterior along its three other sides. The interface from one corner of I to the other is the only boundary-to-boundary interface, because these corners are the only changes of boundary color. Consider three disjoint crossings, open, closed, open in order between the straight sides. Both open paths belong to the cluster of I, while the middle path belongs to the closed cluster of O. At the outer end of either open

path, the edge facing O has these two boundary clusters on opposite sides. It lies on the boundary-to-boundary interface, since a closed interface through that edge would separate the cluster on its inside from its own boundary arc.

Why must the interface return to I between the two contacts with O? Take a simple chain of cells along the middle closed arm. Its two sides face the two open paths because disjoint crossings of a quadrilateral preserve their boundary order. The interface cannot cross this chain through a closed cell or go around its outer end, which meets the closed exterior along O. To pass from one outer contact to the other it must go around the inner end, along the edge facing the open exterior on I. Thus the ordered visits are O, I, O. In this argument a lattice contact is with an incident edge. Its distance from the marked side in the normalized quadrilateral tends to zero by the cell-diameter bound, which is why an edge contact suffices in passing to curves. Color reversal handles the other alternating order.

In the disk coordinate of the cut quadrilateral, the full interface converges to chordal Schramm–Loewner evolution with parameter 6 (SLE_6), up to increasing reparametrization [1, Theorem 7.2 and Lemma 7.3]. Suppose a sequence of curves has the three visits and converges in this metric. Parametrize the curves on $[0, 1]$ so that they converge uniformly, and choose three successive visiting times on each. Compactness yields a subsequence on which the times converge to $t_1 \le t_2 \le t_3$. Since the marked sides converge as closed arcs, the limiting positions lie on O, I, O, respectively. The arcs I and O are disjoint compact sets, so continuity rules out either equality between successive times. This proves closedness, also for the vanishing edge offsets above. The upper bound for closed events under weak convergence now bounds the mesh upper limit by the probability of those visits for SLE_6.

To estimate that probability, realize the same limiting curve in the round half-annulus by its ordinary lattice approximations [7]. Because the curve starts and ends on I, the visits O, I, O break it into four successive portions, each of which traverses $4r < |w| < R/4$. The spare radial distance at both ends ensures that every sufficiently close approximating curve traverses this narrower half-annulus four times as well. In a coupling with uniform convergence, select one complete traversal from each portion of the simple lattice interface. In their spatial order they bound three disjoint strips. Along one bounding segment of each strip, follow the faces on the strip side. They have the same color along the interface, and successive faces either coincide or share an edge at a hexagonal-lattice vertex. They therefore form a connected monochromatic path. Since it lies between traversals, the path uses sampled faces. Trimming the endpoint cells leaves three disjoint arms across $5r < |w| < R/5$. The probability of the limiting visits is consequently at most the lower limit of the probabilities of these three arms in the regular approximations. Summing over their finitely many color orders and applying color switching in a topological rectangle, the half-plane exponent is $3 \cdot 4/6 = 2$ [9, Section 3, Remark 2 and Theorem 3]. This use of a regular reference quadrilateral is what makes the bound independent of the Euclidean shapes of the slit banks. □

11.2 Moving the boundary to an inner circle

For now replace each root by a labelled disk of fixed positive radius whose cells we fill open. A *terminal* is one such disk or a labelled open boundary arc. We record their connection partition Π_n at mesh a_n together with a finite vector H_n of arm and circuit indicators in protected smooth annuli. We evaluate these indicators in the original sampled colors, even if some of their cells are then filled to compute Π_n. This permits us later to condition on arms and still read every terminal connection in that same sample.

In disk coordinates move the boundary to $|w| = 1 - h$, carrying each label to the same interval of angles, and denote the resulting partition by $\Pi_{n,h}$. Both partitions use the same

colors in the common interior. Reserve a window of angular radius τ around each boundary color change. We take τ small enough that the windows are disjoint and h small compared with τ.

Lemma 11.3. *For $0 < \zeta < 1/3$ the two partitions can be compared with error*

$$\limsup_{n\to\infty} \mathbb{P}(\Pi_n \neq \Pi_{n,h}) \leq C_{\tau,\zeta} h^{1-\zeta} + C_\zeta \tau^{1/3-\zeta}.$$

The second term can be omitted for a monochromatic boundary.

Proof. Between successive windows we divide the collar into tiles of width between h and $2h$, up to constant factors at the ends, and move across them in angular order. For fixed h, τ, choose a simple lattice contour about the protected disk approximating the inner circle. In each of the disjoint narrow neighborhoods of the radial dividers, the small cell diameters allow a lattice-edge path from the contour to the outer bank. Stop at the first contact at either end and erase loops. Using the same divider for both adjacent tiles makes their boundaries fit together, so moving one tile replaces a single interval of the current boundary by the other sides of that tile and leaves the colors of its neighbors unchanged. On a monochromatic interval this move amounts to filling the tile with the bank color and putting that color on the newly exposed boundary. In particular an open move can only merge terminal components and a closed move can only separate them.

Around a tile away from the windows, choose a distance R comparable with τ and small enough to exclude the other terminals, the color changes and the protected sets. The two portions of the current bank on either side of the tile have the same color out to that distance. To apply planar duality, isolate a quadrilateral between two transverse cuts. Each cut starts on the current bank on one side of the tile, runs into the disk, and returns to the bank on the other side. For the inner cut we use dividers a bounded number of tiles apart and a concentric arc at depth comparable with h; for the outer cut the separations and depth are comparable with R. The bank between their endpoints forms the two remaining sides, or flanks. Both cuts can be chosen on cell edges. A sampled crossing between them traverses a half-annulus of radii Ch and cR in the original boundary coordinate, with fixed $C, c > 0$. The portion of the old collar behind the current bank is outside this quadrilateral.

Figure 2 shows the two configurations in this quadrilateral. To see how the separating arms arise, we use the following elementary form of planar duality. In a lattice quadrilateral with two open lateral sides, explore the open cluster reachable from the left side. If it misses the right side, its frontier facing right separates the lateral sides and joins the two transverse cuts. The cells just beyond this frontier are closed, since an open neighbor would have been reached. Following them produces a closed crossing between the cuts. The one-cell choices at the transverse cuts are absorbed by the radial margins.

Suppose first that an open tile move changes the partition. Some terminal previously disconnected from the bank now reaches it through the tile. Follow its old open path to the tile and select a simple subpath between the two transverse cuts, trimming it at its last inner and first subsequent outer contact in the outward direction. The path divides the quadrilateral in two. In the quadrilateral on the left, an open crossing from the path to the open flank would have joined the terminal to the bank before the move. Since those clusters were distinct, planar duality for triangular-lattice site percolation forces a closed crossing between the inner and outer cuts on that side. The same argument on the right forces a second closed crossing. The two separators are disjoint because they are on opposite sides of the open path. Neither can use the open flank, and the middle open path itself avoided the bank. We have obtained three sampled arms in closed, open, closed order.

On a closed tile move use the configuration *after* the move. If two terminals have lost their connection, follow their former connecting path from each end until it first reaches the tile. The two surviving pieces belong to distinct open components incident to the newly exposed interval. Each reaches beyond the outer cut, since the terminals lie outside the chosen neighborhood. Take a simple crossing between the cuts in each piece. The region between the crossings is itself a quadrilateral, with the two open paths as its lateral sides and subarcs of the cuts as its other sides. An open crossing between the lateral sides would reconnect the two terminal components after the move. Duality therefore forces a closed crossing between the cuts, now *between* the open paths. The outer flanks lie outside this middle quadrilateral, so its closed arm cannot run along the fixed closed bank. Here the three sampled arms are open, closed, open. In both cases all three arms lie on the interior side of the current bank. Their cells still have their original sampled colors, allowing us to apply Lemma 11.2 in the original domain at every move.

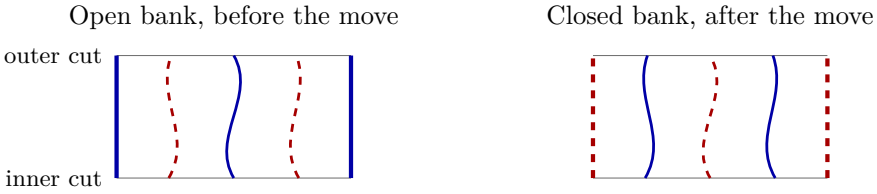

Figure 2: The quadrilateral around one tile, straightened so that the inner and outer cuts are horizontal. Solid curves are open, dashed curves are closed, and the vertical sides are the two flanks of the bank. On the left, a terminal path is disconnected from both open flanks, so a closed arm separates it from each. On the right, two terminal paths have become disconnected and a closed arm separates them. In both cases the three interior curves use sampled cells.

There are $O(h^{-1})$ tiles, each with change probability of mesh upper limit at most $C_\zeta(h/R)^{2-\zeta}$. Summing over them costs $C_{\tau,\zeta}h^{1-\zeta}$. Move each remaining tip window in one piece. Only one open bank is incident to a tip. A component in the common exterior that already meets this bank cannot acquire a new label just by meeting it again inside the window. A change therefore requires a different terminal component to reach the window through sampled open cells. Since every other terminal lies a fixed distance away, Lemma 11.2 bounds this probability by $C_\zeta\tau^{1/3-\zeta}$. Summing over the finitely many tips proves the estimate. □

If the only open arc shrinks to a point, include the whole arc in one window. Its label becomes isolated unless a sampled arm reaches from the window to a distant terminal. If instead the complementary closed arc shrinks, both open flanks belong to the same wired label, and the same one-arm bound controls a change. We thus obtain the monochromatic endpoint conventions in Theorem 11.1.

11.3 The joint limit for disks and roots

We first pass to the limit at fixed positive scales. For each $h > 0$ the inverse disk maps and their derivatives converge on a neighborhood of $\{|w| \le 1 - h\}$, so the inner circles and their marked arcs form a regular family as in Lemma 5.9. In the absence of holes, apply the crossing tests from its proof jointly with H_n. Join two terminals by a graph edge whenever a sampled open cluster touches both, using the incident-cell convention at each wired set. Since an open path splits at its visits to wired sets, the connected components of this finite graph recover the full wired partition, including the boundary labels [1, Section 11.1]. Its

joint limit with H_n is invariant under conformal transport: the interior crossing and circuit laws have that invariance, and the regularizations at the smooth arcs and their endpoints have vanishing errors in both domains [4, Theorem 9.5].

For closed holes use disjoint thin exterior collars, avoiding the annuli that define H_n. At fixed width there is positive probability of a surrounding closed circuit in every collar, so the preceding joint convergence allows us to condition on these events. Explore each circuit from the hole side as in [2, Lemma 7.1] and [1, Lemma 13.1]. Because this exploration reveals no sites strictly outside the selected circuits, the exterior sites keep their product law. Filling the enclosed regions closed preserves all connections among the exterior terminals. Each filled region lies between two deterministic offsets of its hole. On a surrounding cut the strip estimate of [1, Sections 12–13] bounds the error in replacing it by the hole itself, uniformly over bounded completions, including the wired labels. Taking the collar widths to zero therefore recovers the desired joint limit. For transport by f, take the collars on the domain side of the hole boundaries. At fixed collar width, the circuit events, the protected indicators and the buffered connection tests are functions of the crossing configuration restricted to the perforated domain. Their joint law is invariant under f by [4, Theorem 9.5]. Thus the conditional comparisons use the image collars. Their widths tend to zero as well, since the corresponding analytic Jordan boundaries admit conformal reflection in local charts. The strip estimate applies on both sides, as in the unrooted partition argument of [2, Lemma 7.1].

The indicators H_n are supported away from the boundary collar. Under our coupling they coincide before and after the move, so the total variation distance between the laws of (Π_n, H_n) and $(\Pi_{n,h}, H_n)$ is at most $\mathbb{P}(\Pi_n \neq \Pi_{n,h})$. At fixed h the inner-circle law has the unique limit just obtained. Hence any two subsequential limits of the original laws differ by at most twice the upper bound in Lemma 11.3. Letting first h and then τ tend to zero proves uniqueness.

We now compare the two outer boundaries under the map in the theorem. Write F for f in disk coordinates. On the outer circle let $F(e^{i\theta}) = e^{i\alpha(\theta)}$, with α an increasing lift of the boundary correspondence. Since F extends conformally across the circle, $\alpha'(\theta) = |F'(e^{i\theta})|$ is bounded above and away from zero. Taylor expansion in the inward radial direction gives, uniformly in θ,

$$1 - |F((1-h)e^{i\theta})| = h\alpha'(\theta) + O(h^2).$$

The image of the inner circle therefore lies between the circles of radii $1 - Ch$ and $1 - ch$, for some $0 < c < C$. Its angular coordinate is $\alpha(\theta) + O(h)$ and has positive derivative for small h by convergence in C^1. Thus the image is a radial graph, and the tip carried by it lies within $O(h)$ of its target angle.

To compare the partitions, couple this graph and the target outer circle in the same coloring. Outside the tip windows, use the radial dividers in the proof of Lemma 11.3, stopping each at the graph. Each tile still has width and depth comparable with h. A change of partition therefore requires the same three sampled arms, with total probability at most $C_{\tau,\zeta} h^{1-\zeta}$ in mesh upper limit. For fixed τ each displaced endpoint stays inside its tip window when h is small. The one-arm estimate there costs at most $C_\zeta \tau^{1/3-\zeta}$. The protected indicators lie inside both contours and agree in this comparison. At fixed h the positive-scale partition on the source inner circle has the same law as its image on the graph, by the interior and hole comparisons above. Letting $h \downarrow 0$ and then $\tau \downarrow 0$ identifies the joint laws on the two outer boundaries. At a monochromatic endpoint there are no tip windows.

Proof of Theorem 11.1. Choose disjoint interior disks $B(q_i, d_i)$ around the m roots. Write A_i for the event that the lattice root has an open arm to its disk boundary. Every admissible partition requires all the A_i. Since they concern disjoint disks, its normalized weight is its

probability conditional on $\bigcap_i A_i$ times

$$c_\Phi^m \prod_{i=1}^m \frac{\mathbb{P}(A_i)}{\pi_a} \longrightarrow c_\Phi^m \prod_{i=1}^m d_i^{-x},$$

where a is the mesh and c_Φ is the density constant of Section 4 [3, (2.1)].

Take $0 < \varepsilon < t/2 < \min_i d_i/8$ and wire each disk $B(q_i, t)$ with the label of its root. Under $\bigcap_i A_i$, every open circuit surrounding $B(q_i, t)$ inside $B(q_i, d_i/2)$ meets the root arm. Consequently any new path through a wired disk can be rerouted along that circuit, and the same circuit connects the root to every path that uses its label. Crossing estimates in disjoint annuli of fixed radius ratio bound the probability of missing all such circuits by a quantity tending to zero as $t \downarrow 0$. Positive association gives the same upper bound after the root-arm conditioning.

Replace this conditioning by requiring sampled arms from radius ε to d_i in the original colors. By the coupling of [3, Lemma 2.1 and Remark 2.2], applied in the disjoint root disks as in [1, Lemma 11.1], the two conditional samples agree outside common open circuits inside $B(q_i, t)$, with error tending to zero as $\varepsilon \downarrow 0$ at fixed t. On agreement the wired partitions are identical, since every site at which the samples can differ is inside a wired disk. At fixed ε, t the conditional wired probability is a ratio of joint probabilities whose limits we have just proved, and the denominator has a positive limit. Two subsequential rooted weights thus differ by at most the comparison errors times a bounded one-arm normalization. First send ε to zero and then t to zero. This proves convergence for each partition, including those of limiting weight zero.

For covariance, transport all three neighborhoods of each root with f. The conditional probabilities at fixed scales are conformally invariant. On a sufficiently small root neighborhood, both f and f^{-1} have bounded distortion, so the transported sets are bounded between concentric disks of comparable radii. The same circuit comparison therefore removes their inner cutoffs [1, Section 14, (14.1)–(14.3)]. What remains at root q_i is the normalized one-arm probability to its outer neighborhood V, proportional to $\operatorname{crad}_V(q_i)^{-x}$ by [5, Theorem 2.1]. As $\operatorname{crad}_{f(V)}(f(q_i)) = |f'(q_i)| \operatorname{crad}_V(q_i)$, the ratio of the original normalization to the transported one is $|f'(q_i)|^x$. Independence across the disjoint outer neighborhoods supplies the stated product.

It remains to pass from convergence along lattice domains to continuity in the continuum data. Let $D_j \to D$ be any sequence of separated marked configurations, where a configuration includes the domain, roots, holes and labelled arcs. Denote the limiting vector for a fixed configuration by $W(D_j)$. Follow an approximating sequence for each fixed D_j until its mesh is below $1/j$ and two errors are at most $1/j$. The first error is the distance of its marked data from D_j in a metric for the marked topology described above. The second is the sum of the absolute differences between its partition weights and the coordinates of $W(D_j)$. We can meet both requirements on the same mesh because the sequence approximates D_j and, along that sequence, each of the finitely many weights converges. The triangle inequality for the marked topology then takes these lattice approximations to D. The varying-domain argument above forces their weight vectors to tend to $W(D)$, hence $W(D_j) \to W(D)$ by the triangle inequality.

If convergence were nonuniform on a compact family, we could find marked configurations and lattice approximations with mesh and approximation error tending to zero, but with their weight vectors a fixed positive distance apart in the finite partition norm. On a subsequence the marked configurations converge. The varying-domain result for the lattice weights and continuity for the continuum weights then give the same limiting vector, a contradiction. □

12 Local Ward estimates and conformal images of circles

A circle centered at a source usually ceases to be a circle after a conformal change of coordinates. To estimate the change in its angular average, we first bound derivatives with respect to the source position. Theorem 11.1 allows us to move the interior sources and the marked boundary together while keeping track of which clusters connect them.

12.1 Derivatives on a fixed protected source patch

We obtain the ordinary source derivatives needed in the radial equation by integrating the stress field around the moving insertion. The contour lies in the protected interior, where its distance to the other insertions can be bounded below.

Lemma 12.1 (Finite-tip local regularity)**.** *Let all source points lie a distance comparable with r apart in a fixed protected disk, while the finite boundary tips lie outside that disk. For every fixed nonnegative integer j, the scalar finite-tip responses satisfy*

$$\left|\nabla_w^j \{r^y \langle (L_r - aE^\circ)(0)\Phi(w)\, C_\beta\rangle\}\right| \le C_j r^{-x-j}, \qquad |w| \asymp r. \tag{12.1}$$

The same estimate holds with $L_r - aE^\circ$ replaced by E°. Here a is a fixed real constant. The symbol C_β denotes a fixed linear test of the finite labelled partition with absolute value at most one, including its parity marks. Constants are independent of the separation of the boundary tips.

Proof. We first derive the weak Ward identity in a half-plane coordinate, keeping the boundary tips in a compact set of distinct real points. The stress center is ζ and the moving density is at w. Until the last step the local scalar or density-pair regulators have positive radii.

(i) *Transport of each partition.* For a stress ellipse of radius s, eccentricity parameter e and angle ϕ, put $t = es^2e^{2i\phi}$. The map in [2, (8.6)–(8.9)] sends the complement of the round disk at ζ onto the complement of its reflected image and preserves the real boundary. In disk coordinates it extends conformally across the outer circle, including the point corresponding to infinity. The normalized error from replacing the prescribed ellipse by this image tends to zero by the strip estimate [2, (8.8)], after attaching the other sources on their disjoint cuts. Apply Theorem 11.1 to the inverse map g_t on these complements, separately for every partition in the finite-regulator expression. It transports each root q with multiplier $|g_t'(q)|^x$ and each labelled arc with its endpoints. The test C_β thus evaluates the same labelled partition on both sides. In particular this operation also transports the two roots of a regulated logarithmic insertion.

(ii) *Removal of the round hole.* Test the moving interior coordinates and real tip positions against a smooth function supported on separated configurations. For the logarithmic slot also average the regulated pair against smooth kernels in log separation and angle as in Section 6. After a change of variables the inverse Jacobian and the root multipliers act on the test. Its change is $O(|t|)$ in each fixed test seminorm by [2, (8.9)]. At a separated cut the difference caused by the ordinary round hole is $O(s^b)$ for $1 < b < 5/4$ by the four-arm bound used in [2, Section 8.3]. Attaching the remaining sources costs their disjoint-cut norms. The term at $t = 0$ is independent of ϕ, so its second harmonic vanishes. The transported difference is consequently $O(|t|s^b)$ in the tested identity, and contributes $O(s^b)$ after division by es^2. For a scalar regulator the error in replacing its image by its affine disk tends to zero after that division by [2, (8.10)]. We remove the other source regulators at fixed s using (4.5) and (5.8), which are uniform over the

boundary completion. These bounds also identify the temporarily averaged limits with the raw ones.

(iii) *The coefficient of the angular variation.* The normalized integral against $e^{-2i\phi}$ selects the coefficient of t in the inverse map. Its holomorphic terms in the displacement and its spatial derivative at u are $t/(\zeta-u)$ and $t/(\zeta-u)^2$, respectively [2, (8.9)]. Integration by parts in the transported test therefore yields the simple pole $\partial_w/(\zeta-w)$ at the density. Expanding its multiplier supplies the double pole $(x/2)/(\zeta-w)^2$. In the doubled half-plane formula the reflected coordinate contributes the corresponding poles at $\bar{w}$; a real boundary tip u_j contributes only $(\zeta-u_j)^{-1}\partial_{u_j}$, since the arc label has weight zero. At the logarithmic slot the two root variations act on the midpoint and the separation of the pair. The separation derivative also acts on its logarithmic subtraction and produces the $-\kappa E^\circ/2$ double-pole coefficient in (6.8), hence the singular expansion (6.9). Letting $s \downarrow 0$ gives the weak identity. With additional separated stress insertions the same calculation applies at fixed disjoint cuts, by the mixed Ward hierarchy of [2, Theorem 4.4] and Section 6.

Choose a circle about w of radius cr which separates w from every other insertion and from every boundary mark. Integrating $T(\zeta)$ around it selects the simple pole of the density Ward identity. The double pole has zero residue, and every other term is analytic inside the circle. Hence

$$\partial_w\langle(L_r - aE^\circ)(0)\Phi(w)C_\beta\rangle = \frac{1}{2\pi i}\oint_{|\zeta-w|=cr}\langle T(\zeta)(L_r - aE^\circ)(0)\Phi(w)C_\beta\rangle\, d\zeta. \tag{12.2}$$

This is initially a distributional equality. The raw disjoint-source bound on its integrand is $Cr^{-(2+y+x)}$, since the reference length and all local cuts are comparable with r. After multiplying by the contour length and by r^y, we obtain the first derivative bound Cr^{-x-1}.

For each fixed order j, choose j nested circles separated from one another by distances comparable with r, with constants depending on j. On integrating the outer stress against $d\zeta$, its double pole at each inner stress has zero residue. Its simple pole differentiates the correlation in that inner stress coordinate. The integral of this derivative around the corresponding closed inner contour vanishes, since the correlation is single-valued and holomorphic along the contour. Opposite chiralities have no collision pole there by the mixed Ward identity. Thus each additional integral differentiates the moving density once more. A stress source costs r^{-2} and its contour has length of order r, so the finite stress hierarchy bounds the normalized jth derivative by $C_j r^{-x-j}$. Using conjugate contours for the antiholomorphic derivatives also controls every mixed derivative. Since the distributional derivatives of all orders are locally bounded, the correlation has a smooth representative in the interior variables, for which the Ward identities hold pointwise.

The constants in these estimates come from the source-row bounds and the norm-one exterior completion. They are therefore independent of the angular separation used during the derivation. Exhausting the set of distinct boundary angles by compact subsets extends the bounds to that whole set. □

Along $w = re^{i\phi}$ at fixed ϕ, a spatial derivative in $\log r$ acts by $w\partial_w + \bar{w}\partial_{\bar{w}}$. The factors of w and $\bar{w}$ supply one power of r per spatial derivative in (12.1). Differentiating the prefactor r^y multiplies it by y. On a fixed logarithmic window this gives a bound $C_j r^{-x}$ for the j-th derivative with respect to $\log r$ of a normalized packet. Differentiating its running reference length produces $-\kappa E^\circ$ by (5.83). These additional terms obey the same bound.

12.2 Interpolation after first-mode decay

Let $u(t)$ be a first angular mode on a unit logarithmic window about $t = \log r$. Suppose the one-arc equation of Section 13 gives $|u| \le Cr^{7/10}$. Lemma 12.1 gives $|u^{(5)}| \le Cr^{-x}$. The elementary five-point finite-difference estimate, obtained by cancelling the Taylor coefficients through order four, is

$$|u'(t)| \le C(\delta^{-1}\|u\|_\infty + \delta^4\|u^{(5)}\|_\infty).$$

Choose $\delta = r^{(7/10+x)/5}$. It follows that

$$|u'(t)| \le Cr^{(4/5)(7/10)-x/5} = Cr^{647/1200} \le Cr^{21/40}, \qquad 0 < r \le 1. \tag{12.3}$$

Lemma 13.2 derives the first-mode bound from the raw first-derivative estimates.

12.3 A uniform conformal-germ estimate

For a normalized univalent map f, write $f(w) = w + a_2w^2 + O(w^3)$ on a fixed disk. Two such maps are compared in the C^1 norm on a slightly larger disk. Denote their distance by δ. By Cauchy's formula the difference of their n-th Taylor coefficients is bounded by $C_n\delta$. After subtracting the quadratic term of $f - g$, its remainder on the smaller disk is bounded by $C\delta|w|^3$.

Lemma 12.2 (Dependence on the normalized germ)**.** *In the disk let C_θ denote completion by a compensating odd mark on its single wired open arc of angular length θ. For $\Xi = M$ or $\Xi = B$, write $\Xi_r(f)$ for its scalar value in this experiment when we transport the original averaging circle by f, including the density conformal multiplier. If $f(0) = g(0) = 0$ and $f'(0) = g'(0) = 1$, then*

$$|\Xi_r(f) - \Xi_r(g)| \le C\|f - g\|_{C^1} r^{61/40}. \tag{12.4}$$

Consequently its $r^{3/2}$ coefficient is independent of the normalized germ.

Proof. Put $b_0 = C_{LL} - a_L C_\circ$ and let U_k, V_k denote Fourier coefficients in ϕ with weight $e^{-ik\phi}$. For B, set

$$S_r(w) = r^y\langle (L_r - a_L E^\circ)(0)\Phi(w)C_\theta\rangle, \qquad U(r,\phi) = S_r(re^{i\phi}) - b_0\langle \Phi(0)C_\theta\rangle,$$

and use V for the analogous centered $E^\circ\Phi$ packet. Applying the same boundary completion to each row makes these quantities real numbers. The transported expression is

$$B_r(f) = \mathrm{av}_\phi\, |f'(re^{i\phi})|^x S_r(f(re^{i\phi})) - b_0\langle \Phi(0)C_\theta\rangle.$$

This follows from primary transport of the density and the normalization $f'(0) = 1$. The logarithmic field at the center therefore has no scale anomaly under this map.

On a smaller disk the straight interpolation $f_\lambda = (1-\lambda)g + \lambda f$ has derivative within $1/2$ of one by distortion, uniformly for $0 \le \lambda \le 1$. It is injective there. We differentiate the average with respect to λ and expand about the identity germ. Replacing f_λ by the identity in the linear variation introduces the quadratic error estimated below. Expand its variation as $\dot f(w) = \dot a_2 w^2 + O(\delta w^3)$. The quadratic term changes the radial coordinate by $r\Re(\dot a_2 re^{i\phi})$, the angle by $\Im(\dot a_2 re^{i\phi})$, and the density multiplier by $2x\Re(\dot a_2 re^{i\phi})$. Integration by parts in ϕ thus gives its first variation as

$$\frac{r\dot a_2}{2}\,[DU_{-1} + (2x - 1 - y)U_{-1} + \kappa V_{-1}] + \text{the conjugate-mode term}, \qquad D = r\partial_r. \tag{12.5}$$

Differentiating $S_r(re^{i\phi})$ with respect to r differentiates both its spatial argument and its reference length. The latter derivative is $-\kappa r^y \langle E^\circ(0)\Phi(re^{i\phi})C_\theta\rangle$ by (5.83), which moves to the other side with the positive sign in (12.5). The angular average of each leading scalar subtraction against a first harmonic is zero.

Lemma 13.2 below uses only the undeformed one-arc equation and the raw bound (12.1). That first-mode decay and (12.3) bound (12.5) by $C\delta r^{1+21/40} = C\delta r^{61/40}$. The cubic and higher terms, and the quadratic Taylor remainder, are bounded with the first two raw derivative estimates of Lemma 12.1. They contribute at most $C\delta r^{2-x} = C\delta r^{91/48}$, which is smaller. Uniform distortion bounds control the interpolation on the fixed small disk. Integration along it proves (12.4). The proof for M is the same with the logarithmic term omitted. Since $61/40 > 3/2$, division by $r^{3/2}$ proves the last assertion. □

13 The one-arc equation and its first scalar correction

With one open boundary arc, a surviving odd mark has only one possible destination. The width of the arc is still random under exploration. We use the equation for its angular width to calculate the first correction to the averaged response.

13.1 Radial exploration of the wired arc

Put the central insertion at 0 in $\mathbb{D}$, and let the wired arc run counterclockwise from 1 to $e^{i\theta}$, where $0 < \theta < 2\pi$. The complementary arc is dual-wired (closed). The open boundary class is marked as odd. Keep the previously fixed normalization of Φ and denote its positive full-wire value at the origin by $m_{\mathrm{w}} = \langle\Phi(0)\rangle_{2\pi}$. Write $w = re^{i\phi}$ and $D_r = r\partial_r$. For this boundary condition we define

$$S_E(r,\phi,\theta) = r^y\langle E^\circ(0)\Phi(re^{i\phi})\rangle_\theta, \qquad S_L(r,\phi,\theta) = r^y\langle L_r(0)\Phi(re^{i\phi})\rangle_\theta. \tag{13.1}$$

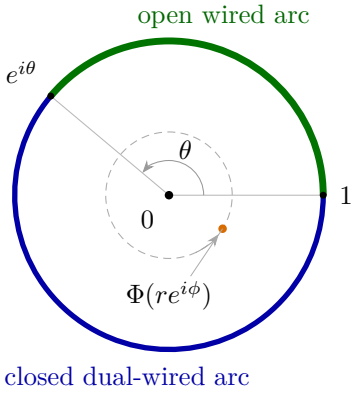

Figure 3: The canonical one-arc problem defining (13.1). The density moves around the small averaging circle while the central scalar or logarithmic source stays fixed. The estimate includes both limits in which a boundary arc disappears. The later four-tip transfer in Section 14 retains the conformal image of this original averaging circle.

The subscript denotes the alternating boundary colors, with the compensating odd mark on the open arc. We use radial Schramm–Loewner evolution with parameter 6 (SLE_6), in the capacity time for which $\mathrm{crad}(0) = e^{-t}$, with initial conformal radius one [10, Theorem 3]. At a stopped time with the protected neighborhoods intact, Theorem 11.1 identifies the

partition probabilities at fixed source regulators in the marked remaining domain. Indeed, first restrict to a compact class of marks. Any sequence of remaining domains in that class has a marked-convergent subsequence. The joint driving, map and mark convergence up to compact stopping is the argument of [2, Section 7.1 and the proof of the angular equation in Section 7]. Conditional on that stopped state the remaining filling has its product law. Fixed-regulator convergence and the uniform local Cauchy bounds then give the martingale identity for the completed response. Localization in time permits us to work up to the first boundary collision.

The chordal exploration becomes ordinary radial SLE_6 up to separation of the protected source from the target because the additional force coefficient in the coordinate change is $6 - 6 = 0$ [10, Theorem 3, p. 662]. In the frame rotating with the radial driving point, the Loewner equation gives

$$\begin{aligned} d\theta_t &= -\sqrt{6}\, dB_t + \cot(\theta_t/2)\, dt, \\ d\log r_t = v_{\mathrm{rad}}(r_t, \phi_t)\, dt, &\qquad d\phi_t = -\sqrt{6}\, dB_t + v_{\mathrm{ang}}(r_t, \phi_t)\, dt, \end{aligned} \tag{13.2}$$

The drift v_{rad} of the logarithmic radius and the angular drift v_{ang} are the real and imaginary parts of $(1 + w)/(1 - w)$ at $w = re^{i\phi}$. Their expansions and that of the derivative multiplier are

$$\begin{aligned} v_{\mathrm{rad}} &= 1 + \sum_{n \geq 1} r^n (e^{in\phi} + e^{-in\phi}), \\ v_{\mathrm{ang}} &= -i \sum_{n \geq 1} r^n (e^{in\phi} - e^{-in\phi}), \\ J &= 1 + \sum_{n \geq 1} (n+1) r^n (e^{in\phi} + e^{-in\phi}). \end{aligned} \tag{13.3}$$

In the last line we compute $J\, dt = d \log |g_t'(w)|$ by differentiating the radial Loewner vector field $w(1 + w)/(1 - w)$, which gives the factor $n + 1$. The central derivative is $g_t'(0) = e^t$.

To derive the interior equation from the stopped martingale identity, we test against a smooth function compactly supported in $(\log r, \phi, \theta)$. After localizing the smooth stochastic flow to this support, a change of variables moves the diffusion onto the test function. Its adjoint semigroup has derivative at time zero equal to the formal adjoint of the Itô generator there, so the martingale identity implies the distributional equation

$$\Big[3(\partial_\theta + \partial_\phi)^2 + \cot(\theta/2)\partial_\theta + v_{\mathrm{rad}} D_r + v_{\mathrm{ang}} \partial_\phi + y(1 - v_{\mathrm{rad}}) + xJ \Big]\, S_E = 0. \tag{13.4}$$

Indeed, the two occurrences of $-\sqrt{6}\, dB_t$ in (13.2) give the first term, the central field contributes y, the factor r^y contributes $-y v_{\mathrm{rad}}$, and the moving density contributes xJ.

The logarithmic reference must be transported at the same time. The convention $D_r L_r = -\kappa E^\circ$ implies

$$L_{e^{dt} r} = L_{r_t} + \kappa (v_{\mathrm{rad}} - 1)\, dt\, E^\circ + o(dt), \tag{13.5}$$

because $r_t = r(1 + v_{\mathrm{rad}}\, dt) + o(dt)$. Thus the left side of (13.4), with S_L in place of S_E, equals $-\kappa(v_{\mathrm{rad}} - 1) S_E$. The symbol κ throughout this calculation is the logarithmic mixing constant. The SLE parameter in (13.2) is 6.

Set

$$A_k = 3(\partial_\theta + ik)^2 + \cot(\theta/2)\partial_\theta, \qquad h(\theta) = \sin(\theta/4)^{1/3}. \tag{13.6}$$

Direct differentiation gives $(A_0 + x)h = 0$, $h(0) = 0$, and $h(2\pi) = 1$. The scalar one-point density is $m_{\mathrm{w}} h$. The quantity m_{w} is finite by the one-arm bound and positive by arm

extension to a full wired boundary. This follows either from the one-point version of (13.4), or from the same differential equation and the endpoint conditions proved below.

Let $C_\circ$ and C_{LL} be the leading fusion constants of S_E and S_L. For the fixed scalar a_L used in the completed packet, put $b_0 = C_{LL} - a_L C_\circ$ and define the centered functions

$$V = S_E - C_\circ m_{\mathrm{w}} h, \qquad U = S_L - a_L S_E - b_0 m_{\mathrm{w}} h. \tag{13.7}$$

The leading fusion estimate recalled earlier gives, for some $\gamma > 0$,

$$\|U(r,\cdot,\cdot)\|_\infty + \|V(r,\cdot,\cdot)\|_\infty \le C_\gamma r^\gamma. \tag{13.8}$$

Only convergence to zero in this estimate will be needed to remove the scalar ground state. The nonzero-mode argument below uses the raw local bounds instead of differentiating (13.8).

To display every forcing term, write

$$\mathcal{V}_r = (v_{\mathrm{rad}} - 1)D_r + v_{\mathrm{ang}}\partial_\phi - y(v_{\mathrm{rad}} - 1) + x(J-1). \tag{13.9}$$

Equations (13.4)–(13.7) give

$$\begin{aligned}
&[D_r + 3(\partial_\theta + \partial_\phi)^2 + \cot(\theta/2)\partial_\theta + x]V = -\mathcal{V}_r V - C_\circ m_{\mathrm{w}} \mathcal{V}_r h,\\
&[D_r + 3(\partial_\theta + \partial_\phi)^2 + \cot(\theta/2)\partial_\theta + x]U = -\mathcal{V}_r U - b_0 m_{\mathrm{w}} \mathcal{V}_r h - \kappa(v_{\mathrm{rad}} - 1)(V + C_\circ m_{\mathrm{w}} h).
\end{aligned} \tag{13.10}$$

For any periodic function f, use the Fourier convention

$$f_k(r,\theta) = \frac{1}{2\pi}\int_0^{2\pi} e^{-ik\phi} f(r,\phi,\theta)\, d\phi. \tag{13.11}$$

Multiplication of the convergent series in (13.3) then gives the exact identity

$$(\mathcal{V}_r f)_k = \sum_{n\ge 1} r^n \left\{ [D_r - y + x(n+1) + k - n] f_{k-n} + [D_r - y + x(n+1) - k - n] f_{k+n} \right\}. \tag{13.12}$$

This identity shows explicitly why the scalar correction involves the first angular modes and their radial derivatives.

13.2 The endpoint conditions

To choose the endpoint conditions for A_k, we follow the clusters as one of the boundary arcs shrinks. This distinguishes the solutions that remain bounded at a singular endpoint.

Lemma 13.1 (Boundary conditions at a vanishing arc)**.** *For fixed $0 < r < 1/4$, the functions U and V vanish as $\theta \downarrow 0$. Their scalar Fourier modes select the regular branch at $\theta = 2\pi$. Every nonzero Fourier mode vanishes at both endpoints.*

Proof. Keep the source neighborhoods inside $\{|z| < 1/2\}$. When the wired arc has length θ, a nonzero response to its odd mark requires a boundary arm from this arc to a fixed macroscopic distance. By Lemma 11.2, for each sufficiently small $\zeta > 0$ this event has probability at most $C\theta^{1/3-\zeta}$. After the exploration, the local row bound controls the signed source by a constant depending on r. Their product tends to zero with θ, which proves the assertion at the left endpoint.

At the other endpoint, couple the boundary condition with a closed arc of length $\delta = 2\pi - \theta$ to the full wired boundary. A change visible from $\{|z| < 1/2\}$ requires an open connection to

that small arc separated from the remaining wired boundary by two closed dual connections. These are three boundary arms. This description also covers a marked cluster losing its only wired attachment. Hence the half-plane three-arm estimate, with the same local row bound, yields

$$\sup_{\phi} |f(r,\phi,2\pi-\delta) - f(r,\phi,2\pi)| \le C_{r,\zeta}\delta^{2-\zeta}, \qquad f = U, V. \tag{13.13}$$

Here the three-arm exponent is 2 [9, Theorem 3]. The full wired disk is invariant under rotations about the origin. The source at the origin and both logarithmic reference conventions are scalar. Consequently the full-wire response is independent of ϕ, proving $f_k(r, 2\pi) = 0$ for $k \neq 0$.

(13.13) also determines the scalar operator domain. At fixed r, the equations above and the local source derivative bounds make $(A_0 f_0)(r,\theta)$ bounded. Since

$$A_0 g = 3m^{-1}(mg')', \qquad m(\theta) = \sin(\theta/2)^{2/3}, \tag{13.14}$$

integration near 2π gives $g(2\pi-\delta) - g(2\pi) = c\delta^{1/3} + O(\delta^2)$. Taking $0 < \zeta < 5/3$ in (13.13) forces $c = 0$. Equivalently, the right endpoint flux mg' is zero. For nonzero modes the additional regular first-order terms in A_k do not change its two indicial exponents, 0 and 1/3. Their vanishing endpoint values therefore select the killed realization at both ends. The scalar realization is killed at the left endpoint and regular at the right. □

13.3 The first angular harmonics

When the image of the averaging circle is slightly deformed, its first harmonics contribute to the angular average. We estimate how fast these harmonics decay as the circle shrinks.

Lemma 13.2 (First angular modes)**.** *For $f = U, V$, uniformly in $0 \le \theta \le 2\pi$,*

$$|f_1(r,\theta)| + |f_{-1}(r,\theta)| \le Cr^{7/10}. \tag{13.15}$$

Proof. We first prove a semigroup estimate for the killed realization of $A_k + x$, with $k = 1$ or -1. In $L^2(m(\theta)\,d\theta)$, put $v = \theta/2$ and make the unitary change of unknown, up to a constant factor,

$$f(\theta) = e^{-ik\theta}\sin(v)^{-1/3}u(v). \tag{13.16}$$

Direct differentiation gives

$$A_k + x \;\sim\; -\frac{3}{4}H_{a,b} + \frac{3}{16}, \qquad H_{a,b} = -\partial_v^2 + a(a-1)\csc^2 v - 2b\cot v, \quad a = \frac{2}{3}, \quad b = -\frac{2ik}{3}. \tag{13.17}$$

The killed branch $f = O(\theta^{1/3})$ becomes $u = O(v^{2/3})$. It is the Friedrichs branch of the inverse-square operator. Its closed sectorial form has domain $H_0^1(0,\pi)$ because the inverse-square coefficient is $-2/9 > -1/4$, and the $\cot v$ term is infinitesimally form bounded by the Hardy inequality and Cauchy–Schwarz. The resolvent is compact by the compact embedding $H_0^1(0,\pi) \subset L^2(0,\pi)$.

We give the spectral argument because its boundary condition and imaginary parameter are relevant here. The real-parameter Rosen–Morse eigenvalue formula is classical [12, (34), (49)–(50)]. The following factorization checks its applicability in the present realization. For $a > 1/2$ define the differential expressions

$$B_a = \partial_v - a\cot v + b/a, \qquad B_a^\sharp = -\partial_v - a\cot v + b/a. \tag{13.18}$$

The superscript $\sharp$ denotes this expression, not a Hilbert space adjoint when b is imaginary. Multiplication gives

$$\begin{aligned} H_{a,b} &= B_a^\sharp B_a + a^2 - b^2/a^2, \\ H_{a+1,b} &= B_a B_a^\sharp + a^2 - b^2/a^2. \end{aligned} \tag{13.19}$$

Thus B_a sends an eigenfunction of $H_{a,b}$ with eigenvalue E to an eigenfunction of $H_{a+1,b}$ with the same eigenvalue, unless it annihilates it. This statement respects the endpoint domains. Indeed, the Friedrichs expansion at zero is

$$u(v) = c\, v^a (1 - bv/a + O(v^2)); \tag{13.20}$$

the two leading terms cancel in $B_a u$, leaving $O(v^{a+1})$. At π the expansion has $+b(\pi - v)/a$ and gives the same cancellation. The exceptional kernel is the one-dimensional space spanned by $\sin(v)^a \exp(-bv/a)$, with eigenvalue $a^2 - b^2/a^2$.

Repeated application of $B_a, B_{a+1}, \dots$ must eventually reach such a kernel. Otherwise the fixed eigenvalue E would belong to $H_{a+N,b}$ for every N. Since b is purely imaginary, the real part of its quadratic form is that of $H_{a+N,0}$. The first line of (13.19) at $b = 0$ gives $\operatorname{Re} E \geq (a+N)^2$, a contradiction as $N \to \infty$. Conversely, lowering the displayed ground functions by the $B_j^\sharp$ produces a nonzero Friedrichs eigenfunction at each level. The kernel of $B_j^\sharp$ has endpoint behavior v^{-j} and contains no square-integrable function for $j > 1/2$. The operator has compact resolvent, so this exhausts its spectrum. Its eigenvalues are

$$E_n = (n+a)^2 - \frac{b^2}{(n+a)^2}, \qquad n = 0, 1, 2, \dots. \tag{13.21}$$

From (13.17), the corresponding positive decay rates of $A_k + x$ are

$$\lambda_{n,k} = \frac{3}{4}(n + 2/3)^2 - \frac{3}{16} + \frac{k^2}{3(n+2/3)^2}. \tag{13.22}$$

For $|k| = 1$ their minimum is $\lambda_{0,k} = 43/48$. All $n \geq 1$ give a larger value. For example the first eigenfunction in the original variable is $\sin(\theta/2)^{1/3} e^{-ik\theta/2}$, with the displayed ground eigenvalue.

The closed sectorial form generates an analytic semigroup. Its compact resolvent and the preceding spectral bound imply an L^2 decay estimate at every rate $\eta < 43/48$. One may obtain this estimate directly by moving the resolvent contour to $\operatorname{Re} z = -\eta$. The sectorial resolvent bound controls the unbounded parts of that contour. It also gives an ordinary supremum norm estimate after a fixed positive time. Indeed, the analytic semigroup maps L^2 into the operator domain and hence into its form domain, while

$$|u(v)| \leq \min(v, \pi - v)^{1/2} \|u'\|_{L^2} \quad \Longrightarrow \quad \|\sin(v)^{-1/3} u(v)\|_\infty \leq C \|u'\|_{L^2}. \tag{13.23}$$

For small times, the Fourier representation of the killed joint diffusion in (13.2), with $v_{\mathrm{rad}} = 1$ and $v_{\mathrm{ang}} = 0$, gives domination by the scalar killed diffusion, times e^{xt}. Combining the two bounds yields

$$\|e^{t(A_k + x)}\|_{\infty \to \infty} \leq C_\eta e^{-\eta t}, \qquad t \geq 0, \quad k = \pm 1, \quad \eta < 43/48. \tag{13.24}$$

It remains to bound the forcing in the coupled equations. The local row estimates and Lemma 12.1 give

$$\|f\|_\infty + \|D_r f\|_\infty + \|\partial_\phi f\|_\infty \leq C r^{-x}, \qquad f = U, V, \tag{13.25}$$

uniformly on fixed multiplicative windows in r. Since $v_{\mathrm{rad}}-1, v_{\mathrm{ang}}, J-1 = O(r)$, every right side in (13.10), including its logarithmic term, is $O(r^{1-x}) = O(r^{43/48})$ in the first modes. Fix $r_0 < 1/4$. Duhamel's formula with $t = \log(r_0/r)$ and (13.24) gives

$$\|f_{\pm1}(r)\|_\infty \le C(r/r_0)^\eta \|f_{\pm1}(r_0)\|_\infty + C\int_r^{r_0} (r/v)^\eta v^{43/48}\,\frac{dv}{v}. \tag{13.26}$$

The integral is $O(r^\eta)$ for $\eta < 43/48$. Taking $\eta = 7/10$ proves the lemma. □

13.4 Forcing of the angular average

Although each first harmonic has zero angular average, the exploration map couples it to the opposite harmonic of its coefficients. Their products survive averaging, so we need to bound the first modes to control the error in the scalar equation.

Lemma 13.3 (Error bound for the angular average)**.** *The scalar modes satisfy*

$$(D_r + A_0 + x)V_0 = F_E, \qquad (D_r + A_0 + x)U_0 = F_B, \qquad \|F_E(r)\|_\infty + \|F_B(r)\|_\infty \le Cr^{61/40}. \tag{13.27}$$

Proof. On a fixed logarithmic-radius window Lemma 12.1 bounds $D_r^5 f_{\pm1}$ by Cr^{-x}. We need only one radial derivative, so we interpolate with the stronger estimate (13.15) for the modes themselves:

$$\|D_r f_{\pm1}(r)\|_\infty \le Cr^{(4(7/10)-x)/5} = Cr^{647/1200} \le Cr^{21/40}, \qquad f = U, V. \tag{13.28}$$

This is (12.3) applied on a fixed multiplicative window.

The scalar Fourier coefficient of $\mathcal{V}_r h$ is zero because h is independent of r and ϕ, and $v_{\mathrm{rad}}-1, J-1$ have zero mean. Consequently (13.10) and (13.12) identify the entire forcing as

$$\begin{aligned} F_E &= -\sum_{n\ge1} r^n[D_r - y + x(n+1) - n](V_{-n} + V_n), \\ F_B &= -\sum_{n\ge1} r^n[D_r - y + x(n+1) - n](U_{-n} + U_n) - \kappa\sum_{n\ge1} r^n(V_{-n} + V_n). \end{aligned} \tag{13.29}$$

For $n = 1$, the derivative terms are bounded by $Cr^{1+21/40}$, and all the remaining terms by $Cr^{1+7/10}$. For $n \ge 2$, (13.25) and the geometric series give a bound Cr^{2-x}. Thus

$$r^{1+21/40} + r^{1+7/10} + r^{2-x} = O(r^{61/40}), \tag{13.30}$$

which proves the assertion. In particular (13.29) includes the change of logarithmic reference and all angular harmonics, not just a truncation of the conformal shape expansion. □

13.5 Jacobi projection and the coefficient at order $r^{3/2}$

The shifted scalar generator has the one-point profile as its zero mode. Centering removes that mode's limiting coefficient, and the first nonconstant mode determines the next possible power of r.

Lemma 13.4 (Uniform one-arc asymptotic)**.** *There are finite constants a_M and a_B such that*

$$\begin{aligned} V_0(r,\theta) &= a_M r^{3/2}\phi_1(\theta) + O(r^{61/40}), \\ U_0(r,\theta) &= a_B r^{3/2}\phi_1(\theta) + O(r^{61/40}), \\ \phi_1(\theta) &= \sin(\theta/4)^{1/3}\big(\cos(\theta/2) + 1/6\big). \end{aligned} \tag{13.31}$$

The error is uniform on the closed interval $0 \le \theta \le 2\pi$. The constants refer to the specified field normalizations and canonical one-arc boundary condition.

Proof. Put $t = \cos(\theta/2)$. Differentiating (13.6) gives the ground-state transformation

$$h^{-1}(A_0 + x)(hu) = \frac{3}{4}[(1-t^2)u'' + (-1/3 - 2t)u']. \tag{13.32}$$

This is the Jacobi generator with parameters $(\alpha, \beta) = (1/6, -1/6)$. Its invariant probability measure is

$$d\pi(t) = \frac{3}{2\pi}(1-t)^{1/6}(1+t)^{-1/6}\,dt, \qquad -1 < t < 1. \tag{13.33}$$

The normalization follows from $2\Gamma(7/6)\Gamma(5/6) = 2\pi/3$. The boundary conditions in Lemma 13.1 select the regular Jacobi realization. In particular no independent right-endpoint trace is added to the differential equation.

From the Jacobi differential equation and orthogonality [13, Tables 18.3.1 and 18.8.1], the eigenvalues of the negative generator in (13.32) are

$$\lambda_n = \frac{3}{4}n(n+1), \qquad n = 0, 1, 2, \dots. \tag{13.34}$$

The first three eigenvalues are $0, 3/2, 9/2$. To project onto the ground state 1 and the next polynomial $t + 1/6$, we use their norms under the Jacobi measure. Evaluating the beta integrals for the first excited mode, we find

$$\int (t + 1/6)\,d\pi(t) = 0, \qquad \int (t + 1/6)^2\,d\pi(t) = \frac{35}{108}. \tag{13.35}$$

Thus the first two spectral coefficients of a bounded function $f(\theta)$ are

$$\ell_0(f) = \int \frac{f}{h}\,d\pi, \qquad \ell_1(f) = \frac{108}{35}\int (t + 1/6)\frac{f}{h}\,d\pi, \tag{13.36}$$

where $\theta = 2\arccos t$ inside the integrals. Both functionals are bounded in the ordinary supremum norm because $d\pi/h$ is a constant multiple of $(1+t)^{-1/6}\,dt$, which is integrable at both endpoints. Write $P_0 f = h\ell_0(f)$ and $P_1 f = \phi_1 \ell_1(f)$.

Let T_s denote the semigroup of the scalar realization of $A_0 + x$. The Jacobi expansion, conjugated by h, gives

$$\|T_s - P_0 - e^{-3s/2}P_1\|_{\infty\to\infty} \le Ce^{-9s/2}, \qquad s \ge 1. \tag{13.37}$$

To check this estimate in the stated norm, use the endpoint bound $\|P_n^{(1/6,-1/6)}\|_\infty \le (7/6)_n/n! = O((1+n)^{1/6})$ from [13, (18.14.1)], and the squared norm $\|P_n^{(1/6,-1/6)}\|^2_{L^2(\pi)} \asymp (1+n)^{-1}$ from [13, Table 18.3.1]. Since $d\pi/h$ is integrable, the resulting series is bounded by $C\sum_{n\ge 2}(1+n)^{4/3}e^{-3n(n+1)s/4}$, which is at most the right side of (13.37) for $s \ge 1$. For $0 \le s \le 1$ we use the maximum principle for the scalar generator, which bounds $\|T_s\|_{\infty\to\infty}$ by e^{xs}.

Apply the projections to (13.27), first with $(f, F) = (V_0, F_E)$ and then with $(f, F) = (U_0, F_B)$. The ground coefficient satisfies $D_r\ell_0(f) = \ell_0(F)$. By (13.8) its limit at zero is zero, and hence

$$\ell_0(f(r)) = \int_0^r \ell_0(F(v))\,\frac{dv}{v} = O(r^{61/40}). \tag{13.38}$$

For the first coefficient the differential equation is $(D_r - 3/2)\ell_1(f) = \ell_1(F)$. Since $61/40 > 3/2$, the forcing is integrable against $v^{-5/2}\,dv$ near zero. In particular the coefficient

$$c_f = r_0^{-3/2}\ell_1(f(r_0)) - \int_0^{r_0} v^{-5/2}\ell_1(F(v))\,dv \tag{13.39}$$

is finite, and integrating the differential equation from zero to r yields

$$\ell_1(f(r)) = c_f r^{3/2} + O(r^{61/40}). \tag{13.40}$$

The coefficient in (13.39) is independent of the chosen r_0 by the same differential equation.

Finally apply Duhamel's formula to $(I - P_0 - P_1)f$. Its initial contribution is $O(r^{9/2})$, and (13.37) bounds the forcing integral by

$$C \int_r^{r_0} (r/v)^{9/2} v^{61/40} \frac{dv}{v} \le C r^{61/40}. \tag{13.41}$$

The part of the integral with $r \le v \le er$ uses the short-time bound and has the same order. Combining (13.38), (13.40), and (13.41) proves (13.31), with $a_M = c_{V_0}$ and $a_B = c_{U_0}$. □

The integral in (13.39) converges with margin $61/40 - 3/2 = 1/40$. Section 18 identifies which linear combination of its coefficients vanishes.

14 Radial exploration with four boundary tips

When one of the two interfaces finishes, the remaining marks see a single open arc. Before that time we must follow both the four boundary angles and the image of the small circle around the density. Two domains with the same angles can give different circles. We keep the local conformal map to estimate this difference.

We write $\mathbb{E}$ for expectation, with a superscript or subscript when the exploration law is changed.

14.1 The three boundary identifications

After the explored exterior has been saved, call the remaining quadrilateral clean when its four alternating arcs are the whole boundary word and all exterior identifications are deferred to completion. It has two active open banks, denoted by A and B. All occupations, port labels, and identifications outside this component were recorded by the exploration. Before imposing any additional external identification of A with B, an odd source has three possible nonzero states

$$U_A = \{A \text{ odd},\ B \text{ even};\ A \neq B\}, \qquad U_B = \{A \text{ even},\ B \text{ odd};\ A \neq B\},$$
$$J = \{A = B \text{ odd}\}.$$

Indeed, total parity is odd. A disappearing odd class is killed and a disappearing even class is erased. These are the finite-mesh parity rules used in the density construction [2, Section 4.2 and Lemma 4.1].

For a signed row $\nu = aU_A + bU_B + cJ$, we may attach the compensating odd mark to A, attach it to B, or wire the banks together before attaching it. If F_A, F_B, F_J denote the resulting responses, the parity rule relates them to the three partition coordinates by

$$F_A = a + c, \qquad F_B = b + c, \qquad F_J = a + b + c. \tag{14.1}$$

We can therefore recover the three coordinates from the boundary experiments:

$$a = F_J - F_B, \qquad b = F_J - F_A, \qquad c = F_A + F_B - F_J, \tag{14.2}$$

and hence

$$\|\nu\|_{\mathrm{var}} \le 2|F_A| + 2|F_B| + 3|F_J|. \tag{14.3}$$

To restore the exterior wiring we push the row forward under the map that identifies the wired blocks. This map has variation norm at most one, whatever the number of original exterior ports. Equations (14.1)– (14.3) are applied at a common mesh, after the genuine four-tip reduction.

14.2 Change of measure in a quadrilateral

Normalize the source to 0 and its conformal radius to 1. In the balanced parametrization the four boundary marks have arguments

$$0, \quad Z_1, \quad \pi, \quad \pi + Z_2, \qquad 0 < Z_1, Z_2 < \pi.$$

The opposite marks are targets. The other two are the current starts. Radial time t is chosen so that the conformal radius of the remaining source component is e^{-t}, as in [11, Section 4].

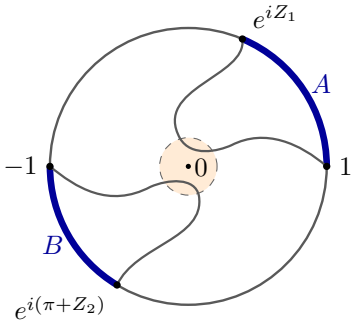

Figure 4: A quadrilateral with alternating boundary colors. The thick arcs are the two open banks A, B. The thin interior curves show one pairing in which both interfaces reach a small disk about the source. The four-arm survival exponent is $5/4$. Rescaling the density contributes $-5/48$ to the exponent of the mixed response, leaving $55/48$ in the radial recurrence of Section 15.

Write $Z = (Z_1, Z_2)$ for this angular state and F for the inverse uniformizing map, with physical lengths divided by the current conformal radius and axes rotated so that $F(0) = 0$ and $F'(0) = 1$. At time t write F_t for the updated normalized map. Let α be either of the two noncrossing link patterns, let $p_\alpha(Z)$ be its probability under the percolation law, and let $G_\alpha(Z)$ be its conditional two-curve Green function, the leading coefficient of the probability that both interfaces visit a small disk about the source [11, Theorem 1.1]. At the percolation parameter, Cardy's factor cancels the hypergeometric denominator in the conditional Green function. With a common positive normalization of the Green functions, the four-tip calibration of [2, Section 5.6, (4.13) and (5.24)] is therefore

$$p_\alpha(Z) G_\alpha(Z) = g(Z), \qquad g(Z) = \left[\sin Z_1 \sin Z_2 \cos \frac{Z_1 - Z_2}{2} \right]^{1/3}. \tag{14.4}$$

The omitted constant is common to the two patterns and cancels in every Radon–Nikodym ratio below. Equivalently, the full product of the six boundary chord lengths is $16 \sin Z_1 \sin Z_2 \cos((Z_1 - Z_2)/2)$.

Write τ_4 for the first loss of the four-tip source component. The conditional exploration and Zhan's four-sided radial law Q [11, Sections 3.4 and 4] are related, up to this time, by

$$\mathbb{E}_\alpha[\mathbf{1}_{\{t<\tau_4\}} H] = e^{-yt} G_\alpha(Z) \mathbb{E}_Z^Q \left[\frac{H}{G_\alpha(Z_t)} \right], \qquad y = \frac{5}{4}, \tag{14.5}$$

for nonnegative measurable functions of the stopped exploration. This is the change of measure on the stopped filtration in [11, (3.34)–(3.36) and proof of Lemma 5.4]. Integrable signed functions follow by their positive and negative parts.

Write $Q_t H(Z,F) = \mathbb{E}^Q_{Z,F} H(Z_t, F_t)$. Let H be one integrable unconditioned remaining response, measurable from the stopped state and the completion fixed by the exploration. The unconditioned remaining response gives the same function H of the stopped state for both initial link patterns. Summing over the original link patterns gives

$$\sum_\alpha p_\alpha(Z)\mathbb{E}_\alpha\left[\mathbf{1}_{\{t<\tau_4\}} H(Z_t,F_t)\right] = e^{-yt} g(Z)\, Q_t\left(\frac{H}{g}\right)(Z,F). \tag{14.6}$$

Here the common transformed law follows either by applying (14.5) to both labelings, or by observing that the combined transform in each case is by the same function $p_\alpha G_\alpha = g$. In the resulting sum of terminal factors,

$$\sum_\alpha \frac{1}{G_\alpha(Z_t)} = \frac{\sum_\alpha p_\alpha(Z_t)}{g(Z_t)} = \frac{1}{g(Z_t)},$$

which proves (14.6). The growth rule uses the same two starts and targets for both link patterns.

The two target images remain opposite. Their common rotation has finite variation given by the radial Loewner vector field at a target. The growth speeds are functions of Z [11, Section 4]. Two evolutions following the same reduced angular path therefore accumulate the same frame increment. In these coordinates the original averaging circle is carried into the disk by F^{-1}, defined on a fixed smaller disk by distortion. A change in F changes that inverse by at most a constant times the change in F in C^1 on a slightly larger disk. This follows from the inverse derivative formula and the uniform lower derivative bound there.

14.3 Dependence on the initial conformal map

Fix a disk $\{|z|<\eta\}$ with $\eta>0$ sufficiently small, and measure normalized germs in C^1 on that disk. All normalized univalent maps have uniform bounds on a slightly larger fixed disk. For two such maps $F, \widetilde{F}$,

$$F(z) - \widetilde{F}(z) = O(z^2)$$

there, with a universal constant, because their constant and linear terms agree. If both maps are driven for a further time u by the same angular path, the inverse Loewner map has derivative of modulus e^{-u} at the source. Its image of the fixed smaller disk has radius at most Ce^{-u} by distortion. Applying the preceding quadratic estimate and then multiplying by the normalizing factor e^u gives

$$d(F_u, \widetilde{F}_u) \le Ce^{-u} d(F,\widetilde{F}), \qquad u \ge 1. \tag{14.7}$$

The difference has a double zero and is bounded by $Cd(F,\widetilde{F})|z|^2$ on a smaller disk. Applying the Cauchy estimate on a smaller protected disk controls the derivative by the same bound. On a bounded interval the inverse Loewner map is a disk self-map fixing zero. Schwarz's lemma keeps the argument in the chosen disk, and the chain rule bounds its derivative there. Thus $d(F_u,\widetilde{F}_u) \le C_T d(F,\widetilde{F})$ after a fixed buffer of disks is chosen. These are the bounded-block and contracting estimates used below. The phase factors produced by the target frame have modulus one and are common to the two maps.

This contraction also constructs a stationary germ over a two-sided stationary angular path. Start a normalized map at time $-T$ and observe its normalized germ at time 0. For two choices with starting times earlier than $-T$, their difference at time 0 is at most Ce^{-T} by (14.7). The limit is measurable, is independent of the initial normalized map, and is invariant under time shifts. Denote the resulting stationary expectation of functions of (Z, F) by Π.

14.4 A weighted relaxation estimate

For the balanced angular process, [11, Lemma 5.1 and Corollary 5.3] give the uniform relative-density estimate

$$|k_t(Z, Z') - \pi(Z')| \le C_{t_0} e^{-11t/4} \pi(Z'), \qquad t \ge t_0 > 0. \tag{14.8}$$

The density in these coordinates is

$$\pi(Z_1, Z_2) = \frac{1}{3\pi} (\sin Z_1 \sin Z_2)^{1/3} (\sin Z_1 + \sin Z_2). \tag{14.9}$$

Indeed, the change of variables used in that calculation is

$$X = \cos \frac{Z_1 + Z_2}{2}, \qquad Y = \sin \frac{Z_1 - Z_2}{2},$$

with $1 - X^2 - Y^2 = \sin Z_1 \sin Z_2$ and Jacobian $(\sin Z_1 + \sin Z_2)/4$. Substituting these identities in [11, (5.12)] gives (14.9).

Define

$$w(Z) = 1 + g(Z)^{-1},$$

and let $\mathcal{B}$ be the class of measurable functions for which

$$\begin{aligned} \|H\|_{\mathcal{B}} = & \sup_{Z,F} \frac{|H(Z,F)|}{w(Z)} \\ & + \sup_{Z, F \neq \widetilde{F}} \frac{|H(Z,F) - H(Z,\widetilde{F})|}{w(Z) d(F, \widetilde{F})} < \infty. \end{aligned} \tag{14.10}$$

No angular derivative is required in this definition. From (14.4) and (14.9),

$$\frac{\pi(Z)}{g(Z)} = \frac{2}{3\pi} \sin \frac{Z_1 + Z_2}{2} \left(\cos \frac{Z_1 - Z_2}{2} \right)^{2/3}. \tag{14.11}$$

In particular, $\pi(w) < \infty$, including at the corners where the boundary tips collide.

Lemma 14.1 (Convergence of the angle and conformal map to equilibrium)**.** *For $H \in \mathcal{B}$ and $t \ge 1$,*

$$\sup_{Z,F} |Q_t H(Z,F) - \Pi H| \le C e^{-11t/15} \|H\|_{\mathcal{B}}. \tag{14.12}$$

The same estimate holds in the weighted supremum norm $\|H\|_{w,\infty} = \sup |H|/w$. At time zero, $\|H - \Pi H\|_{w,\infty} \le C \|H\|_{\mathcal{B}}$.

Proof. Split $t = v + u$. By the common-part coupling of probability measures, (14.8) permits the angular state at time v to be coupled with its stationary law so that each failure marginal is dominated by $Ce^{-11v/4}\pi$. Conditional on the coupled angles, sample the two corresponding germs according to their conditional laws. This preserves each joint state law.

On successful coupling, drive the two states with the same future angular path for time u. Their common angular marginal is dominated by π at time v and remains so at time t. Hence (14.7) and (14.10) bound the successful part of the difference by

$$C\|H\|_{\mathcal{B}}e^{-u}\pi(w).$$

On failure, stationarity propagates the two bounds $Ce^{-11v/4}\pi$ to the final time. The absolute-value part of the norm therefore bounds the failed part by

$$C\|H\|_{\mathcal{B}}e^{-11v/4}\pi(w).$$

This uses domination of the failure marginals, not only a bound on the failure probability. It is the reason the singular weight causes no loss of exponent.

Choose $v = 4t/15$ and $u = 11t/15$. The displayed bounds prove (14.12) when both subintervals exceed fixed positive constants. The remaining bounded time interval is absorbed in C using (14.8) at a fixed positive time and the bounded germ diameter. Finally $w \geq 1$ gives the weighted version, and $|\Pi H| \leq \|H\|_{\mathcal{B}}\pi(w)$ proves the assertion at time zero. □

15 A radial recurrence in a quadrilateral

In this section Ξ_r denotes either M_r or B_r. Both have total odd parity and obey the matched dilation rule

$$\Xi_r(z) = \lambda^x \Xi_{\lambda r}(\lambda z). \tag{15.1}$$

For B_r, the running reference length in L_r is essential for this identity. In particular, no fixed-reference logarithm is introduced during a radial rescaling.

Let $F_\beta(r; Z, F)$ be its response to one of the three completions in (14.1). For a sufficiently small fixed ρ_0, put

$$\rho_m = \rho_0 e^{-m}, \qquad H_m(Z,F) = \frac{F_\beta(\rho_m; Z, F)}{\rho_m^s g(Z)}, \qquad s = y - x = \frac{55}{48}. \tag{15.2}$$

The dependence on the packet and completion is suppressed only in this section. All assertions apply to each of their finitely many choices.

Lemma 15.1 (Exact radial block identity)**.** *The normalized responses satisfy*

$$H_{m+1} = Q_1 H_m + e_m. \tag{15.3}$$

Here e_m is the normalized response on paths which leave the four-tip sector during the next unit of radial time. Moreover,

$$\|H_0\|_{\mathcal{B}} \leq C, \qquad \|e_m\|_{\mathcal{B}} \leq Ce^{-qm}, \qquad q = \frac{17}{48}. \tag{15.4}$$

If the one-arc coefficient in Lemma 13.4 is a_Ξ, then

$$e_m = e^{-qm} e_* + \delta_m, \qquad \|\delta_m\|_{\mathcal{B}} \leq Ce^{-(q+1/40)m}, \tag{15.5}$$

where e_* is independent of the initial normalized germ and is a_Ξ times a profile depending only on the chosen completion and the fixed starting radius ρ_0.

Proof. Choose ρ_0 so small that the source circle and its regulator disks remain protected during one unit of radial time. This choice is uniform because the source component has conformal radius at least e^{-1} until the end of that block, and Koebe's theorem supplies a fixed Euclidean protecting disk. Thus the stopped exploration does not query the local source regulators.

On a surviving path the factor e^{-y} comes from (14.6), and rescaling the remaining domain by e contributes e^{x} by (15.1). Dividing by the normalization in (15.2) leaves

$$e^{s+x-y} = 1.$$

Consequently the paths that survive contribute $Q_1 H_m$ and those that exit contribute e_m. Adding the two proves (15.3).

At a four-tip exit time $\tau \le 1$, the remaining source component has at most two active tips. By parity its response either vanishes or comes from one open bank carrying the odd mark. The exterior then acts by the same contraction for every local packet, since the transcript fixes its completion. The one-arc bound of Lemma 13.4 and the bounded rescaling during the block give an exit response of size $C\rho_{m+1}^{p}$, where $p = 3/2$. After division by $\rho_{m+1}^{s} g(Z)$ this is bounded by $C\rho_{m+1}^{q} w(Z)$.

For the germ-Lipschitz seminorm, the canonical exploration law depends on Z but not on the initial conformal map. Apply Lemma 12.2 to the two resulting one-arc source curves, using that a bounded radial block changes their germ distance by at most a fixed factor. Its bound is $C\rho_{m+1}^{q+1/40} w(Z)$ after division by $\rho_{m+1}^{s} g(Z)$. This proves the estimate for e_m in (15.4). The fixed-radius Ward bound of Lemma 12.1 proves the assertion for H_0.

For the leading term, write the one-arc asymptotic as $a_\Xi r^p \phi_1$ plus its uniform remainder. Its contribution at exit time τ is

$$a_\Xi \rho_{m+1}^{p} e^{(x+p)\tau} \phi_1,$$

using the same exterior completion. The expectation of this expression, divided by $\rho_{m+1}^{s} g(Z)$, is $e^{-qm} e_*$. Its angular profile and its completion depend only on the canonical exploration, so e_* is independent of F and is linear in a_Ξ. The weighted supremum bound on δ_m follows from the one-arc remainder estimate. The leading term has zero germ-Lipschitz seminorm, and the preceding shape estimate gives the same rate for the seminorm of δ_m. This proves (15.5). □

Proposition 15.2 (The stationary coefficient and first radial correction)**.** *There is a constant*

$$K_\beta = \Pi H_0 + \sum_{j=0}^{\infty} \Pi e_j \tag{15.6}$$

such that $H_n \to K_\beta$ in weighted supremum norm. More precisely,

$$H_n = K_\beta + e^{-qn} h_* + O_{w,\infty}\big(e^{-(q+1/40)n}\big), \tag{15.7}$$

where

$$h_* = e^{q} \sum_{k=0}^{\infty} e^{qk} (Q_1^k - \Pi) e_* - \frac{\Pi e_*}{1 - e^{-q}}. \tag{15.8}$$

The series converges in weighted supremum norm and depends linearly on e_*.

Proof. By (15.4) and $\pi(w) < \infty$, the scalar series in (15.6) converges absolutely. Iterating (15.3) and subtracting that series gives

$$H_n - K_\beta = (Q_1^n - \Pi)H_0 + \sum_{j=0}^{n-1}(Q_1^{n-1-j} - \Pi)e_j - \sum_{j=n}^{\infty}\Pi e_j. \tag{15.9}$$

Lemma 14.1 applies to every positive-lag term. For the zero-lag term, its time-zero weighted bound applies instead. Thus (15.4) first gives $H_n - K_\beta = O_{w,\infty}(e^{-qn})$.

Substitute (15.5) into (15.9). Multiplying the leading convolution by e^{qn} and writing $k = n - 1 - j$ gives

$$e^q \sum_{k=0}^{n-1} e^{qk}(Q_1^k - \Pi)e_*.$$

Because $11/15 > q$, the decay of $Q_1^k - \Pi$ dominates the factor e^{qk}, and the series converges. The leading stationary tail is

$$-e^{qn}\sum_{j=n}^{\infty} e^{-qj}\Pi e_* = -\frac{\Pi e_*}{1 - e^{-q}}.$$

These two expressions give (15.8).

The remaining convolution is bounded, before normalization, by

$$C\sum_{j=0}^{n-1} e^{-(11/15)(n-1-j)}e^{-(q+1/40)j}.$$

Since

$$\frac{11}{15} - q = \frac{91}{240} > \frac{1}{40},$$

this is at most $Ce^{-(q+1/40)n}$. The initial-data term, the omitted leading-series tail, and the stationary remainder tail satisfy the same bound. This proves (15.7). □

Algebraically, (15.8) satisfies

$$(e^{-q}I - Q_1)h_* = e_*.$$

Absolute convergence follows from $11/15 > q$.

To pass from radii on a geometric sequence to every sufficiently small radius, let its starting radius ρ_0 range over one compact multiplicative interval. The preceding estimates are uniform on this interval. The leading exit coefficient in (15.5) is ρ_0^q times a common profile, and the factor ρ_0^q cancels on restoring the r^{-p} normalization. To compare the critical constants for two choices of ρ_0, apply the exact block identity for the fractional time between the starting radii. As the common small scale tends to zero the exit contribution is $O(r^q)$, while Q_t preserves constants, so the two choices have the same critical constant.

Lemma 15.3 (Detection of the leading coefficient in a quadrilateral)**.** *Fix one of the three boundary completions and a nondegenerate balanced quad. If its response satisfies*

$$F_\beta(r; Z, F) = o(r^s),$$

then $K_\beta = 0$. In particular, a finite r^{-p} limit for that fixed response implies this cancellation. If only a linear combination of the boundary completions is accessible to the test, the conclusion holds only for the corresponding linear combination of their amplitudes.

Proof. Restoring the normalization in (15.7) gives $r^{-s}F_\beta(r; Z, F) \to g(Z)K_\beta$. In the interior angular state space $g(Z) > 0$, and $p > s$. This proves all assertions by linearity. To use a distributional test with a moving center, one also needs positivity on a set of positive area. Proposition 17.2 supplies that step. □

16 Expansion on an arbitrary observation circle

We now put back the parts of the exploration outside the first quadrilateral. The number of connections there is unrestricted. A long delay before the first four-tip domain appears requires six arms, whose probability controls the accumulated error.

16.1 Balancing the four marked points

The balanced parametrization imposes no separation hypothesis on an initial quad. Label its four tips cyclically by $1, 2, 3, 4$, choose targets $\{2, 4\}$ and starts $\{1, 3\}$, and grow the start in the shorter arc between the two targets. Both noncrossing pairings connect each chosen start to a chosen target. Therefore this exploration need not be conditioned on a link pattern.

Before the four-tip component is lost, write $a, b > 0$ for the two angular distances from that start to the targets, with $a + b = \Delta \le \pi$. The radial Loewner equation gives

$$\frac{d\Delta}{dt} = \cot(a/2) + \cot(b/2) \ge 2\cot(\Delta/4) \ge 2. \tag{16.1}$$

Consequently the targets become opposite or the exploration leaves the four-tip sector within time $\pi/2$. The source conformal radius remains at least $e^{-\pi/2}$ times its initial value. On survival, the domain Markov property gives the unconditioned quadrilateral law and the balanced estimate applies. On exit, the one-arc estimate applies. The same norm-one completion restores all exterior labels.

The survival and exit estimates thus combine with their original probabilities, so the bounds on the response and its coefficients are uniform over the initial four-tip geometry.

16.2 The contribution from six or more tips

We use the common exploration transcript of [1, Lemma 8.1 and Theorem 8.4]. At fixed source radii and protection scales, the interior response is a finite row on the remaining labelled arcs. On each compact family of separated angles, Theorem 11.1 allows us to replace that row, including its root attachments, by its continuum value with a uniformly vanishing error in variation norm. An exterior completion has norm at most one, so it preserves this error bound even when it depends on the mesh and on the transcript. By [1, Theorem 8.4(ii)–(iii)], the probability of angles outside such a compact family can be made arbitrarily small at fixed scales. There the raw norm on the protected cut still bounds the integrand independently of those angles. We now remove the source regulators by (4.5) and (5.8). When comparing finitely many radii we use one transcript and one exterior completion for all of them, before summing over the possible reduction scales.

For a late first reduction at dyadic scale t, the preceding comparable scale still has at least six active tips. With an arbitrarily small loss $\zeta > 0$, its probability is at most $C(t/d)^{35/12-\zeta}$ by the alternating six-arm exponent [9, Theorem 4]. A local error of order $r^{p+\varepsilon}$ therefore contributes at most

$$Cr^{p+\varepsilon}t^{-(x+p+\varepsilon)}\left(\frac{t}{d}\right)^{35/12-\zeta}, \qquad \varepsilon = \frac{1}{40}. \tag{16.2}$$

Configurations with at most four tips from the outset enter at scale comparable to d. For those that first reduce later, we sum (16.2) over the possible reduction scales. The sum is dominated by its largest scale because

$$\frac{35}{12} - x - p - \varepsilon = \frac{21}{16} - \frac{1}{40} = \frac{103}{80} > 0. \tag{16.3}$$

For $0 < \zeta < 103/80$ the resulting geometric series is bounded by

$$Cd^{-x}(r/d)^{p+\varepsilon}.$$

The part with at least six tips down to scale comparable to r has raw norm at most Cr^{-x} and contributes at most

$$Cr^{-x}(r/d)^{35/12-\zeta}.$$

After r^{-p} normalization this decays with exponent $35/12 - x - p - \zeta$, which is larger than ε. The tail of the coefficient of order p has the same bound, since its local norm at scale t is at most $Ct^{-(x+p)}$ and the same six-arm probability applies. The critical coefficient has local norm at most $Ct^{-(x+s)} = Ct^{-5/4}$. Its tail is summable because

$$\frac{35}{12} - (x+s) = \frac{5}{3} > 0.$$

After multiplication by r^s, its omitted tail is bounded by the same unresolved six-tip contribution. These estimates will now construct both coefficients directly in the existing completion, without postulating a space of continuum frontier records.

Proposition 16.1 (Completed two-term expansion)**.** *For each packet $\Xi_r \in \{M_r, B_r\}$, define the two-scale rows at a common mesh and cut by*

$$\begin{aligned} C_{\Xi,r} &= \frac{\Xi_r - 2^p \Xi_{r/2}}{r^s(1-2^{p-s})}, \\ D_{\Xi,r} &= \frac{\Xi_r - 2^s \Xi_{r/2}}{r^p(1-2^{s-p})}. \end{aligned} \tag{16.4}$$

They have limits C_Ξ, D_Ξ in the completed-record norm, and

$$\|\Xi_r - r^s C_\Xi - r^p D_\Xi\|_{d,*} \le Cd^{-x}(r/d)^{p+1/40}. \tag{16.5}$$

Their norms satisfy

$$\|C_\Xi\|_{d,*} \le Cd^{-(x+s)}, \qquad \|D_\Xi\|_{d,*} \le Cd^{-(x+p)}.$$

The row C_Ξ is obtained by completing the stationary amplitudes $K_{\Xi,\beta}$. In particular, if

$$K_{\Xi,A} = K_{\Xi,B} = K_{\Xi,J} = 0, \tag{16.6}$$

then $C_\Xi = 0$ and $r^{-p}\Xi_r \to D_\Xi$ in the original completed-record norm. Condition (16.6) is separate for $\Xi = M$ and for $\Xi = B$.

Proof. At a fixed genuine four-tip reduction, substitute (15.7) into (16.4). The first combination cancels the term of order p and has error $O(r^{q+\varepsilon})$ after its r^{-s} normalization. The second cancels the term of order s and has error $O(r^\varepsilon)$ after its r^{-p} normalization. The arbitrary-quad startup gives the same assertions before balancing.

First compare the radii r and br, with $1/2 \le b \le 1$. Use the same finite-mesh exploration until the first reduction, stopping above the larger source scale. On the resolved shells the common local coefficients cancel between the two scales. Apply the preceding shell sum and the three-column inverse before the norm-one exterior completion. On the unresolved part both source radii are comparable with r, so their raw normalized bounds have the same

order and the six-arm estimate applies to both. This proves the corresponding comparable-scale Cauchy estimates, uniformly in b. Summing along a dyadic chain and using one final comparable-scale step gives, for arbitrary $r, r' > 0$,

$$\begin{aligned} \|C_{\Xi,r} - C_{\Xi,r'}\|_{d,*} &\le Cd^{-(x+s)}\big[(r/d)^{q+\varepsilon} + (r'/d)^{q+\varepsilon}\big], \\ \|D_{\Xi,r} - D_{\Xi,r'}\|_{d,*} &\le Cd^{-(x+p)}\big[(r/d)^{\varepsilon} + (r'/d)^{\varepsilon}\big]. \end{aligned} \tag{16.7}$$

We take the mesh limit with the protected scales fixed as in Section 4.3. Since the resulting families are Cauchy in the original norm, completeness supplies their limits C_Ξ, D_Ξ. The same shell estimates without differencing give their asserted norm bounds.

The definitions have the exact algebraic identity

$$\Xi_r = r^s C_{\Xi,r} + r^p D_{\Xi,r}.$$

Letting $r' \downarrow 0$ in (16.7) and using $s + q = p$ now proves (16.5). If (16.6) holds, every local critical coefficient is zero. Its absolutely summable completed contribution and hence C_Ξ are zero. □

Under (16.6), two radii r, r' satisfy

$$\left\|r^{-p}\Xi_r - r'^{-p}\Xi_{r'}\right\|_{d,*} \le Cd^{-(x+p)}\left[(r/d)^{\varepsilon} + (r'/d)^{\varepsilon}\right]. \tag{16.8}$$

16.3 A single coefficient direction

The one-arc eigenspace at $p = 3/2$ is one-dimensional. Write the two one-arc coefficients as $a_M\phi_1$ for M_r and $a_B\phi_1$ for B_r. The exit operation in Lemma 15.1 is linear and independent of the source packet. Hence their leading forcing terms are a_M and a_B times the same completion-dependent profile.

By (15.8), the resulting four-tip coefficients have the same proportionality, and the completed exploration preserves it. The initial-data term supplies no further coefficient at this order, because $11/15 > 17/48$. Therefore the coefficients D_M, D_B in (16.5) lie in a common one-dimensional direction, whether or not their critical coefficients vanish.

Proposition 17.2, proved below, establishes (16.6) for M. It follows that $C_M = 0$ and that the strong limit D_M of $r^{-p}M_r$ agrees with the weak insertion Ψ on the separated tests of Paper II, since both use the same extraction. Its known nonzero correlation implies $a_M \neq 0$, since $a_M = 0$ would force $D_M = 0$ by the resolvent construction. Consequently

$$D_B = \frac{a_B}{a_M}\Psi. \tag{16.9}$$

We determine the scalar a_B/a_M in Section 18. The term of order r^s has its own coefficient C_B.

17 Cancellation for the scalar field

Three boundary experiments distinguish the three coordinates of the stationary coefficient for E°. We apply the scalar null identity to each experiment to show that all three coordinates vanish.

Lemma 17.1 (Weak null fusion in a fixed quadrilateral)**.** *Fix a simply connected domain with four distinct alternating boundary tips, and one of the boundary completions C_A, C_B, C_J of (14.1). On a compact source set in its interior,*

$$\langle M_r(z) C_\beta\rangle = O_{\mathcal{D}'}(r^{3/2}), \qquad \beta \in \{A, B, J\}. \tag{17.1}$$

The distributional tests act on z. The domain, its tips, and the exterior completion remain fixed when these derivatives are taken.

Proof. First keep the two insertion coordinates separated and hold the density coordinate fixed during scalar localization. The localization proof of the scalar null identity in [2, Propositions 8.2–8.3 and Theorem 9.1] applies with this boundary completion. Indeed, on a fixed protected source patch its transcript is independent of the scalar coordinate. On a transcript with at most six active tips, the conditional null identity is an identity for the entire finite boundary-partition response. Each of C_A, C_B, C_J is a deterministic linear completion of norm at most one, so it preserves that identity. The remaining transcripts have at least eight alternating arms. The same source and stress-row bounds as in that proof give the tested remainder

$$C_\zeta R^{21/4-\zeta} R^{-5/4-2} = C_\zeta R^{2-\zeta}.$$

We first complete the density through its own fixed cut, so the eight-arm probability is evaluated under the original annular filling law. After integration by parts, all derivatives act on the compact source test. We may therefore send R to zero in the displayed bound and obtain both null equations for this boundary experiment.

Write $w = z + s$ for the density coordinate. It remains to use these equations as $s \to 0$. Work on a smaller source patch and choose a fixed contour Γ enclosing the whole pair. Set

$$H(z,s) = \langle E^\circ(z)\Phi(z+s)C_\beta\rangle, \qquad P(z,s) = |s|^y H(z,s), \qquad C(z) = C_\circ\langle\Phi(z)C_\beta\rangle,$$

and let P_n be the nth angular coefficient of P. For a local expression F, write

$$\mathcal{J}F(z) = \frac{1}{2\pi i}\oint_\Gamma \frac{T(w)F(z)}{w-z}\,dw, \qquad \mathcal{A} = 4\partial_z^2 - 6\mathcal{J}.$$

The finite-tip Ward identity proved in Lemma 12.1 permits the contour surrounding the scalar to be enlarged to Γ. The residue at the density is $-h_\Phi H/s^2 + (\partial_s H)/s$. Thus the scalar null equation becomes

$$-\frac{2}{3}(\partial_z - \partial_s)^2 H + \frac{h_\Phi}{s^2}H - \frac{1}{s}\partial_s H + \mathcal{J}H = 0, \tag{17.2}$$

and likewise in the conjugate variables. This contour representation does not differentiate the exterior boundary or its completion.

By the leading completed-row estimate (4.6), $P_0 - C = O_{\mathcal{D}'}(r^\gamma)$ and $P_n = O_{\mathcal{D}'}(r^\gamma)$ for $n \neq 0$. The same bounds hold after adding the separated stress on Γ, by bounded row gluing. In particular, $\mathcal{A}P_n = O_{\mathcal{D}'}(r^\gamma)$ for $n \neq 0$, with a fixed larger source-test seminorm. Each nonzero Fourier packet is kept as the angular integral of $P - C$ before taking its norm. This is precisely the grouping used in the local contour construction of [2, Theorem 4.11 and Sections 13.6–13.7].

Put $T_r = r\partial_r$ and $p = 3/2$. Substitution in (17.2) gives

$$(T_r + n)(T_r + n - p)P_n = -r(9 - 4n - 4T_r)\partial_z P_{n-1} - r^2\mathcal{A}P_{n-2}, \tag{17.3}$$

$$(T_r - n)(T_r - n - p)P_n = -r(9 + 4n - 4T_r)\partial_{\bar z} P_{n+1} - r^2\overline{\mathcal{A}}P_{n+2}. \tag{17.4}$$

These are the Euler equations of [2, Section 12, (12.5)–(12.11)], now with the fixed contour replacing its exterior Ward operator. For P_1, equation (17.4) has roots $1, 5/2$ and a right side of the form $T_r f + g$, where $f, g = O_{\mathcal{D}'}(r^{1+\gamma})$. Integration in $\log r$ therefore gives $P_1 = a_1 r + O_{\mathcal{D}'}(r^{1+\gamma})$, with the same statement for $T_r P_1$. Substitution in (17.3) identifies $a_1 = -5\partial_z C$. Conjugating the same calculation, we find

$$P_{-1} = -5r\partial_{\bar z} C + O_{\mathcal{D}'}(r^{1+\gamma}), \qquad T_r P_{-1} = -5r\partial_{\bar z} C + O_{\mathcal{D}'}(r^{1+\gamma}).$$

We compare these coefficients against a smooth test on a fixed logarithmic-radius window, transferring radial derivatives to that test. Substituting the first modes into (17.3) at $n = 0$, we find

$$T_r(T_r - p)P_0 = 25r^2\partial_z\partial_{\bar{z}}C + O_{\mathcal{D}'}(r^{2+\gamma}).$$

The two homogeneous powers are 1 and r^p. The leading fusion fixes the constant term as C, and the particular solution is $O_{\mathcal{D}'}(r^2)$. Consequently $P_0 - C$ is $O_{\mathcal{D}'}(r^p)$, proving (17.1). All cutoff limits have been taken at fixed s before this final collision limit. □

Proposition 17.2 (Cancellation of the three M amplitudes)**.** *For the angular average M associated with E°, the constants in* (15.6) *satisfy*

$$K_A^M = K_B^M = K_J^M = 0. \tag{17.5}$$

Proof. Fix a nondegenerate quadrilateral as in Lemma 17.1. The first term of Proposition 15.2, transported to a variable source point in a compact interior set, is

$$r^{-s}\langle M_r(z)C_\beta\rangle \longrightarrow K_\beta^M\,\mathcal{G}_D(z), \qquad s = y - x = \frac{55}{48}. \tag{17.6}$$

To justify this statement also for a moving source, first divide lengths by $d_z = \mathrm{crad}_D(z)$. Let σ be the balancing time of (16.1) and let S be survival to that time. Conditional on S, the four labels survive in their cyclic order. On exit before balancing the response is $O(r^p)$ by the one-arc estimate. The Markov decomposition thus gives

$$\mathcal{G}_D(z) = d_z^{-y}\,\mathbb{E}_z[\mathbf{1}_S e^{y\sigma} g(Z_\sigma)].$$

The formula includes $\sigma = 0$ for a balanced configuration. The error after division by r^s is locally uniform since $\sigma \le \pi/2$ and $g\,w = 1 + g$ is bounded. Take a disk quadrilateral whose four separated angles are balanced at its center. On a small neighborhood of the center the balancing time on survival is at most the initial deviation from opposition divided by two, by (16.1). There is positive probability that the driver stays in a small angular interval up to that time. Before a collision its law is locally absolutely continuous with respect to Brownian driving (ordinary radial driving here), and on this event all four angles stay separated by continuity of the Loewner flow. Hence the displayed integrand is positive on an event of positive probability throughout that neighborhood. Local boundedness and this positivity suffice for distributional testing.

Since $p > s$, equation (17.1) says that the left side tends to zero as a source distribution. Pair with a nonnegative, nonzero smooth test supported in that compact set. The integral of $\mathcal{G}_D$ is positive, so $K_\beta^M = 0$. Apply this argument separately to the three fixed completions. □

The proof uses the null equation at the scalar being fused with the density. A null equation at a different, separated E° insertion does not reproduce it for $L_r\Phi$. Thus (17.5) supplies no cancellation of K_β^B.

18 The subleading field and the stationary logarithmic coefficient

Tests at two different radii distinguish the two powers of r. To identify the coefficient at order $r^{3/2}$ we also need a distant field with a nonzero pairing. The field Ψ itself supplies that test.

18.1 Identification of the two coefficients

Proposition 16.1 constructs two terms in the original norm for each packet. Write them as

$$\Xi_r = r^s C_\Xi + r^p D_\Xi + O_{d,*}(d^{-x}(r/d)^{p+1/40}), \qquad s = \frac{55}{48}, \quad p = \frac{3}{2}, \tag{18.1}$$

with the dimensional factors for each coefficient understood as in that proposition. For M, Proposition 17.2 eliminates the first coefficient, so $r^{-p}M_r$ converges in norm to D_M. Its pairings with the separated fields of Paper II converge to the corresponding pairings of Ψ, since Paper II defines Ψ by this same limit. We therefore write Ψ for D_M on the complete record.

The series (15.8) depends linearly on the one-arc exit coefficient. Returning to the observation circle preserves that linearity, so all the D_Ξ lie in the same one-dimensional subspace. We know one nonzero element of it, namely $D_M = \Psi$, whose two-point function is (4.8). We can therefore write $D_B = c\Psi$ for some scalar c.

Pair (18.1) for B with a fixed separated Ψ. This is an admissible bounded completion by the strong M construction just obtained. Dividing first by r^s and using (10.16) gives

$$\langle C_B(z)\Psi(v)\rangle = 0.$$

Once this pairing vanishes, division by r^p shows that $\langle D_B(z)\Psi(v)\rangle = 0$ as well. This pairing equals $c\langle\Psi(z)\Psi(v)\rangle$, so (4.8) forces $c = 0$. Since $a_M \neq 0$, relation (16.9) also forces $a_B = 0$ in the one-arc projection.

Theorem 18.1 (Mixed fusion in the complete-record norm)**.** *The centered angular average M_r for E° satisfies*

$$\|M_r - r^p\Psi\|_{d,*} \le Cd^{-x}(r/d)^{p+1/40}. \tag{18.2}$$

For the logarithmic field of Theorem 5.1, there is a scalar odd coefficient $\Omega = C_B$ of scaling dimension $x + s = y = 5/4$ such that

$$\|B_r - r^s\Omega\|_{d,*} \le Cd^{-x}(r/d)^{p+1/40}, \tag{18.3}$$

$$\|N_r - r^s\Omega - a_L r^p\Psi\|_{d,*} \le Cd^{-x}(r/d)^{p+1/40}. \tag{18.4}$$

The scaling dimension refers to the dilation rule for this coefficient. Its norm at cut d is bounded by $Cd^{-5/4}$, by Proposition 16.1. In particular, the full-record estimate with $B_r = O(r^{p+1/40})$ holds exactly when $\Omega = 0$.

Proof. The preceding comparisons identify both coefficients in (18.1). By the dilation rule (15.1) the first coefficient has degree $x + s = y$, and substituting $N = B + a_L M$ proves (18.4). To see uniqueness, subtract two proposed expansions and divide their difference by r^s. The term of order r^p vanishes in the limit because $p > s$, so the first coefficients agree. Dividing the remaining difference by r^p identifies the second coefficients, since the remainder divided by r^p still tends to zero in the original norm. In particular,

$$\|r^{-s}B_r - \Omega\|_{d,*} \le Cd^{-5/4}(r/d)^{91/240}, \tag{18.5}$$

$$\sup_{1/2\le b\le 1} \|M_r - b^{-p}M_{br}\|_{d,*} \le Cd^{-x}(r/d)^{61/40}. \tag{18.6}$$

The exponent in the first bound is $61/40 - s = 91/240$. For the second we subtract the expansions at r and br after multiplying the latter by b^{-p}, so their Ψ terms cancel. □

18.2 Disjoint insertions and the stationary coefficient

We may apply the norm estimate in several disjoint disks. At disk i of radius d_i put $X_i = r_i^{-3/2} M_{r_i}$. Theorem 18.1 gives $\|X_i - \Psi_i\|_{d_i,*} \le C d_i^{-77/48} (r_i/d_i)^{1/40}$ and $\|X_i\|_{d_i,*} + \|\Psi_i\|_{d_i,*} \le C d_i^{-77/48}$. Expand the difference of the tensor products by changing one factor at a time. After any joint completion its norm is bounded by

$$C_m \left(\prod_{i=1}^{m} d_i^{-77/48} \right) \sum_{i=1}^{m} (r_i/d_i)^{1/40}.$$

Since the right-hand side is a sum of single-disk errors, the radii may tend to zero independently at fixed distinct centers. Pairing with separated fields recovers [2, Theorem 4.11].

The vanishing of $\langle \Omega(z)\Psi(v) \rangle$ does not determine the signed measure Ω. A simple example explains the issue. On the partitions of three named sites the nonzero row

$$\delta_{123} - \delta_{12|3} - \delta_{13|2} - \delta_{23|1} + 2\delta_{1|2|3}$$

has zero mass and zero pair-sign moments. Since the independent symmetric block signs also have vanishing odd moments, every three-sign test integrates to zero against this row. Here δ_π denotes the unit mass on the indicated partition. For the percolation coefficient, it would suffice to exhibit fixed boundary experiments of weak order $o(r^{55/48})$ whose completion weights span the surviving stationary coordinates. Equivalently one could establish cancellation directly in the series (15.6).

Conclusion

Closing a disk defines the scalar field E°. In a density collision the same field occurs because each annulus in which the two clusters can first connect contributes to its logarithmic coefficient. The finite part L_ℓ carries this normalization into collisions with a third density and into the limit of two pairs shrinking at unrelated rates.

For the mixed collision, one can now distinguish the two open banks of a quadrilateral all the way back to the original observation circle. On that circle the first correction for E° is $r^{3/2}\Psi$ for every bounded exterior test. The corresponding logarithmic fusion has the same subleading field with the coefficient fixed by (10.15). A possible additional contribution is entirely contained in the three quadrilateral amplitudes of Ω in Section 18.

Use of generative AI

The research programme was conceived by the author before generative AI was used in this project. ChatGPT 6 (OpenAI) was used extensively in proposing and developing proof strategies, mathematical arguments and calculations, and in drafting and revising the manuscript. Anthropic Claude Fable 5.2 Max has been used to double check the content. The author takes responsibility for the content of the manuscript.

References

[1] A. Gandolfi, *Towards a conformal field theory of critical percolation. I. The bulk stress tensor and Ward identities*, manuscript of 15 November 2026, Hexagon 2611.00497v1.

[2] A. Gandolfi, *Towards a conformal field theory of critical percolation. II. Scalar responses and null identities*, manuscript of 17 November 2026, Hexagon 2611.00651v1.

[3] F. Camia, *Conformal covariance of connection probabilities and fields in 2D critical percolation*, Comm. Pure Appl. Math. **77** (2024), 2138–2176. doi:10.1002/cpa.22171.

[4] F. Camia, R. P. Conijn and D. Kiss, *Conformal measure ensembles for percolation and the FK-Ising model*, in *Sojourns in Probability Theory and Statistical Physics–II*, Springer Proc. Math. Stat. **299** (2019), 44–89. arXiv:1507.01371v3.

[5] F. Camia, *On the density of 2D critical percolation gaskets and anchored clusters*, arXiv:2312.11047.

[6] F. Camia and C. M. Newman, *Two-dimensional critical percolation: The full scaling limit*, Comm. Math. Phys. **268** (2006), 1–38. arXiv:math/0605035.

[7] F. Camia and C. M. Newman, *Critical percolation exploration path and SLE(6): A proof of convergence*, Probab. Theory Related Fields **139** (2007), 473–519. arXiv:math/0604487v2.

[8] G. F. Lawler, O. Schramm and W. Werner, *One-arm exponent for critical 2D percolation*, Electron. J. Probab. **7** (2002), paper 2, 1–13. arXiv:math/0108211.

[9] S. Smirnov and W. Werner, *Critical exponents for two-dimensional percolation*, Math. Res. Lett. **8** (2001), 729–744. arXiv:math/0109120v2.

[10] O. Schramm and D. B. Wilson, *SLE coordinate changes*, New York J. Math. **11** (2005), 659–669. Journal version.

[11] D. Zhan, *Two-curve Green's function for 2-SLE: The interior case*, Comm. Math. Phys. **375** (2020), 1–40. arXiv:1806.09663v2.

[12] C. B. Compean and M. Kirchbach, *The trigonometric Rosen–Morse potential in the supersymmetric quantum mechanics and its exact solutions*, J. Phys. A **39** (2006), 547–557. doi:10.1088/0305-4470/39/3/007. arXiv:quant-ph/0509055.

[13] NIST Digital Library of Mathematical Functions. `https://dlmf.nist.gov/`.

[14] A. A. Belavin, A. M. Polyakov and A. B. Zamolodchikov, *Infinite conformal symmetry in two-dimensional quantum field theory*, Nucl. Phys. B **241** (1984), 333–380. doi:10.1016/0550-3213(84)90052-X.

[15] Y. He, *Logarithmic operators in $c = 0$ bulk CFTs*, SciPost Phys. **19** (2025), 008. doi:10.21468/SciPostPhys.19.1.008.

[16] F. Camia and Y. Feng, *Logarithmic correlation functions in 2D critical percolation*, J. High Energy Phys. **08** (2024), 103. arXiv:2403.18576.

[17] F. Camia and Y. Feng, *Conformally covariant probabilities, operator product expansions, and logarithmic correlations in two-dimensional critical percolation*. arXiv:2407.04246v2, 26 August 2025.

[18] F. Camia and Y. Feng, *The percolation energy field and its logarithmic partner*. arXiv:2508.16047v2, 1 June 2026.

[19] C. Garban, G. Pete and O. Schramm, *Pivotal, cluster and interface measures for critical planar percolation*, J. Amer. Math. Soc. **26** (2013), no. 4, 939–1024. arXiv:1008.1378v5.

[20] P. Nolin, *Near-critical percolation in two dimensions*, Electron. J. Probab. **13** (2008), no. 55, 1562–1623. arXiv:0711.4948.

[21] O. Schramm and S. Smirnov, *On the scaling limits of planar percolation*, Ann. Probab. **39** (2011), no. 5, 1768–1814. arXiv:1101.5820.

[22] V. Gurarie, *Logarithmic operators in conformal field theory*, Nucl. Phys. B **410** (1993), 535–549. arXiv:hep-th/9303160v2.

[23] A. Kupiainen, R. Rhodes and V. Vargas, *Local conformal structure of Liouville quantum gravity*, Comm. Math. Phys. **371** (2019), no. 3, 1005–1069. doi:10.1007/s00220-018-3260-3. arXiv:1512.01802v3.

[24] G. Baverez and M. D. Wong, *Fusion asymptotics for Liouville correlation functions*, Ann. Inst. Henri Poincaré Probab. Stat. **61** (2025), no. 3, 2004–2035. doi:10.1214/24-AIHP1489. First preprint version, arXiv:1807.10207v1 (2018).